Dissertation

submitted to the

Combined Faculties for the Natural Sciences and for Mathematics

of the Ruperto–Carola University of Heidelberg, Germany

for the degree of

Doctor of Natural Sciences

Put forward by

Bao, Xiao-Hui

born in Liaoning, China

Oral examination: 22.07.2010

Quantum Information with Entangled Photons and Cold Atomic Ensembles

Referees: Prof. Dr. Jian-Wei Pan

Prof. Dr. Matthias Weidemüller

Zusammenfassung

Quanteninformation mit verschränkten Photonen und kalten atomaren Ensembles

In der Quanteninformationsverarbeitung gelten Photonen als die besten Kandidaten für die Übertragung und Atome als die besten Kandidaten für die Speicherung von Information. Die Kombination dieser beiden Systeme verspricht eine faszinierende Zukunft für die praktische Anwendung von Konzepten der Quanteninformation. Die Arbeiten, die im Rahmen dieser Dissertation vorgestellt werden, lassen sich größtenteils in zwei Teilbereiche einordnen. Der ersten Teil beschreibt die Manipulation von verschränkten Photonen und beinhaltet die Demonstration eines zerstörungsfreien CNOT-Gatters, die Erzeugung von schmalbandigen verschränkten Photonen mithilfe einer durch einen Hohlraumresonator verstärkten parametrischen Fluoreszenzquelle und die Realisierung von Interferenz zwischen schmalbandigen Photonenquellen. Der zweite Teil behandelt die Manipulation von atomaren Ensembles. Der Hauptzweck dieses Teils ist die Vergrößerung der Übertragungsentfernung für die Quantenkommunikation durch das Konzept des Quantenrepeaters. Die in diesem Teil vorgestellten experimentellen Arbeiten beinhalten die Verlängerung der Speicherzeit von Quantenspeichern auf 1ms durch Vergrößerung der Wellenlänge der gespeicherten Spinwelle, die Realisierung des verschränkungsgestützten Spinwelleninterferometers, der Demonstration von effizientem Verschränkungsaustausch mithilfe von Quantenspeichern und die Realisierung der Quantenteleportation zwischen atomaren Ensembles.

Abstract

Quantum Information with Entangled Photons and Cold Atomic Ensembles

In quantum information science, photons are the best candidate for transmitting information, and atoms are the best candidate for storing information. The combination of these two systems provides a fascinating future for practical applications of the quantum information concepts. The work presented in this thesis mainly consists of two parts. The first part is about manipulation of entangled photons, including the demonstration of a nondestructive CNOT gate, the creation of narrowband entangled photons through cavity-enhanced spontaneous parametric down-conversion, and the realization of interference between narrowband photon sources. The second part is about manipulation of atomic ensembles. The main purpose for this part is to extend the quantum communication distance using the concept of quantum repeater. Within this part, the experimental work includes, the extension of storage lifetime of quantum memories to 1 ms by increasing the wavelength of stored spinwave, the realization of entanglement assisted spinwave interferometer, the demonstration of efficient entanglement swapping with quantum memories, and the realization of quantum teleportation between atomic ensembles.

Contents

Chapter 1

Introduction

In this chapter, we give an introduction to the basic concepts in quantum information science, including qubit, quantum cryptography, quantum teleportation, entanglement swapping, quantum repeater and quantum computing. Experimental processes are also discussed in each section.

1.1 Qubit

A quantum bit, i.e., qubit, is the basic unit in quantum information science. It can be an arbitrary superposition state of the logic bit "0" and "1", which is usually written the following way

$$|\psi\rangle = \alpha|0\rangle + \beta|1\rangle. \tag{1.1}$$

A qubit can be the spin state of a single particle, for instance, spin-up corresponds to $|0\rangle$ and spin-down corresponds to $|1\rangle$. It can also be an superposition of arbitrary two internal states of an atom or ion. For the case of a photon, it can be the polarization, momentum, arriving time, or even the frequency, etc. For the case of an atomic ensemble, it can be the superposition state of two spacial modes of spinwave. In one word, any system which has two distinct states that are able to interfere each other can be viewed as a qubit.

1.2 Quantum cryptography

The essence of quantum cryptography is the so called no-cloning theory, which says that an arbitrary quantum state of a single particle can not be cloned. The proof is rather

simple. First we assume that it is possible to clone the single particle state, which means that there is an unitary transformation which can realize the following operations

$$\begin{aligned} U|\psi\rangle_1|0\rangle_2 &= |\psi\rangle_1|\psi\rangle_2 \\ U|\phi\rangle_1|0\rangle_2 &= |\phi\rangle_1|\phi\rangle_2 \end{aligned} \tag{1.2}$$

with particle 1 carrying the state to be cloned, and particle 2 being the target particle to carry the cloned state, $|\psi\rangle$ and $|\phi\rangle$ are two arbitrary states. By taking the conjugate transpose operation of the first equation and multiplying with the second equation, we have

$$\langle\psi|\phi\rangle(\langle\psi|\phi\rangle - 1) = 0. \tag{1.3}$$

However since $|\psi\rangle$ and $|\phi\rangle$ are two arbitrary state, it is not possible to fulfill the above equation. Therefore the assumption made is incorrect, such a cloning machine is not available. In this way we proved the no cloning theory.

The first quantum cryptography protocol was proposed by Charles Bennett and Gilles Brassard in 1984 [1], which was later named as the BB84 protocol. The basis idea is following. First, the sender A prepares a single particle with a state which is randomly chosen among four states, including $|0\rangle$, $|1\rangle$, $|+\rangle$ and $|-\rangle$ with $|\pm\rangle = 1/\sqrt{2}(|0\rangle \pm |1\rangle)$ and sends it the receiver B through public channels; Second, B measures the received particles in a basis which is randomly chosen between $|0\rangle/|1\rangle$ and $|+\rangle/|-\rangle$; Third, A and B public broadcast their information of bases chosen. If the bases are same, they will share one bit of correlated key, if not they just discard this event. In case of an eavesdropper, in order to get some information about the keys A and B build, he will inevitably induce some disturbance to the state A sends, according to the no-cloning theory. By comparing a small part of their keys, A and B can easily find the existence of the eavesdropper.

Subsequently in 1991 Artur K. Ekert proposed a quantum cryptography protocol [2] using entangled photons, with the security guaranteed by the famous Bell's theory. Afterwards in 2006, we proposed a scheme based on hyper-entangled photon pairs [3], which can give higher efficiency and better security. All the above protocols are within the discrete variable regime. For the continuous variable regime, the first cryptography protocol was proposed by T. C. Ralph in 1999 [4]. In the aspect of experimental realizations, after the invention of the decoy-state schemes [5, 6], the absolute secure communication distance has overcome 100 km in 2007 [7–9]. Nowadays, commercial quantum cryptography products become available from the companies like id Quantique, MagiQ Technologies, etc.

1.3 Quantum teleportation and entanglement swapping

In order to transmit a quantum state from location A to another distant location B, we can encode the quantum state to a single-photon and transmit it directly to B. This direct transmission method suffers from the problem of channel loss. In case of long distance transmission, the success probability is rather low, most of the states will be lost during the transmission.

In 1993 C. H. Bennett *et al.* proposed the protocol of quantum teleportation [10], which is schematically shown in Fig. 1.1(a). In this protocol, an auxiliary entangled pair of particles are utilized. We assume that the state to be teleported is $|\psi\rangle = \alpha|0\rangle + \beta|1\rangle$ which is carried by particle 1. The auxiliary entangled pair between location A and B is $|\Psi^-\rangle_{23}$, with particle 2 in location A and particle 3 in location B. $|\Psi^-\rangle_{23}$ is the one of the four famous Bell states with the from of

$$\begin{aligned} |\Psi^{\pm}\rangle_{ij} &= 1/\sqrt{2}(|0\rangle_i|1\rangle_j \pm |1\rangle_i|0\rangle_j) \\ |\Phi^{\pm}\rangle_{ij} &= 1/\sqrt{2}(|0\rangle_i|0\rangle_j \pm |1\rangle_i|1\rangle_j). \end{aligned} \tag{1.4}$$

The joint state for these three particles can be written as

$$|\Psi\rangle = |\psi\rangle_1 \otimes |\Psi^-\rangle_{23}. \tag{1.5}$$

We can rewrite the right part in the Bell basis of particle 1 and 2 as following

$$\begin{aligned} |\Psi\rangle = 1/2\{&|\Phi^+\rangle_{12} \otimes (\alpha|1\rangle_3 - \beta|0\rangle_3) \\ &+|\Phi^-\rangle_{12} \otimes (\alpha|1\rangle_3 + \beta|0\rangle_3) \\ &-|\Psi^+\rangle_{12} \otimes (\alpha|0\rangle_3 - \beta|1\rangle_3) \\ &-|\Psi^-\rangle_{12} \otimes (\alpha|0\rangle_3 + \beta|1\rangle_3)\}. \end{aligned} \tag{1.6}$$

Therefore if we make a joint Bell state measurement (BSM) between particle 1 and 2 at location A, the remaining state for particle 3 at location B is rather similar with the initial state of particle 1, with only difference of a single-qubit unitary rotation. If we send the BSM result through a classical channel to location B, and make the corresponding unitary operation on particle 3, we can recover the original state of particle 1 on particle 3. In this way, the quantum state is "teleported" from location A to B. Since the classical signal can not travel faster than speed of light, the teleportation process does not violate the special relativity theory.

The first teleportation experiments were realized with photons by D. Bouwmeester and J.-W Pan *et al.* in the group of Anton Zeilinger in the end 1997 [11], and by D. Boschi

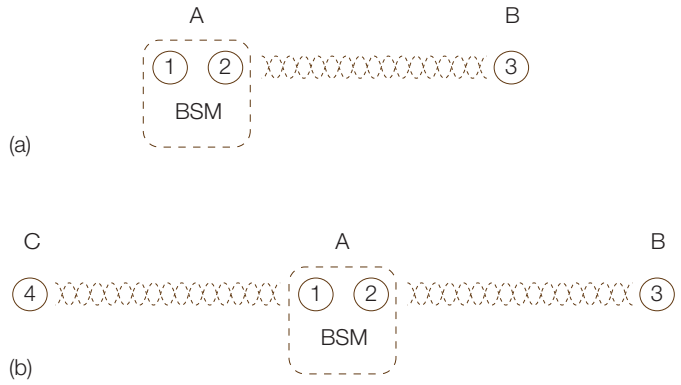

FIGURE 1.1: Quantum teleportation (a) and entanglement swapping (b).

et al. in the group of F. De Martini in the beginning of 1998 [12]. Teleportation in continuous variable regime was first realized by A. Furusawa *et al.* in 1998 [13]. In 2004, Wineland group [14] and Blatt group [15] realized the quantum teleportation between two ions with a separation of several μm only. This distance was improved to 1 m by Monroe group in 2009 [16]. Very recently, we realized the teleportation between two atomic ensembles which are connected by 150 m fibers (see Chap. 11 for detail).

The process of entanglement swapping is quite similar as shown in Fig. 1.1(b). In the quantum teleportation protocol, if initially particle 1 is entangled with another particle 4 in location C, after the BSM, particle 4 will be entangled with particle 3. In this way entanglement is build between location B and C. The type of entanglement between 3 and 4 is determined by the BSM result. By actively feeding forward this information and making the corresponding single-qubit rotation, particle 3 and 4 can be entangled in a single form. Entanglement swapping constitutes the basis of quantum repeater which will be discussed in Sec. 1.4. The first experimental realization of entanglement swapping was made by J.-W. Pan *et al.* in 1998 [17].

1.4 Quantum repeater

In order to efficiently transfer a quantum state to a distant location, we can use the teleportation process. The main problem is changed to the creation of remote entanglement in a deterministic way. Since photons are the best candidate for long distance transmission, in the following part of this section we restrict our discussion with photons. One method to create this type of deterministic entanglement is shown in Fig. 1.2(a). First a pair of local entangled photons is created in the remote site A and B respectively. For each site, one photon is stored with a quantum memory and the other is transmitted to a middle site. If both of the two flying photons can reach the middle site, through the process of entanglement swapping, we can entangle the remaining two stationary

photons. In this way remote entanglement can be created deterministically. However the above scheme is not so efficient actually. The probability for a photon from site A or B to reach the middle site is $p = e^{-\alpha L/2}$, with L the distance between A and B, α the channel loss rate. Therefore, the time consumption for the creation of a pair of remote entanglement is

$$t_c = \frac{1}{p \cdot p}\frac{L}{C} = e^{\alpha L}\frac{L}{C}, \tag{1.7}$$

with C the speed of light, and the resource consumption, i.e., how many pairs of local entanglement are used, is

$$R_c = \frac{1}{p \cdot p} \cdot 2 = 2e^{\alpha L}. \tag{1.8}$$

We can see that both the time and resource consumption scale exponentially as a function of distance L, which is a signature of inefficiency.

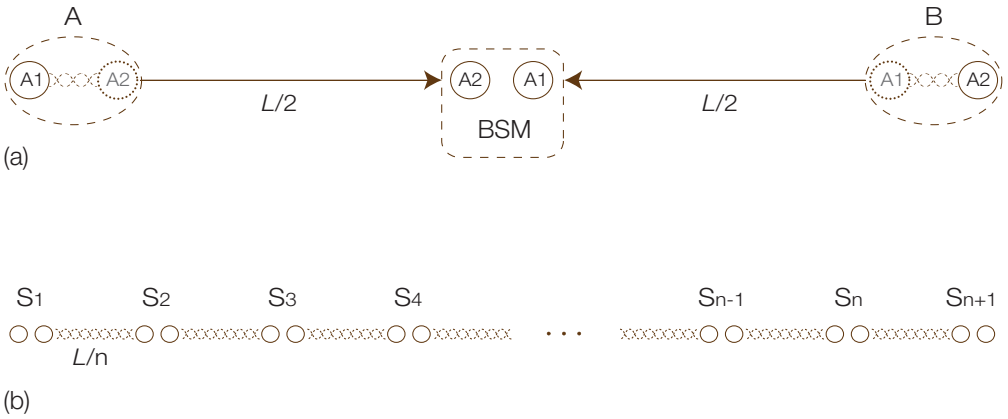

FIGURE 1.2: The quantum repeater protocol with (a) creation of remote entanglement (b) entanglement connection between different sections.

The basic idea of quantum repeater [18] is shown in Fig. 1.2(b). A long-distance channel is split into n small sections, with section distance of $\Delta = L/n$. For each section, the method in Fig. 1.2(a) is used to create entanglement. By replacing L with Δ in Eq. 1.7 and Eq. 1.8, we get the time and resource consumption for each section

$$\begin{aligned} t_{\text{sec}} &= e^{\alpha\Delta}\frac{\Delta}{C} \\ R_{\text{sec}} &= 2e^{\alpha\Delta}. \end{aligned} \tag{1.9}$$

After the creation of remote entanglement for each section, through a series of entanglement swapping in the intermediate sites (S_2 to S_n in Fig. 1.2), remote entanglement can be built between the beginning site (S_1) and the ending site (S_{n+1}) of the original

channel. The total time and resource consumption are

$$t_{\text{total}} \simeq t_{\text{sec}} + \frac{L}{C} = e^{\alpha\Delta}\frac{\Delta}{2C} + \frac{L}{C}$$
$$R_{\text{total}} = nR_{\text{sec}} = \frac{2L}{\Delta}e^{\alpha\Delta}. \tag{1.10}$$

The term L/C is corresponding to the transmission of classical signal of BSM results during the process of entanglement connection. From the result in Eq. 1.10, we can see that the time and resource consumption is only linearly dependent on the channel length L. In comparison with Eq. 1.7 and Eq. 1.8, the efficient is improved significantly, especially when L is very large and Δ is relatively small. In the above analysis of quantum repeater, we have not considered the non-perfection during entanglement creation for each section, and the noise induced during BSM. If these practical issues are being considered, after several stages of entanglement connection, the fidelity of remote entanglement will drop obviously. The solution for this problem is using the protocol of quantum purification [19], in which process, by discarding some of the entangled pairs conditioned on the joint measurement between different pairs, the fidelity for the left can be improved.

From the experimental view, in order to realize the quantum repeater protocol, the main difficulty is to find a method to efficiently store the photonic states. An experimental feasible scheme for quantum repeater was proposed by L.-M. Duan *et al.* in 2001 [20]. Subsequently, along this line of research there were several groups started to work on this scheme. Non-classical correlation between a single-photon and spinwave stored in an atomic ensemble was first observed in 2003 by A. Kuzmich *et al.* [21]. Single-photon storage through electromagnetically induced transparency (EIT) was realized by M. D. Eisaman *et al.* in [22] and T. Chaneliere *et al.* in [23] in 2005. A basic quantum repeater node was realized by C.-W. Chou *et al.* in 2007 [24] with a single-photon interference scheme, and by Z.-S. Yuan *et al.* in 2008 [25] with a two-photon interference scheme. In 2009, the storage lifetime was improved from several tens μs to the regime of several ms by us in [26] and R. Zhao in [27].

1.5 Quantum computing

The vast study of quantum computing starts from the discovery of Shor's algorithm in 1994 [28]. Until now Shor's algorithm is still the most important quantum algorithm. With this algorithm, the factorization of large integers can be done much efficiently. The speed is exponentially faster than the most efficient known classical algorithms. While the widely used public-key cryptography scheme known as RSA is based on the

computational complexity of factoring large integers, therefore Shor's algorithm largely threatens most of the secure communication systems. Another famous algorithm is the so called Grover's algorithm discovered in 1996 [29], which can speed up the search of an unsorted database from $O(N)$ to $O(N^{1/2})$.

A typical quantum computing process consists of three steps, initial state preparation, a series of gate operations (also called as a quantum circuit), and state measurement. Usually the realization of arbitrary gate operation in the second step is most difficult for most of the physical realizations. It was proved that arbitrary gate operation can be decomposed into a series of single-qubit operations and two-qubit controlled-not (CNOT) gates [30]. Therefore, one main task for the experimentalists working in different physical approaches for quantum computing is to build the CNOT gate, and improve the gate fidelity as high as possible. So far, the CNOT gate has been realized in many physical systems, including nuclear magnetic resonance [31], ion trap [32], linear optics [33], quantum dot [34], and super-conductors [35]. Another important aspect is the scalability. So far the ion trap approach shows the best scalability, with the best result of manipulating eight qubits [36].

Apart from the standard quantum circuit model which has been discussed above, R. Raussendorf and and H. J. Briegel proposed another theoretical model of quantum computing [37], called one-way quantum computing or measurement based quantum computing. In the one-way model, the computing starts from the preparation of a large two-dimensional entangled cluster state, arbitrary gate operations are realized through single-qubit measurements and feedback. The main task in this model is the creation of initial entanglement. For the experimental realizations, one promising approach is using neutral atoms trapped in optical lattice. Some preliminary result of creating highly entangled states in optical lattice has been observed in 2003 by O. Mandel *et al.* in [38]. Primary difficulties include unavailability of single-site addressing technique, and measuring the highly entangled state quantitatively. Recently there has been a new scheme without harnessing single-site addressing proposed by K. B. Soderberg *et al.* in [39]. The first one-way quantum computer was realized with photons by P. Walther *et al.* in 2005 [40]. The main difficulty for optical one-way computing is the scalability, i.e., how to create large entangled states efficiently.

Chapter 2

Creation of Entangled Photons

Entanglement is the main resource in quantum communication and quantum computing. In this chapter, we introduce the creation of entangled photons. At the beginning, a brief introduction to spontaneous parametric down-conversion (SPDC) is given. Then the creation of different types of entanglement is reviewed including the degree of momentum, arriving time and polarization. After that we discuss about the generation of multi-photon entanglement and hyper-entanglement. In the end of this chapter, creation of entangled photons in other systems is reviewed, and the methods of entanglement detection are introduced.

2.1 SPDC in nonlinear media

SPDC has been the main method to generate entangled photons so far. When a nonlinear crystal with second-order nonlinear susceptibility of $\chi^{(2)}$ is pumped by a laser, with a rather low probability, a pump photon splits into two photons (traditionally called *signal* and *idler*). This process is subject to energy conservation and momentum conservation, which is expressed as

$$\hbar\omega_p = \hbar\omega_1 + \hbar\omega_2 \tag{2.1}$$

$$\hbar\mathbf{k}_p = \hbar\mathbf{k}_1 + \hbar\mathbf{k}_2 \tag{2.2}$$

where ω is the frequency, $\mathbf{k}$ is the wave vector of the three photons. The second equation is called phase-matching condition, which determines the spacial and spectral distribution of the down-converted photons. The frequencies of the two photons can be very near or faraway and the propagation directions of them can be colinear or not. Determined by the polarizations of the generated photons, phase-matching is classified into

two types, Type I (parallel polarization) and Type II (perpendicular polarization). Theoretical description of SPDC was first developed by Hong and Mandel in [41]. Later on Rubin *et al.* studied the specific case for type-II configuration extensively in [42].

2.2 Types of entanglement in SPDC

2.2.1 Momentum entanglement

Usually the emission of down-converted photons has a spacial distribution. Due to the momentum conservation in this process, the emission directions are correlated. This kind of entanglement is usually called the momentum entanglement, or path entanglement. Fig. 2.1 is the typical setup to investigate the momentum entanglement, which was proposed by Horne *et al.* in [43] and first experimentally realized by Rarity *et al.* in [44]. The photons emitted through the paths A, B, C and D satisfy the momentum conservation:

$$\mathbf{k}_A + \mathbf{k}_C = \mathbf{k}_p \qquad \mathbf{k}_B + \mathbf{k}_D = \mathbf{k}_p. \tag{2.3}$$

Then the photons through path A and D are mixed on a 50:50 beam-splitter (BS), and photons through B and C on another 50:50 BS. If there is coincident event between detector D_1 (D_{1u} or D_{1d}) and detector D_2 (D_{2u} or D_{2d}), we can not distinguish whether the photons are from path A and C or from B and D. So the state can be expressed as:

$$|\psi\rangle = 1/\sqrt{2}(|A\rangle_1|C\rangle_2 + e^{i\phi}|D\rangle_1|B\rangle_2). \tag{2.4}$$

The phase between the two terms are determined by the path-length difference between $B+D$ and $A+C$. In the above discussion, we just post-select four paths in the emission distribution. Using this method, higher-dimensional entanglement can be easily realized by post-selecting more paths.

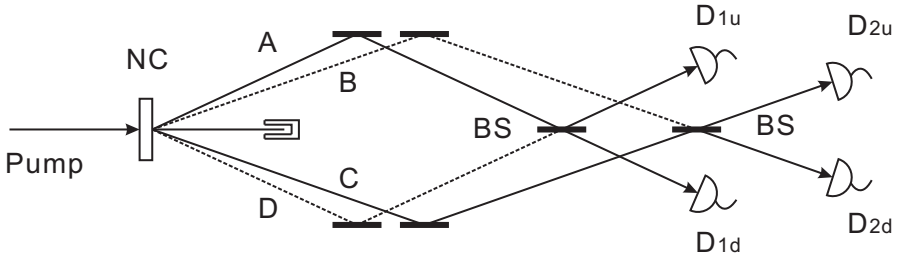

FIGURE 2.1: Momentum entanglement

There is a variation of this kind of entanglement, in which the pump is reflected back passing through the NC for a second time [45, 46]. For each time the pump passes through, only two directions are selected. There is coherence between these two cases,

hence leading to the momentum (path) entanglement. Higher-dimensional entanglement can be realized by passing the pump through several NCs.

2.2.2 Time entanglement

The interference of photon pair generated at different time points within the coherence time of the pump laser gives rise to what is usually called energy-time entanglement. This kind of entanglement was first proposed by Franson for the case that an excited atom emits two photons simultaneously [47], and was later experimentally realized with a SPDC source [48, 49]. This type of entanglement originates from the time coherence of the pump.

Fig. 2.2 is a typical setup to generate the energy-time entanglement through the SPDC process. Usually the ultra-violate (UV) pump laser used has a long coherence length which is usually larger than several meters. The generated photon pairs are detected after passing through an unbalanced Mach-Zehnder (MZ) interferometer. The path-length difference between the two arms which is usually several tens centimeters are much longer than the coherence length of the down-converted photons (several hundred microns). If both of the detectors detect a photon simultaneously, there are two possibilities causing this event, either both of the two photons passing through the long arm of each unbalanced interferometer, or both passing the short one. In principle, we can not distinguish these two possibilities, thus it can be expressed in a superposition state:

$$|\psi\rangle = 1/\sqrt{2}(|L\rangle_1|L\rangle_2 + |S\rangle_1|S\rangle_2). \tag{2.5}$$

Accordingly the photons passing through the long arm are generated "early", and the photons passing through the short arm are generated "late", compared with the detection time. So the above state can be also denoted as:

$$|\psi\rangle = 1/\sqrt{2}(|E\rangle_1|E\rangle_2 + |L\rangle_1|L\rangle_2). \tag{2.6}$$

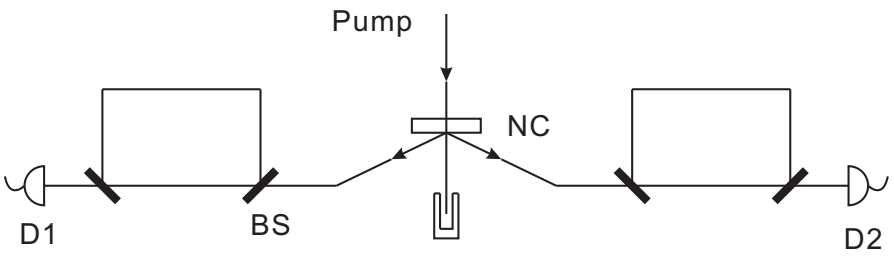

FIGURE 2.2: Energy-time entanglement

Actually the down-converted photons generated at any time within the pump coherence time can be entangled. The discrete entanglement above is just a post-selection of the complete state. The method can be further generalized to create higher-dimensional entanglement [50].

Brendel *et al.* developed a new kind of time entanglement called time-bin entanglement [51], in which a pulsed pump laser was utilized. Compared with the energy-time entanglement, the coherence of the pump laser is not important. The necessary coherence is produced by transmitting the pump through a similar unbalanced MZ interferometer. The pulsed character also provides the possibility to use gated single-photon detectors in the infrared band. This type of time-bin entanglement has been vastly utilized by Gisin's group in the quantum cryptography experiments (see [52] for instance) and multi-photon experiments (see [53] for instance).

2.2.3 Polarization entanglement

Polarization degree is often preferable, due to the availability of high-precision polarization rotating elements and the relative insensitivity of most materials to thermally induced birefringence. In the earlier experimental realizations [54, 55], down-converted photons with definite polarizations were superposed on a beam-splitter and entanglement was observed only for the post-selected events in which the two photons traveled to different output ports. However, the photons were actually created in product states. In latter experiments [56, 57], colinear type-II configuration was utilized. In this case, a photon pair with different polarizations was generated colinearly. Spatially separated polarization entanglement can be generated by splitting the two photons wiht a beamsplitter and post-selecting the case of one photon in each output port. Kwiat *el al.* developed the first true polarization-entangled source [58]. The configuration is sketched in Fig. 2.3.

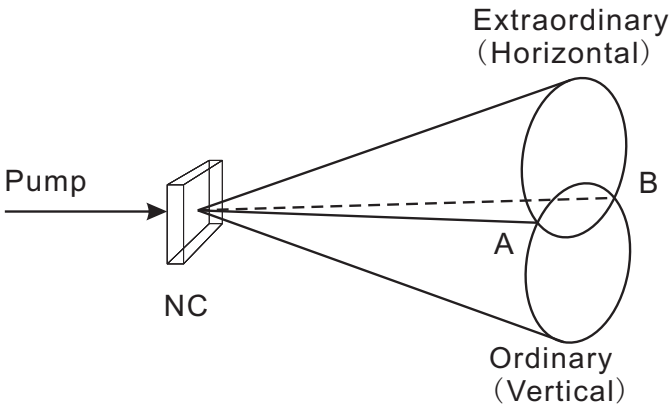

FIGURE 2.3: Polarization entanglement

The NC is Type-II configured, with the emitted extraordinary (horizontal polarized) photons and ordinary (vertical polarized) photons forming separate cones. The intersections of these two cones define two spatial modes (A and B). If the photon in mode A is of horizontal polarization, then the photon in mode B will be of vertical polarization, or vice versa, due to the type-II phase-matching. So the two-photon state detected in the modes A and B can be expressed as:

$$|\psi\rangle = 1/\sqrt{2}(|H\rangle_1|V\rangle_2 + e^{i\phi}|V\rangle_1|H\rangle_2) \tag{2.7}$$

where H corresponds to horizontal polarization, and V corresponds to vertical polarization. Usually compensators (a half-wave plate followed by a half-thickness NC) are inserted in path A and B to achieve high visibility. The relative phase ϕ between the two terms can be adjusted by slightly tilting the compensating NC. Other Bell states can be easily generated by manipulating one photon with waveplates.

In the above configuration, only the photons generated at the cone intersections are entangled and collected, which results in relatively low coincident count rate (3.6×10^5 s^{-1} in [59]). In [60], Kwiat *et al.* proposed a two-crystal source, in which all down-converted photons at a given color are entangled. In this source, the two crystals are all type-I configured and the pump is 45 degree polarized. The pump photon has equal probability to be down-converted either in the first crystal to generate two photons with H polarization or in the second one to generate two photons with V polarization. These two possibilities are indistinguishable, hence generating the polarization entanglement. This source suffers from the problem of angle dependent phase shift, which can be compensated by utilizing specially designed crystals [61]. Another method to generate higher brightness polarization-entangled photons with two crystals is the interferometric source (proposed in [62], see [63] for an experimental realization) in which two type-II configured colinear sources are combined on a polarizing beam-splitter interferometricly. The colinear cofiguration offers the possibility to lock the phase of the entangled state by locking the pump phase [63].

2.3 Multi-photon entanglement

Apart from the fundamental interests,[1] many quantum communication protocols necessitate multi-particle entanglement, such as quantum secret sharing [65, 66], third-man quantum cryptography [67], quantum "Guess My Number" protocol [68, 69], teleportation of composite systems [70], one-way quantum computing [37], etc.

[1] For instance, multi-particle entanglement enables non-statistical contradiction between quantum mechanics and local realism [64].

So far most of the multi-photon entanglement sources are based on the interference of two SPDC sources. Previously it was assumed that extremely fast ($\sim 10^{-14}$ s) detectors were required to interfere independent SPDC sources [71]. Afterwards this difficulty was solved by utilizing a pulsed laser (usually a femto-second laser with pulse duration smaller than the coherence time of the down-converted photons) as the pump [72]. Fig. 2.4 is a typical setup to generate three-photon or four-photon entanglement, which was proposed by Zeilinger *et al.* [73] and experimentally demonstrated in [74].

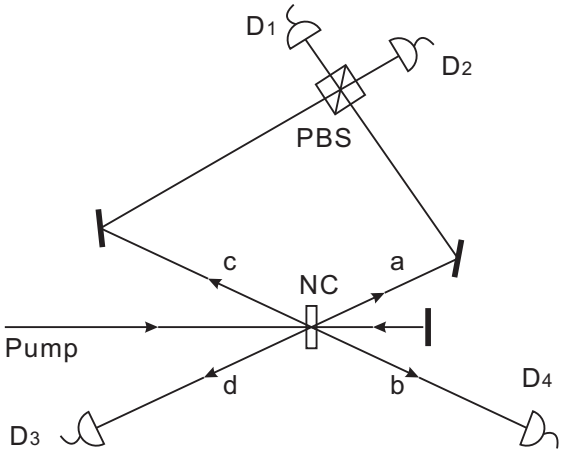

FIGURE 2.4: Multi-photon polarization entanglement

A UV femto-second laser is utilized as the pump, a polarization entangled photon pair is generated when the pump passing through the NC for the first time, and another pair is generated when the pump pulse is reflected and passing the NC for the second time. Then one photon from each pair (photon a or c) is sent to a polarizing beam-splitter (PBS). The path length difference between a and c is adjusted to make the two photons arrive at the PBS simultaneously. The joint state of the two pairs can be expressed as:

$$|\psi\rangle = 1/2(|H\rangle_a|H\rangle_b + |V\rangle_a|V\rangle_b) \otimes (|H\rangle_c|H\rangle_d + |V\rangle_c|V\rangle_d). \tag{2.8}$$

A PBS transmits H polarization, and reflects V polarization. So if two photons with same polarization come into a PBS from different paths, they will exit through different paths. If with different polarizations, they will exit through the same path. Usually only the case that one and only one photon in each output path is detected, so the PBS in this situation acts as a post-selection tool, which post-selects the case that the incident photons have the same polarization. The post-selected 4-photon state can be expressed as:

$$|\psi\rangle = 1/\sqrt{2}(|H\rangle_1|H\rangle_2|H\rangle_3|H\rangle_4 + |V\rangle_1|V\rangle_2|V\rangle_3|V\rangle_4). \tag{2.9}$$

This state is called 4-photon Greenberger-Horne-Zeilinger (GHZ) state. In the experiment the overlapping on the PBS is crucial to the quality of the entanglement. Usually

narrowband interference filters are added in front of each detector to make the coherence length of the detected photons longer than the pulse duration of the pump.

If one photon is measured in the $|+\rangle/|-\rangle$ basis with $|\pm\rangle = 1/\sqrt{2}(|H\rangle \pm |V\rangle)$, the other 3-photon state will be projected to a 3-photon GHZ state. This method can be further generalized to create larger multi-photon GHZ states. By interfering two pairs of polarization entangled photons and an attenuated laser pulse, Zhao *et al.* demonstrated the entanglement of five photons [75]. Subsequently the same idea was applied to three pairs to generate entanglement of six photons [76]. With this method, only the GHZ type entanglement can be generated. Eibl *et al.* demonstrated another type of four-photon entanglement source [77], exploiting the single passed case. The advantage of no requirement of interference is obvious, but this setup also has the restriction that only a specific type of entanglement can be generated. So far, a practical method to generate any type of multi-photon entanglement is still not available.

2.4 Hyper-entanglement

In the previous sections, we consider each degree of freedom (momentum, time, polarization, etc.) separately. In some cases, two photons emitted from the SPDC process can be entangled in two or more degrees of freedom simultaneously, which is usually called hyper-entanglement [78]. Hyper-entanglement may have interesting applications due to the extra entangled resource carried by the two photons. This includes the complete Bell state analyzer [79], entanglement purification [80], two-photon GHZ type tests of local realism [81], deterministic and efficient quantum cryptography [82], etc.

The hyper-entanglement with polarization and momentum degrees was realized independently by Yang *et al.* [46] and by Cinelli *et al.* [83]. The two realizations are a little bit different, one with type-II configuration and the other with type-I configuration. The one by Yang *et al.* is easier to understand, which is shown in Fig. 2.5. In this setup, the nonlinear crystal is configured to generate polarization entanglement [58]. One polarization entangled pair is generated either when the pump transmits through the NC for the first time, or when it is reflected and transmits through the NC for the second time. To make these two possibilities indistinguishable, it is necessary to make the spacial modes identical on each of the two beam-splitters (BS) respectively. Ideally, after adjusting the relative phases, this hyper-entanglement can be expressed as:

$$|\psi\rangle = 1/2(|H\rangle_1|H\rangle_2 + |H\rangle_1|H\rangle_2) \otimes (|a\rangle_1|b\rangle_2 + |c\rangle_1|d\rangle_2). \tag{2.10}$$

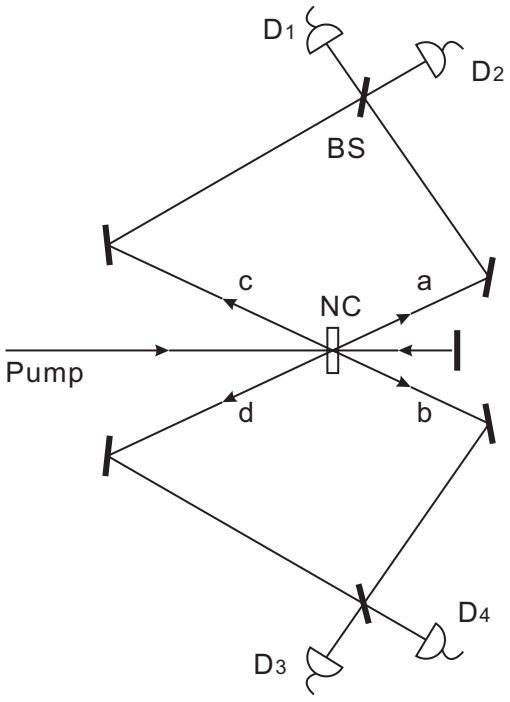

FIGURE 2.5: Hyper-entanglement in polarization and momentum degree

The momentum degree is sensitive to the path length difference on the order of several nanometers, therefore the above hyper-entanglement is not suitable for long-distance transmission. One alternative [82] is to use the time degree (either time-energy type or time-bin type) instead of the path degree. Hyper-entanglement in three degrees of freedom simultaneously was demonstrated by Barreiro *et al.* [84]. The three degrees are polarization, energy-time and orbital angular momentum.

2.5 Creation of entangled photons in other systems

Excluding SPDC in bulk crystals, there has been some other methods which are also able to create entangled photons. Four-wave mixing in microstructured fibers [85] is one of them. The main advantage is that entangled photons are created inside fibers, there is no need for coupling into additional single-mode fibers as in the case of bulk crystals. Quantum dot is another method to create entangled photons. The first experimental realization was made by R. M. Stevenson *et al.* in 2006 [86]. The main advantage for quantum dot sources is the potential realization of on-demand entangled photons. The on-demand character is rather important for efficient preparation of large-scale entangled states. Four-wave mixing in atomic ensembles is also a method to created entangled photons. Experimental realization of nonclassically correlated photon pairs includes the work by V. Balic *et al.* in [87] and the work by J. K. Thompson *et al.*

in [88], etc. The primary advantage for these atomic ensemble based sources is that the frequency linewidth of the created entangled photons are typically of several MHz only, which matches the linewidth requirement of quantum memories. Another method to create narrowband entangled photons is using the process of cavity-enhanced SPDC, which will be discussed in detail in Chap. 4.

2.6 Entanglement detection

For two-particle entanglement, an usual way to verify entanglement is to measure the Bell-CHSH inequality [89, 90]. A violation of this inequality implies existence of entanglement. In this inequality there is a value S defined as

$$S = |E(\phi_A, \phi_B) - E(\phi_A, \phi'_B) + E(\phi'_A, \phi_B) + E(\phi'_A, \phi'_B)| \tag{2.11}$$

where ϕ_A and ϕ'_A are two measurement settings for particle A, and ϕ_B and ϕ'_B for particle B, and $E(\alpha, \beta)$ is the correlation coefficient between these two particles which is defined as

$$E(\alpha, \beta) = \frac{N_{++} + N_{--} - N_{+-} - N_{-+}}{N_{++} + N_{--} + N_{+-} + N_{-+}} \tag{2.12}$$

with N_{ij} the coincidence count between detector A_i and B_j. Local realistic theory predicts that $S > 2$ for arbitrary measurement settings. Violation of this inequality is a direct proof of entanglement. Since the first violation in 1981 by A. Aspect *et al.* [91], this method has become the standard way to test two-particle entanglement.

For multi-particle entanglement, there has been some further development of the original Bell's theory, like the Greenberger-Horne-Zeilinger (GHZ) theory [64]. Quantum state tomography [92] is a general method to measure the density matrix of arbitrary entangled states, however the number of measurements scale exponentially as a function of particle number n. In contrast the method of entanglement witness [93] is able to detect entanglement with much fewer measurements, which is more appropriate for the detection of multi-particle entanglement when n is large [36, 76].

Chapter 3

Nondestructive CNOT Gate without Using Entangled Ancilla

In this chapter, we present and experimentally demonstrate a novel optical nondestructive controlled-NOT gate without using entangled ancilla. With much fewer measurements compared with quantum process tomography, we get a good estimation of the gate fidelity. The result shows a great improvement compared with previous experiments. Moreover, we also show that quantum parallelism is achieved in our gate and the performance of the gate can not be reproduced by local operations and classical communications.

3.1 Motivation

The controlled-NOT (CNOT) or similar entangling gates between two individual quantum bits (qubits) are essential for quantum computation [30, 94]. Also entangling gates can be utilized to construct a complete Bell-state analyzer which is required in various quantum communication protocols [10, 19, 95]. Photons are one of the best candidates for qubit due to the robustness against decoherence and ease of single-qubit operation. So far there have been several experiments implementing the optical CNOT gate [33, 96–101]. These experiments can be divided into two groups, one is the destructive CNOT gate [33, 96–99] which means that one have to measure the output of the gate to verify a successful operation, imposing a great limitation for its further implementations, and the other is the nondestructive gate [100, 101].

For a nondestructive CNOT gate, the information whether the operation succeeds or not is provided. This information can then be utilized for future conditional operations on

the photonic qubits to achieve efficient linear optical quantum computation. Also with this information arbitrary entangled state can be constructed in an efficient way, especially the cluster state for one-way quantum computation [37, 102]. So nondestructive CNOT gate is much more important than the destructive one. To build a nondestructive gate, usually ancilla photons are unavoidably required. Previous scheme [103] requires an entangled photon pair as assistance. The well developed SPDC (spontaneous parametric down-conversion) [58] entangled photon source will be unsuitable due to the probabilistic character. Generating entangled photons directly from quantum dots [86, 104] is still at its beginning and the fidelity is to be improved. Making use of entangled photons generated from single photons [105–107] is another solution, but it will make the setup much more complicated and reduce the success probability a lot under the present technology. Also the imperfections of the entangled photon pair will cause a degradation to the fidelity of the gate, making high-precision gate operation even more difficult to achieve.

3.2 Our new scheme

In our scheme, the qubit we consider refers to the polarization state of photons. We define the polarization state $|H\rangle$ as logic 0 and $|V\rangle$ as logic 1. Let's assume that the input sate of the control qubit is $|\psi\rangle^c = \alpha|H\rangle + \beta|V\rangle$ and of the target qubit is $|\psi\rangle^t = \gamma|H\rangle + \delta|V\rangle$. As shown in Fig. 3.1(a), two auxiliary photons with polarization state of $1/\sqrt{2}(|H\rangle + |V\rangle)$ and $|H\rangle$ are required. Then the total state of the input four photons can be expressed as:

$$\begin{aligned} |\Psi\rangle_1 = \frac{1}{2}(\alpha|H\rangle_c + \beta|V\rangle_c)\ (|H\rangle_{a1} + |V\rangle_{a1}) \\ (|+\rangle_{a2} + |-\rangle_{a2})\ (\gamma|H\rangle_t + \delta|V\rangle_t) \end{aligned} \tag{3.1}$$

where the subscript (c, a1 ,a2 and t) represents each path of the four photons, state $|+\rangle$ equals to $1/\sqrt{2}(|H\rangle + |V\rangle)$ and $|-\rangle$ equals to $1/\sqrt{2}(|H\rangle - |V\rangle)$. First the four photons transmit through PBS-1 which transmits state $|H\rangle$ and reflects state $|V\rangle$ and PBS-2 which transmits state $|+\rangle$ and reflects state $|-\rangle$. Let's consider the case that there is one photon in each output path. Then the four-photon state will change to

$$\begin{aligned} |\Psi\rangle_2 =& [\alpha|H\rangle_1|H\rangle_2 + \beta|V\rangle_1|V\rangle_2]\otimes \\ & [(\gamma+\delta)|+\rangle_3|+\rangle_4 + (\gamma-\delta)|-\rangle_3|-\rangle_4] \end{aligned} \tag{3.2}$$

with a probability of 1/4. This state expanded in the Bell basis of photon 2 and photon 3 is shown as follows:

$$\begin{aligned}|\Psi\rangle_2 = \quad & I_1 I_4 U_{14}|\psi\rangle_1^c\ |\psi\rangle_4^t \otimes |\Phi^+\rangle_{23} \\ & +I_1\sigma_{x4}U_{14}|\psi\rangle_1^c\ |\psi\rangle_4^t \otimes |\Psi^+\rangle_{23} \\ & +\sigma_{z1}I_4U_{14}|\psi\rangle_1^c\ |\psi\rangle_4^t \otimes |\Phi^-\rangle_{23} \\ & +\sigma_{z1}\sigma_{x4}U_{14}|\psi\rangle_1^c\ |\psi\rangle_4^t \otimes |\Psi^-\rangle_{23}\end{aligned} \tag{3.3}$$

where U refers to the CNOT operation; $|\Phi^{\pm}\rangle$ and $|\Psi^{\pm}\rangle$ are standard Bell states in $|H\rangle/|V\rangle$ basis; σ_x and σ_z are Pauli operators with the form $\sigma_x = |H\rangle\langle V| + |V\rangle\langle H|$, $\sigma_z = |H\rangle\langle H| - |V\rangle\langle V|$.

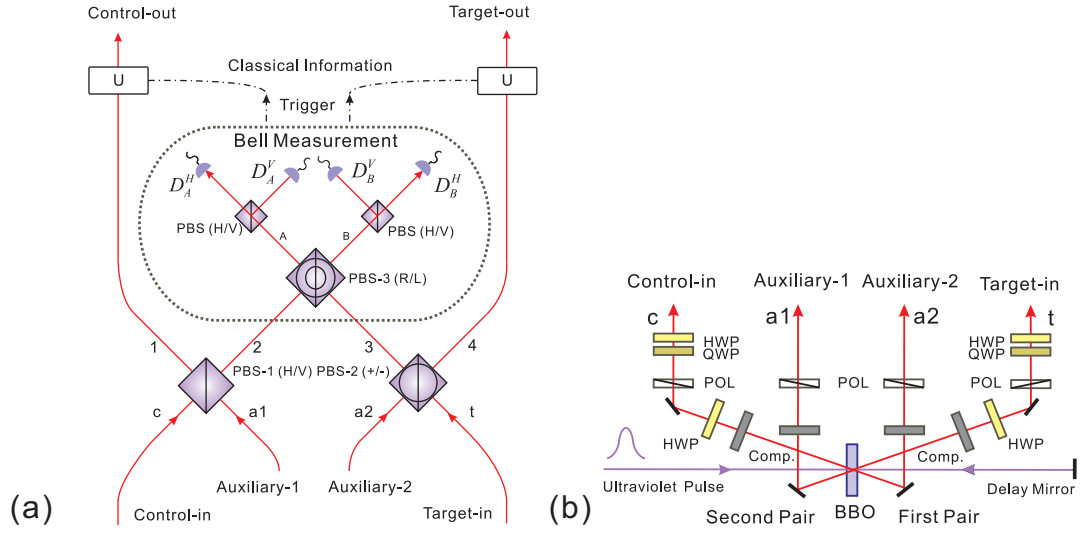

FIGURE 3.1: (a) Our scheme to implement nondestructive CNOT gate with polarization beam splitters (PBS) in $|H\rangle/|V\rangle$ basis, in $|+\rangle/|-\rangle$ basis and in $|R\rangle/|L\rangle$ basis. PBS in $|+\rangle/|-\rangle$ basis (PBS-2) is constructed with a PBS in $|H\rangle/|V\rangle$ basis and four half-wave plates (HWP); PBS in $|R\rangle/|L\rangle$ basis (PBS-3) is constructed with a PBS in $|H\rangle/|V\rangle$ basis and four quarter-wave plates (QWP). This gate works like this: four photons (control qubit, target qubit and two auxiliary qubit) enter from the bottom; if there is a coincident count between detector D_A and detector D_B, a successful CNOT gate operation will be made after sending one bit classical information and doing the corresponding single-qubit unitary operations on photon 1 and 4. Then the state of photon 1 is exactly the output of the control qubit; and the state of photon 4 is exactly the output of the target qubit. In our proof-of-principle experiment, for simplification only the coincident events between D_A^H and D_B^H are registered, and a HWP is added to do the corresponding σ_z operation on photon 1. (b) Experimental setup to generate the required four photons. Near infrared femtosecond laser pulses (≈200 fs, 76 MHz, 788 nm) are converted to ultraviolet pulses through a frequency doubler LBO (LiB_3O_5) crystal (not shown). Then the ultraviolet pulse transmits through the main BBO ($\beta - BaB_2O_4$) crystal (2mm) generating the first photon pair, then reflected back generating the second photon pair. Compensators (Comp.) which is composed of a HWP(45°) and a BBO crystal (1mm) are added in each arm. The observed 2-fold coincident count rate is about $1.2 \times 10^4/s$. In each arm we add a polarizer to do the disentanglement and set the initial product four-photon state to $|H\rangle_c|+\rangle_{a1}|H\rangle_{a2}|H\rangle_t$. Additional wave plates are added in path c and path t to prepare arbitrary polarization states.

From Eq. 3.3 we can see that if the jointly measured result of photon 2 and photon 3 is the state $|\Phi^+\rangle$, then the state of photon 1 and photon 4 is exactly the output state of the CNOT operation; if the measured result is other state ($|\Phi^-\rangle$, $|\Psi^+\rangle$ or $|\Psi^-\rangle$), then corresponding single qubit operations on the state of photon 1 and photon 4 are required to get the result of the CNOT operation. But within the linear optical technology only two of the four bell states can be distinguished. In our scheme as shown in Fig. 3.1(a), the two Bell states are $|\Phi^-\rangle$ and $|\Psi^+\rangle$. $|\Phi^-\rangle$ corresponds to the coincidence between D_A^H and D_B^H or between D_A^V and D_B^V and $|\Psi^+\rangle$ corresponds to the coincidence between D_A^H and D_B^V or between D_A^V and D_B^H. In conclusion if there is a coincident count between D_A (D_A^H or D_A^V) and D_B (D_B^H or D_B^V), then one bit of classical information will be sent to do the corresponding single qubit operation as shown in Fig. 3.1(a), and after that the state of photon 1 and photon 4 will be the exact output state of the CNOT operation. The total success probability is 1/8.

For each PBS (PBS-1 and PBS-2) the output can be divided into three cases: one in each output path; two in first path and zero in the second; zero in the first and two in the second. Consider PBS-1 and PBS-2 jointly, there will be nine cases as follows:

Group 1	1 : 1 : 1 : 1		
Group 2	1 : 1 : 2 : 0	1 : 1 : 0 : 2	2 : 0 : 1 : 1
	0 : 2 : 1 : 1	2 : 0 : 0 : 2	0 : 2 : 2 : 0
Group 3	2 : 0 : 2 : 0	0 : 2 : 0 : 2	

where $n_1 : n_2 : n_3 : n_4$ corresponds to the photon numbers in each path (1, 2, 3 or 4). Group 1 is what we expected, just as what we have discussed. In group 2 the total number of photons on the path 2 and path 3 does not equal to 2, so the cases in this group will not give a correct trigger signal with assistance of photon number resolving detectors [108]. For the cases in group 3, the total photon number of path 2 and path 3 equals to 2. Roughly thinking, these two cases will lead to a coincidence between D_A and D_B, which will ruin this scheme. But considering the photon bunching effect [109], we will find that it is not possible for a correct trigger signal, because two photons either one in $|H\rangle$ and the other in $|V\rangle$ or one in $|+\rangle$ and the other in $|-\rangle$ will go to the same output path when they pass through a PBS in the R/L basis (PBS-3 in Fig. 3.1),where $|R\rangle = 1/\sqrt{2}(|H\rangle + i|V\rangle)$ and $|L\rangle = 1/\sqrt{2}(|H\rangle - i|V\rangle)$.

3.3 Experimental realization

Our scheme works ideally with true single-photon input. But at present manipulating multi single-photons simultaneously is still a difficult task [110]. In our proof-of-principle experiment, we utilized disentangled photons from SPDC [58] sources as the four input photons of the CNOT gate as shown in Fig. 3.1(b). Perfect spacial and temporal overlap on the three PBS are necessary, which is highly related to the fidelity of the gate. In the experiment narrow-band interference filters are added in front of each detector to define the exact spectral emission mode, resulting in a coherence time longer than the pulse duration. All the photons are collected with single-mode fibers to define the exact spacial mode. Additional translators are added in path a1 and a2 to achieve good temporal overlap on PBS-1 and PBS-2. Previously to get the perfect temporal overlap between photons from different pairs on PBS-3, people have to measure the four-fold coincident counts as a function of scanning position of the delay mirror (as shown in Fig. 3.1(b)). But usually the four-fold count rate is very low (at the order of 1/sec typically), which usually makes the scanning process take a long time. In our experiment, we can overcome this difficulty by utilizing the two-photon Mach-Zehnder interference effect as shown in Fig. 3.2. As a result we can scan two-fold coincident counts instead, which is much higher than four-fold coincident counts , and this greatly shortens the process to get photons from different pairs temporal overlapped, usually we can find the temporal overlap on PBS-3 in about several tens of seconds only.

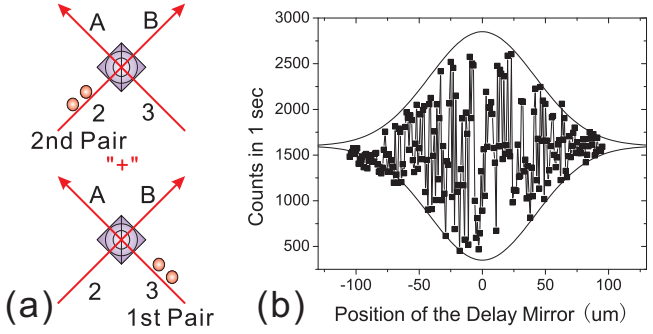

FIGURE 3.2: Two-photon Mach-Zehnder interference as a method to find the overlap on PBS-3. (a) Schematic diagram of the method. After perfect overlaps on PBS-1 and PBS-2 have been achieved, by adjusting polarizers and wave plates, two photons originated from the first pair will be on path 3 with polarization state of $|1R, 1L\rangle_3$ and the other two photons originated from the second pair will be on path 2 with polarization state of $|1R, 1L\rangle_2$. Consider that the probability of generating two pairs simultaneously is rarely low, so the coincident click between detector D_A and detector D_B maybe originate either from the two photons on path 2 or from the two photons on path 3. So the two-photon state before PBS-3 can be expressed as $1/\sqrt{2}(|1R, 1L\rangle_3 + e^{i\phi}|1R, 1L\rangle_2)$ in the case where these two possibilities interfere. Then passing through PBS-3, the state will change to $1/\sqrt{2}(|R\rangle_A|L\rangle_B + e^{i\phi}|L\rangle_A|R\rangle_B)$. So when we move the delay mirror adjusting the phase ϕ, the coincident count between D_A^H and D_B^H will oscillate as a function of the position. (b) Experimental result of the oscillation. We can estimate the overlap position from the best fit of the envelop with Gauss function.

3.4 Experimental results

To evaluate the performance of our gate, first we test the capability to generate entanglement. We choose the input product state as $|+\rangle_c|H\rangle_t$. Corresponding to the CNOT operation, ideally the output state should be $|\Phi^+\rangle_{14}$, which is a maximal entangled state. To verify this, we measure the correlation between the polarizations of photon 1 and photon 4, and the measured visibilities are $(83.8 \pm 5.5)\%$ and $(96.0 \pm 2.8)\%$ for $|H\rangle/|V\rangle$ and $|+\rangle/|-\rangle$ basis, respectively. As we know for states with a visibility above 71%, Bell inequalities [89, 90] can be violated, which is a important criterion for entanglement.

In order to get the most complete and precise evaluation of a gate, previously quantum process tomography [111] has been utilized in former experiments [97, 98, 112]. However, 256 different measurement setups are required to evaluate only a CNOT gate. In contrast, here we utilize a recently proposed method [113] to fully evaluate our gate, in which only 32 measurements are required. From these measurements we can get the upper and lower bound of the gate fidelity.

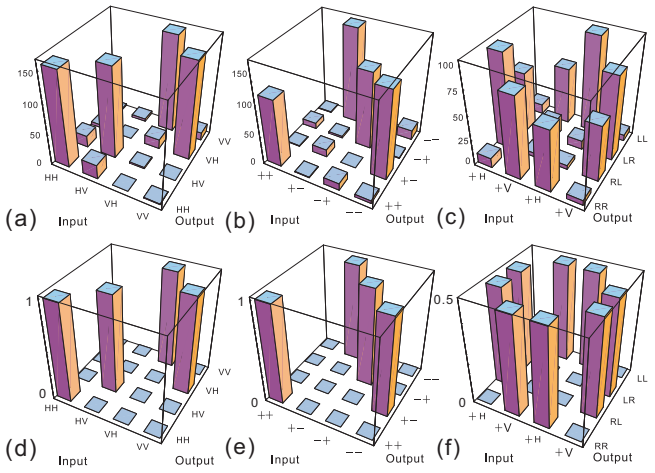

FIGURE 3.3: Experimental evaluation of the CNOT gate, each data point is measured in 320 min for the first three figures. (a) in the computational basis ($|H\rangle/|V\rangle$). (b) in the complementary basis ($|+\rangle/|-\rangle$). For (c), the input control qubit is in the $|+\rangle/|-\rangle$ basis and the input target qubit is in the $|H\rangle/|V\rangle$ basis, while the output qubits are measured in the $|R\rangle/|L\rangle$ basis. (d),(e) and (f) are theoretical values (for the vertical axis, probability is adopted instead of count rate) for (a), (b) and (c), respectively.

As we know, in the computational basis ($|H\rangle/|V\rangle$) under the CNOT operation, the target qubit flips when the control qubit is logic 1 (state $|V\rangle$). However, this process gets reversed in the complementary basis ($|+\rangle/|-\rangle$) that the control qubit will flip if the target qubit is logic 1 (state $|-\rangle$). Measurement of the logic functions in these two bases will give a good estimation of the range of the gate fidelity. The experimental results

are shown in Fig. 3.3(a) and Fig. 3.3(b). Let's define the fidelities in these two bases as

$$\begin{aligned} F_1 = 1/4\ [&P(HH|HH) + P(HV|HV) \\ &+P(VV|VH) + P(VH|VV)\ ] \\ F_2 = 1/4\ [&P(++|++) + P(--|+-) \\ &+P(-+|-+) + P(+-|--)\ ] \end{aligned} \tag{3.4}$$

where each P represents the probability to get the corresponding output state under the specified input state condition. In order to convert the coincident count rates to probabilities, we normalize them with the sum of coincidence counts obtained for the respective input state. In our experiment measured F_1 is $(88 \pm 1)\%$ and F_2 is $(90 \pm 1)\%$. As discussed in detail in Ref. [113], the upper bound and low bound of the gate fidelity can be obtained from these two fidelities as follows:

$$(F_1 + F_2 - 1) \leq F \leq \min(F_1, F_2)\,. \tag{3.5}$$

In our experiment the lower and upper bounds of the gate fidelity are $(78 \pm 2)\%$ and $(88 \pm 1)\%$ respectively. Consider into the imperfections of the polarizers and waveplates used and the slightly higher order events (estimated ratio of 6-photon count rate to 4-photon count rate is only about 0.008), the fidelity of initial state preparation can be better than 98.9%. If the initial state preparation is perfect, the measured gate fidelity will be improved a little bit. We think that most of the degradation of the fidelity is due to the imperfection of PBS and the imperfect overlapping on it.

Recently a new experimental criterion for the evaluation of device performance has been proposed [114]. It was shown that a quantum controlled-NOT gate simultaneously performs the logical functions of three distinct conditional local operations. Each of these local operations can be verified by measuring a corresponding truth table of four local inputs and four local outputs. Specifically, quantum parallelism is achieved if the average fidelity of the three classical operations exceeds 2/3. As a matter of fact the fidelity F_1 and F_2 are just two of the required three fidelities. The third fidelity is defined as

$$\begin{aligned} F_3 = 1/4\ [&P(RL/+H) + P(LR/+H) \\ &+P(RR/+V) + P(LL/+V) + P(RR/-H) \\ &+P(LL/-H) + P(RL/-V) + P(LR/-V)]\,. \end{aligned} \tag{3.6}$$

The experimental result of F_3 is shown in Fig. 3.3(c) with the measured value $(90 \pm 1)\%$. The average fidelity of F_1, F_2 and F_3 is $(89 \pm 1)\%$, exceeding the boundary

2/3, which shows that quantum parallelism of our CNOT gate has been achieved and the performance of the gate can not be reproduced by local operations and classical communications.

3.5 Discussion

In summary, we have presented and experimentally demonstrated a novel scheme to realize the optical nondestructive CNOT gate without using entangled photons but only single photons instead. With much fewer measurements compared with quantum process tomography [111], we got a good estimation of the gate fidelity (between $(78 \pm 2)\%$ and $(88 \pm 1)\%$), showing a great improvement compared with previous experiments (In [101] severe noise from unwanted two-pair events has been subtracted from the experiment result; in [100] five photons were involved to avoid two-pair events, resulting in rather low visibility). Moreover, we have also shown that quantum parallelism was achieved in our CNOT gate. We believe that our experiment and the methods developed in this experiment would have various novel applications in the fields of both linear optical quantum information processing and quantum communication with photons.

Chapter 4

Generation of Narrowband Entangled Photons

In this chapter, we report an experimental realization of a narrow-band polarization-entangled photon source with a linewidth of 9.6 MHz through cavity-enhanced spontaneous parametric down-conversion. This linewidth is comparable to the typical linewidth of atomic ensemble based quantum memories. Single-mode output is realized by setting a reasonable cavity length difference between different polarizations, using of temperature controlled etalons and actively stabilizing the cavity. The entangled property is characterized with quantum state tomography, giving a fidelity of 94% between our state and a maximally entangled state. The coherence length is directly measured to be 32 m through two-photon interference.

4.1 Motivation

The storage of photonic entanglement with quantum memories plays an essential role in linear optical quantum computation (LOQC) [94] to efficiently generate large cluster states [106], and in long-distance quantum communication (LDQC) to make efficient entanglement connections between different segments in a quantum repeater [18]. For the atomic ensemble based quantum memories [23, 115, 116], typical spectrum linewidth required for photons is on the order of several MHz. While spontaneous parametric down-conversion (SPDC) is the main method to generate entangled photons [58], the linewidth determined by the phase-matching condition is usually on the order of several THz which is about 10^6 times larger, making it unfeasible to be stored. Moreover, interference of independent broad-band SPDC sources requires a synchronization precision of several hundred fs [72]. While in LDQC, for the distance on the order of several

hundred km, it becomes extremely challenging for the current synchronization technology [117, 118]. But for a narrow-band continuous-wave source at MHz level, due to the long coherence time, synchronization technique will be unnecessary, while coincidence measurements with time resolution of several ns with current commercial single-photon detectors will be enough to interfere independent sources.

Passive filtering with optical etalons is a direct way to get MHz level narrow-band entangled photons from the broad-band SPDC source, but it will inevitably result in a rather low count rate. In contrast, cavity-enhanced SPDC [119, 120] provides a good solution for this problem. By putting the nonlinear crystal inside a cavity, the generation probability for the down-converted photons whose frequency matches the cavity mode will be enhanced greatly. The cavity acts as an active filter. The frequency of the generated photons lies within the cavity mode, which can be easily set to match the required atomic linewidth. Experimentally, Ou *et al.* [119] has realized a type-I source, in which the two photons generated have the same polarization, making it very difficult to generate entanglement. Wang *et al.* [121] made a further step by putting two type-I nonlinear crystals within a ring cavity to generate polarization entanglement, but unfortunately the output is multi-mode which does not fit the requirement of an atomic quantum memory. While, a type-II configured source (down-converted photons have different polarizations) is more preferable for the ease of generating polarization entanglement, compared with a type-I source. Recently Kuklewicz *et al.* [122] have realized a type-II source, but the output is still multi-mode. So far to the best of our knowledge, a true narrow-band (single-mode) polarization-entangled photon source at MHz level has never been reported yet along this line. Direct generation of narrow-band photon pairs from cold atomic ensembles [88, 123] is another solution, but the setup is usually much more complicated.

4.2 Experimental setup

In our experiment, a flux-grown periodically poled KTiOPO4 (PPKTP) crystal (1cm long) is used as the nonlinear medium. Quasi-phase matching is optimized for a horizontally (H) polarized ultraviolet (UV) pump photon (390 nm) down-converting to a near-infrared photon pair (780 nm) with one polarized in H and the other in vertical (V). The phase-matching bandwidth is 175 GHz. The first side of the PPKTP is high-reflection coated ($R > 99\%$ at 780 nm) to form the double-resonant cavity with a concave mirror ($R \approx 97\%$ at 780 nm) of 10-cm curvature, as shown in Fig. 4.1. The second side of the PPKTP is anti-reflection (AR) coated to minimize losses within the cavity. Both

the PPKTP and the concave mirror are AR coated at 390 nm so that the UV pump interacts only once with the PPKTP in the cavity.

The cavity is intermittently locked using the Pound-Drever-Hall scheme [124]. A mechanical chopper is designed to block the cavity output when the locking beam is switched on, to avoid the leaking beam entering into posterior single-photon detectors. This locking system is only effective for the cavity noise whose frequency is much lower than the locking repetition rate (50 Hz), i.e. the long-term drift. In order to suppress the high frequency noise, especially the strong acoustic noise at subkilohertz, we build the cavity from a single block of stainless steel by digging out the inner part. The PPKTP crystal along with the oven, the thermal electric cooler (TEC) and the concave mirror are fixed firmly inside. The steel block is covered from lateral side with two pieces of organic glass to prevent airflow. Temperature of the PPKTP crystal is controlled to the precision of about 0.002 °C with a high-performance temperature controller. The frequency of the locking beam is the same as the center frequency (ω_0) of the down-converted photons. Since the polarization of the locking beam is rotated to H before entering the cavity, this active locking system can only guarantee the resonance at ω_0 for H. The resonance of the cavity at ω_0 for V is realized by slightly tuning the temperature of the PPKTP.

It has been pointed out that for the case of type-II configured cavity-enhanced SPDC, ideally the output will be single-mode [125]. But considering into the finite finesse of the cavity, the ideal single-mode output will be mixed with several nearby background modes. The quantum state can be expressed as:

$$\begin{aligned} |\Psi\rangle &= \sqrt{\chi_0}|\omega_0\rangle_H|\omega_0\rangle_V \\ &+ \sum_{m=1}^{N=46} \frac{\sqrt{\chi_m}}{2}(|\omega_0 + m\Omega_H\rangle_H|\omega_0 - m\Omega_H\rangle_V \\ &\quad +|\omega_0 - m\Omega_H\rangle_H|\omega_0 + m\Omega_H\rangle_V \\ &\quad +|\omega_0 + m\Omega_V\rangle_H|\omega_0 - m\Omega_V\rangle_V \\ &\quad +|\omega_0 - m\Omega_V\rangle_H|\omega_0 + m\Omega_V\rangle_V) \end{aligned} \tag{4.1}$$

with

$$\frac{\chi_m}{\chi_0} = \frac{4}{1 + \frac{4F^2}{\pi^2}\sin^2\frac{m\Delta\Omega}{\Omega}\pi} \tag{4.2}$$

where Ω_H and Ω_V are the free spectrum ranges (FSR) for H and V respectively, with the average value of Ω (1.9 GHz) and the difference of $\Delta\Omega$ (21 MHz); F is the finesse of the cavity, with the measure value of 166; N is determined by the phase-matching bandwidth of PPKTP. The first term of the right side of Eq. 4.1 is the expected single-mode output. The following four terms in the summation correspond to the case that one

photon is resonant with the cavity while the other is not. For the modes near ω_0, we have $\chi_1/\chi_0 = 1.7$, $\chi_2/\chi_0 = 0.63$, $\chi_3/\chi_0 = 0.31$. When m goes higher, χ_m asymptotically goes to 0. While in the case of equal cavity length ($\Delta\Omega = 0$) [122], each χ_m nearly has the same value. The ratio between the summation of these backgound modes to the center mode is 3.41. In our experiment, we use etalons (FSR = 13.9 GHz, Finesse = 31) to eliminate these nearby modes. The etalons are put into separate copper ovens, and temperature controlled to the precision of 0.01 °C to achieve a stable performance.

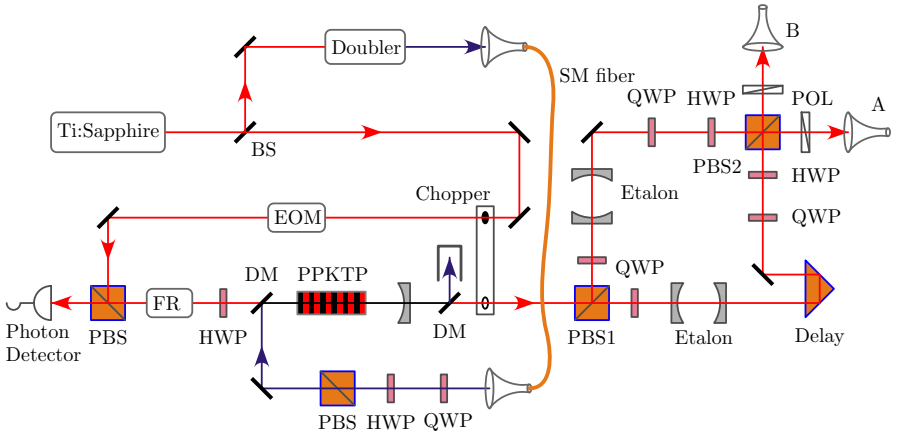

FIGURE 4.1: Layout of the experiment. The generation of polarization entanglement is realized by interfering the two down-converted photons on PBS2. An electro-optic modulator (EOM) phase modulated at 70 MHz is utilized to generate sidebands for the locking beam. A PBS, a Faraday rotator (FR) and a half-wave plate (HWP) is utilized to extract the reflection beam and to generate the error signal for the locking system.

The complete experimental setup is illustratively shown in Fig. 4.1. A frequency-stabilized Ti:Sapphire laser with a linewidth of 75 kHz is utilized as the main laser. A small proportion of the output power is split as the locking beam, and the rest power is sent to an eternal-cavity frequency doubler. The generated UV beam is very elliptical, and we use several cylindrical lenses to convert it to a near-Gaussian beam, which is further coupled into a single-mode fiber and released later with a fiber collimator. Two high-performance dichroic mirrors (DM) are used to combine the UV pump with the locking beam, and later separate the remained UV pump from the cavity output. The generated photon pair is separated on PBS1, and filtered with separated etalons. In our experiment we find that slight reflection from the etalons will cause the double-resonant cavity very unstable. We add a quarter-wave plate (QWP) in each path to form a optical isolator with PBS1 to eliminate the etalon reflection.

4.3 Experimental Results

By making a two-photon interference for the narrow-band photons on PBS2, with one photon polarized in $|+\rangle = 1/\sqrt{2}(|H\rangle + |V\rangle)$ and the other in $|-\rangle = 1/\sqrt{2}(|H\rangle - |V\rangle)$

as input, we are able to generate polarization entanglement for the case one photon in each output port. These two photons are further coupled into single-mode fibers and detected with single-photon detectors.The desired output state is $|\phi^-\rangle = 1/\sqrt{2}(|H\rangle|H\rangle - |V\rangle|V\rangle)$. But during the overlapping on PBS2 there is some phase shift between $|H\rangle$ and $|V\rangle$, leading to an output state of $1/\sqrt{2}(|H\rangle|H\rangle - e^{i\alpha}|V\rangle|V\rangle)$. We insert an adjustable wave-plate in one output path to compensate this phase shift. In order to verify the entanglement property, we first make a polarization correlation measurement at 4 mW pump power, with the result shown in Fig. 4.2(a). The visibility is about 97%, which is far beyond the requirement for a violation of Bell-CHSH inequality [90]. In this inequality the value S is defined as

$$S = |E(\phi_A, \phi_B) - E(\phi_A, \phi'_B) + E(\phi'_A, \phi_B) + E(\phi'_A, \phi'_B)| \tag{4.3}$$

where ϕ_A and ϕ'_A are two polarization measuring angles for photon A, and ϕ_B and ϕ'_B for photon B, and $E(\alpha, \beta)$ is the correlation coefficient between these two photons. Violation of this inequality ($S > 2$) is a direct proof of entanglement. Our measured result is $S = 2.66 \pm 0.03$, for which the inequality is violated by 22 standard deviations. In order to get a more complete characterization of the entanglement, we also make a quantum state tomography [92,126] for our narrow-band entangled source, the result is shown in Fig. 4.2(b). From the tomography result, the calculated fidelity between our state and $|\phi^-\rangle$ is 94.3%.

The correlation time between the down-converted photons is inversely proportional to the bandwidth for a SPDC source [41]. Therefore, a narrow-band source at MHz level should exhibit a correlation time which is much longer compared with the broad-band SPDC source (typically on the order of several hundred fs). In our experiment the detector signal of photon A is sent to a time-to-amplitude converter (TAC) as the start signal, and the signal of photon B is used as the stop signal. The TAC output signal is sent to a multi-channel analyzer. The measured result is shown in Fig. 4.3(a). The data is well agreed with the theoretical expectation with the shape of $e^{-2\pi\Delta\nu|t|}$ [125]. The best fit shows that the linewidth ($\Delta\nu$) is about 9.6 MHz, which is well within the cavity linewidth. The resolution time of the TAC utilized is about 50 ps, but the single-photon detectors only have a resolution time of 350 ps, which is comparable to the cavity round trip time of 520 ps. Therefore [127], this time correlation measurement can not distinguish our source from previous multi-mode cavity-enhanced SPDC sources. To prove the single-mode property of our source we measure the coherence length directly through the two-photon interference experiment. This is done by observing the polarization correlation visibility in $|+\rangle/|-\rangle$ basis between photon A and B, as a function of the relative delay before PBS2. The result is shown in Fig. 4.3(b). We find the coherence length to be 32 ± 3 m, which is consistent with the result from the time correlation

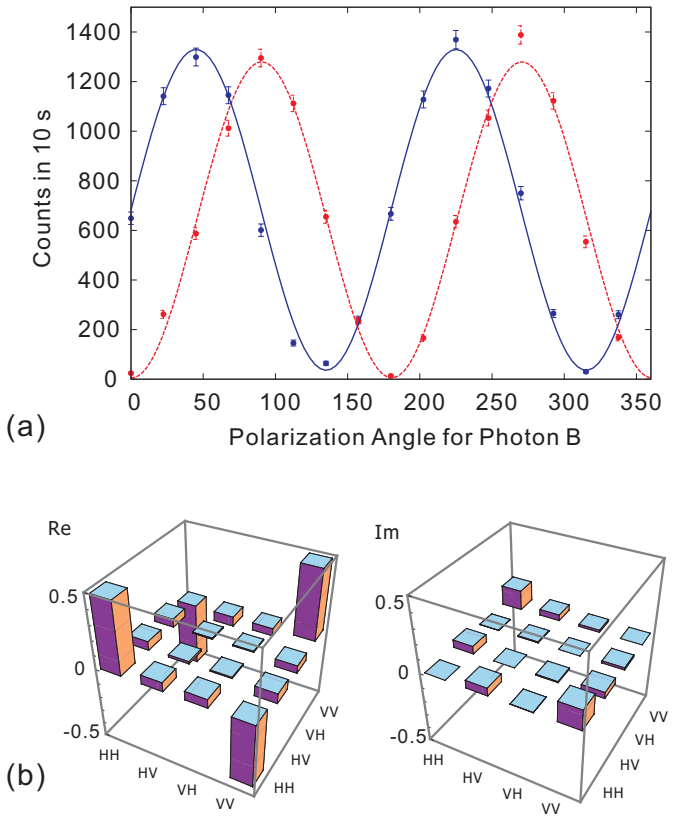

FIGURE 4.2: (a) Polarization correlations for the entangled photon pair. Polarization angle for photon A is fixed to 90° for the red, and −45° for the blue. Error bars represent statistical errors. (b) Tomography measurement result, with the left for the real part, the right for the imaginary part.

measurement in the relation of $\Delta L = \frac{\nu}{\Delta\nu}\lambda$. While for a multi-mode source, determined by the phase-matching condition, the coherence length is usually less than several mm.

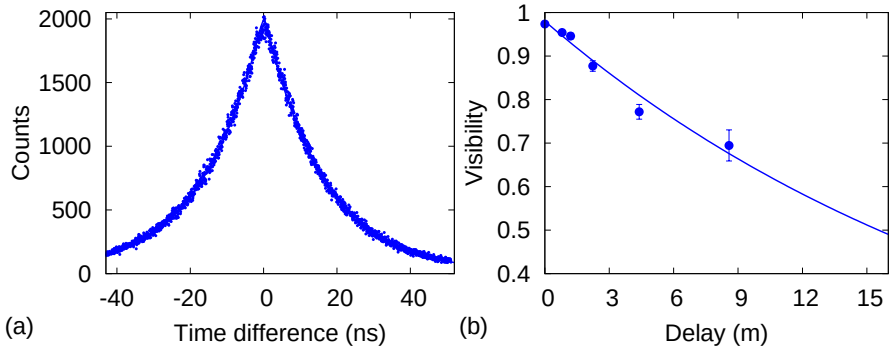

FIGURE 4.3: (a) Time correlation measurement. The data is fitted with a function of $c_0 e^{-2\pi\Delta\nu|t|}$ The FWHM correlation time is 23.0 ns. (b) Visibility in $|+\rangle/|-\rangle$ basis as a function of the relative delay.The data is fitted with a function of $v_0 e^{-x/x0}$. Error bars represent statistical errors.

For a cavity-enhanced SPDC source, in the case of far below threshold (about 1.88 W for our case), the pair generation rate is proportional to the pump power, which is confirmed by our measured result, which is shown in Fig. 4.4. At the pump power of 27 mW, we get a maximal pair generation rate of 1780 s^{-1} and a corresponding maximal spectrum

brightness of 185 $s^{-1}MHz^{-1}$. We fit the data with a proportional function and find that the normalized spectrum brightness is about 6 $s^{-1}MHz^{-1}mW^{-1}$. Further improvement of the brightness could be possible by employing tighter focus, longer crystal and a cavity with higher finesse.

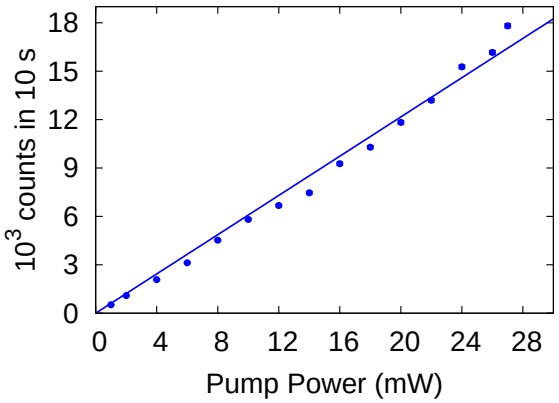

FIGURE 4.4: Pair generation rate as a function of the UV pump power.

4.4 Discussion

In conclusion, we have experimentally generated narrow-band polarization-entangled photon pairs through cavity-enhanced SPDC with a linewidth of 9.6 MHz, which is comparable to the typical linewidth of atomic quantum memories. Single-mode output is realized by setting a reasonable cavity length difference between different polarizations, using temperature controlled etalons and actively stabilizing the cavity. The wavelength chosen is near Rubidium D2 line, making the storage a straightforward task using the method of electromagnetically induced transparency (EIT) in cold atomic ensembles [115] if the UV pump is set to be pulsed. Since the source is probabilistic and the entanglement is generated through post-selection, one may think that it will limit its applications in LDQC. According to a recent theoretical study [128], both of these problems could be eliminated if applying the same trick. When combined with quantum memories, this narrow-band entangled can be used to efficiently build entanglement over large distance for LDQC, and to efficiently generate large cluster states for LOQC, thus it will have extensive applications in future scalable quantum information processing.

Chapter 5

Interference of Narrowband Photon Sources

In this chapter, we report a realization of synchronization-free quantum teleportation and narrowband three-photon entanglement through interfering narrowband photon sources. Since both the single-photon and the entangled photon pair utilized are completely autonomous, it removes the requirement of high demanding synchronization technique in long-distance quantum communication with pulsed SPDC sources. The frequency linewidth of the three-photon entanglement realized is on the order of several MHz, which matches the requirement of atomic ensemble based quantum memories. Such a narrowband multi-photon source will have applications in some advanced quantum communication protocols and linear optical quantum computation.

5.1 Motivation

Quantum teleportation [10] is a process to transfer a quantum state of a photon without transferring the state carrier itself, which plays a central role in quantum communication [129]. It necessitates the interference of a single-photon and an entangled photon pair. Since SPDC is the main method to generate entangled photons [58], typically with a frequency linewidth of several THz. To interfere independent sources, the resolution time of the photon detectors has to be much smaller than the coherence time ($< 1\,\mathrm{ps}$) [130], which is still not available until today. This problem was later solved by utilizing a femtosecond pumping laser and frequency filtering [11, 72]. Since the development of this technique, numerous important advances have been achieved [17, 40, 131–133]. But in this pulsed regime, interference of independent sources requires a synchronization precision of several hundred fs for the pumping lasers. Even though there are some

experimental investigations [117,118] with lasers within a single lab, when one wants to build entanglement over several hundred kilometers, it will become rather challenging.

While in the continuous-wave regime, with the development of the quasi-phase matching technique, it is now possible to narrow the frequency bandwidth for SPDC sources to several tens GHz [134], lowering down the requirement for photon detectors. In [135] Halder *et al.* has demonstrated the feasibility to interfere separate sources through time measurement. In their experiment, Bragg gratings were used to filter out narrow-band photons from a SPDC source, increasing the coherence time to several hundred ps. In order to interfere such entangled sources, a high-demanding superconducting detector with ultra-low time jitter was utilized, which is only available for few groups. Recently, we have reported a narrow-band entangled photon source with a ∼MHz linewidth through cavity-enhanced SPDC [136]. Such a narrow-band source will enable the possibility to interfere separate sources with the widely used commercial sub-ns photon detectors. Also the tolerance of length fluctuations for the quantum communication link will improve from several centimeters in [135] to several meters, which means we can realize quantum teleportation for longer distance, larger time scale, and worse weather condition.

Interference of independent sources is also the main method to generate multi-photon entanglement [76,137,138], which is the main resource for linear optical quantum computation (LOQC) [94]. To efficiently build large entangled states for LOQC, it is required to store the intermediate multi-photon entangled states with a quantum memory [106,139]. But previously due to the usage of SPDC sources, the frequency linewidth of these multi-photon entanglement lies on the order of several THz. While the frequency linewidth required by an atomic ensemble based quantum memory [20, 23, 25, 115] is on the order of several MHz. This frequency mismatch greatly limits the applications of the broadband multi-photon entangled sources. Therefore, creating a narrowband multi-photon entanglement with linewidth of several MHz becomes an urgent task.

5.2 Experimental setup

The schematic diagram of our experimental setup is shown in Fig. 5.1. The entangled photon pairs are generated through cavity-enhanced SPDC. Measured linewidth for this source is 9.6 MHz. Single-mode output is realized by setting a cavity length difference between different polarizations, active cavity stabilization and the use of temperature controlled etalons. Detailed description of this narrow-band entangled source could be found in a former paper of us [136]. The quantum state of these two photons can be

expressed as:

$$|\Phi^-\rangle_{12} = \frac{1}{\sqrt{2}}(|H\rangle_1|H\rangle_2 - |V\rangle_1|V\rangle_2), \tag{5.1}$$

which is one of the four Bell sates, and H represents horizontal polarization, V represents vertical polarization. For a 9 mw input UV power, it is observed that a two-fold coincidence rate of about $200\,\mathrm{s}^{-1}$ at a coincidence time-window of 16 ns.

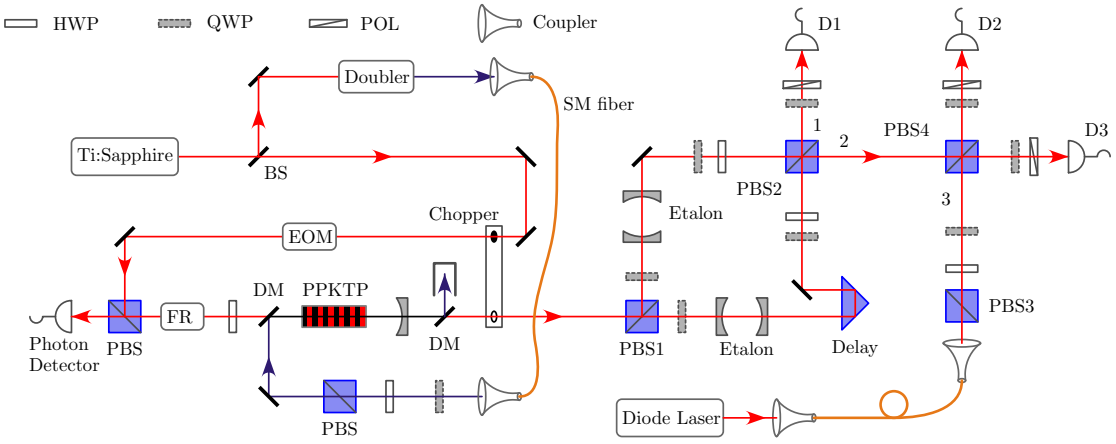

FIGURE 5.1: Experimental setup. A continuous-wave Ti:Sapphire laser locked to one of the ^{87}Rb D_2 hyperfine transitions is divided into two portions by a beam-splitters (BS). The main portion is up-converted to an ultraviolet (UV) beam (390nm) through an external-cavity doubler. Then the UV pump beam (about 9 mw) is coupled into the double-resonant cavity which is composed of a PPKTP (from Raicol) and a concave mirror. The PPKTP is type-II configured that one UV photon gives rise to a H polarized photon and a V polarized photon. After separated on polarized beam-splitter 1 (PBS1), an etalon on each arm is used to filter out single longitudinal mode. The quarter-wave plate (QWP) before each etalon is used to form an optical isolator with PBS1 to eliminate the reflection from the etalon. After rotated to $|+\rangle$ polarization with a half-wave plate (HWP) respectively, the two photons get interfered on PBS2 .The narrow-band entangled photon pair is generated in the case that one photon appears on each output port. The second portion is used to lock the double-resonant cavity actively. A Faraday rotator (FR) and a PBS are utilized to extract the reflected locking beam in order to generate the error signal for the locking. The optical chopper is utilized to switch between the locking and the detecting process. The beam from another completely independent diode laser (locked to the same atomic transition line as the Ti:Sapphire laser) is attenuated to an intensity of about $8.0 \times 10^5\,\mathrm{s}^{-1}$ as the single-photon source to be teleported. A partial Bell state measurement (BSM) of photon 2 and photon 3 is realized with PBS4 and the following polarization analyzers.

The single-photon to be teleported (photon 3 in Fig. 5.1) is generated by attenuating another completely independent diode laser to an intensity of about $8.0 \times 10^5\,\mathrm{s}^{-1}$. The state to be teleported is prepared with a HWP or a QWP. A partial Bell state measurement (BSM) is realized by sending photon 2 and photon 3 through the PBS4 and the following polarization analyzers. When a coincidence of $|+\rangle_2|+\rangle_3$ ($|\pm\rangle = \frac{1}{\sqrt{2}}(|H\rangle \pm |V\rangle)$) clicks between detector D2 and D3, the two photons are projected into the state of $|\Phi^+\rangle_{23} = 1/\sqrt{2}(|H\rangle_2|H\rangle_3 + |V\rangle_2|V\rangle_3)$. Then after a local operation of σ_z on photon 1, the teleportation from photon 3 to photon 1 is finished. In order to get a high-visibility interference on PBS4 between the single-photon and the entangled pair, the coincidence

time window between photon 2 and photon 3 should be much smaller than the correlation time between photon 1 and photon 2 (20ns) [72], in our case we choose it to be 3 ns.

5.3 Experimental results

For the states to be teleported of photon 3, we choose three states, namely, $|H\rangle$, $|+\rangle$, and left-handed ($|\mathrm{L}\rangle$) circular polarization states $1/\sqrt{2}(|H\rangle - i|V\rangle)$. In order to evaluate the performance for the teleportation process, we make a quantum tomography [92] for all the teleported states, with results shown in Fig. 5.2 and fidelities shown in Tab. 5.1. It shows that the fidelities of the six states are well above the classical limit of 2/3 [140]. Thus the success of quantum teleportation is proved.

TABLE 5.1: Fidelities for the teleportation experiment. All the fidelities of the teleportion are well above the classical limit of 2/3.

Polarization	$\|H\rangle$	$\|+\rangle$	$\|L\rangle$
Fidelity	91.0%	79.8%	79.0%

A great advantage to use continuous-wave sources for quantum teleportation and entanglement connection is that the two sources can be completely autonomous. In our experiment, for a 3 ns coincident time window, which is much smaller than the coherent time of the input photons, a perfect overlap between photon 2 and photon 3 at PBS4 is always guaranteed. It removes the high-demanding synchronization technique and provides a much easier way to generate entanglement by using completely independent sources over a large distance.

With similar setup [1], it is now possible to generate the first narrow-band three-photon entanglement. By preparing photon 3 in the state of $|+\rangle$ and photon 1 and 2 in the entangled state of $|\Phi^-\rangle$, the three-fold coincidence among the detector D1, D2 and D3 will lead to a three-photon GHZ state [64]:

$$|\Phi\rangle_{123} = \frac{1}{\sqrt{2}}\left(|H\rangle_1|H\rangle_2|H\rangle_3 - |V\rangle_1|V\rangle_2|V\rangle_3\right). \tag{5.2}$$

To experimentally verify that the desired state of Eq. 5.2 has been successfully generated, we first characterize the components of the three-photon state corresponding to such a three-fold coincidence. This was done by measuring each photon in the H/V basis. The result is shown in Fig. 5.3. The signal-to-noise ratio, which is defined as the ratio of any

[1] For part it is not necessary to make the entangled photon pair and the single photon independent from each other, so photon 3 is got by attenuating the beam from the Ti:Sapphire laser for conveniency.

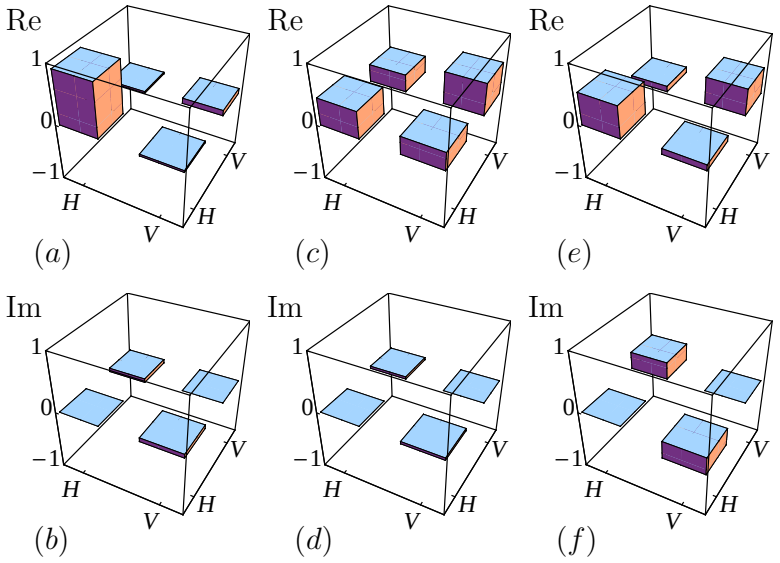

FIGURE 5.2: Tomography results for the teleportation of $|H\rangle$, $|+\rangle$ and $|\mathrm{L}\rangle$. (a) and (b) are the real and imaginary parts for the teleported state of $|H\rangle$ respectively. (c) and (d) are the real and imaginary parts for the teleported state of $|+\rangle$ respectively. (e) and (f) are the real and imaginary parts for the teleported state of $|L\rangle$ respectively.

of the desired three-fold components (HHH and VVV) to any of the 6 other non-desired ones, is about 7.3 : 1.

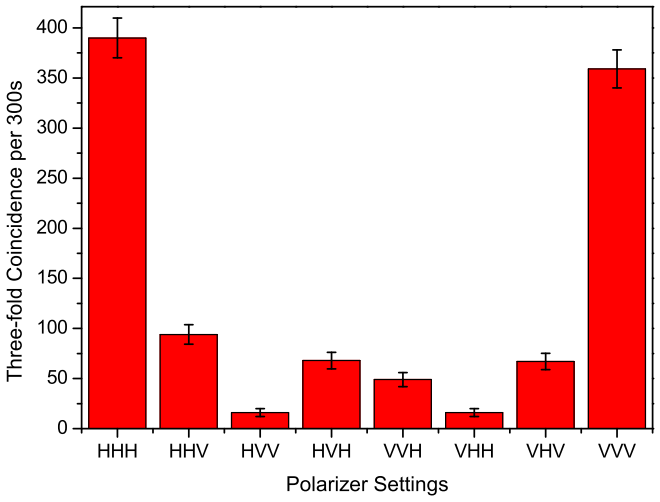

FIGURE 5.3: Measured result for the three-photon entangled state in H/V basis. It shows that the signal-to-noise ratio between the desired three-fold components to any of the 6 other non-desired ones, is about 7.3:1, which confirms that HHH and VVV are the main components of the three-photon state. Error bars represent the statistical errors.

TABLE 5.2: Measured observables of the Mermin inequality (Eq. 5.3) for the three-photon entangled state.

Observable	$\sigma_y^1\sigma_y^2\sigma_x^3$	$\sigma_y^1\sigma_x^2\sigma_y^3$	$\sigma_x^1\sigma_y^2\sigma_y^3$	$\sigma_x^1\sigma_x^2\sigma_x^3$
Value	0.64	0.63	0.67	-0.66
Deviation	0.02	0.02	0.02	0.02

To obtain a further characterization of the entanglement, we make a measurement of the Mermin inequality [141]. In our case, the value of A in the inequality is defined as:

$$A = \sigma_y^1\sigma_y^2\sigma_x^3 + \sigma_y^1\sigma_x^2\sigma_y^3 + \sigma_x^1\sigma_y^2\sigma_y^3 - \sigma_x^1\sigma_x^2\sigma_x^3 \tag{5.3}$$

where σ_i^j corresponds to the i th Pauli matrix on particle j. Violation of the inequality , that is $|\langle A\rangle| > 2$, proves the non-local property of the three photon state. The measured value of the observables are shown in Tab. 5.2. With simple calculation, it is obtained that $|\langle A\rangle| = 2.59 \pm 0.05$, which violates the inequality by 12 standard deviations. Combining the results of components and Mermin obserbales measurements, we can obtain the fidelity between the state generated and the ideal three-photon GHZ state:

$$\begin{aligned} F(\rho) &= \frac{1}{2}({}_{123}\langle HHH|\rho|HHH\rangle_{123} \\ &\quad + {}_{123}\langle VVV|\rho|VVV\rangle_{123}) + \frac{1}{8}|\langle A\rangle| \end{aligned} \tag{5.4}$$

Our result is $F(\rho) = 0.68 \pm 0.01$, which is well above the boundary of 1/2, and thus a proof of true three-photon entanglement [142]. As the linewidth of entangled three-photon is of several MHz, it may have broad application in future LOQC together with atomic quantum memory, especially for the generation of large cluster states [106] that are storable.

5.4 Discussion

In summary, a realization of synchronization-free quantum teleportation and narrowband three-photon entanglement through interfering continuous-wave narrowband sources is reported. Since both for the single-photon and the entangled photon pair utilized are completely autonomous, it removes the requirement of high demanding synchronization technique for the case of pulsed SPDC sources, enabling the possibility to teleport a photonic state between distant locations. The frequency linewidth of the narrowband three-photon entanglement realized is on the order of several MHz, which matches the requirement of atomic ensemble based quantum memories. Such a narrowband

multi-photon source will have applications in some advanced quantum communication protocols and LOQC.

Chapter 6

Quantum Repeater with Cold Atomic Ensembles

6.1 The DLCZ protocol

In order to increase the distance of quantum communication, the concept of quantum repeater was proposed in 1998 by Briegel *et al.* [18]. The main difficulty for its realization is to find an appropriate interface between photonic qubits and stationary qubits. In 2001, Duan *et al.* proposed an experimental feasible protocol [20] based on atomic ensembles. This protocol was later named as the DLCZ protocol by combining the initials of the authors' names. The experimental requirement of this protocol is modest, therefore it led to extensive experimental studies. In this chapter, we analyze in detail the write and read process in the DLCZ protocol, introduce the phase problem in it, present subsequent improved schemes, and make a comparison of the creation speed of remote entanglement and resource consumption for different schemes.

6.1.1 Write process through spontaneous Raman scattering

The basis element in the DLCZ protocol is shown in Fig. 6.1. A Λ type energy level scheme is being considered. It is composed of two ground states, $|g\rangle$ and $|s\rangle$, and an excited state $|e\rangle$, with the optical transition $|g\rangle \leftrightarrow |e\rangle$ and $|s\rangle \leftrightarrow |e\rangle$ allowed. Originally all the atoms are prepared in the state of $|g\rangle$. First, the *write*, a weak pulse which is slightly off-resonant with the $|g\rangle \leftrightarrow |e\rangle$ transition is applied. With a rather small probability, there will be one atom within the ensemble transferred to the state $|s\rangle$ through Raman scattering and a scattered single-photon being created with an angle of θ relative to the

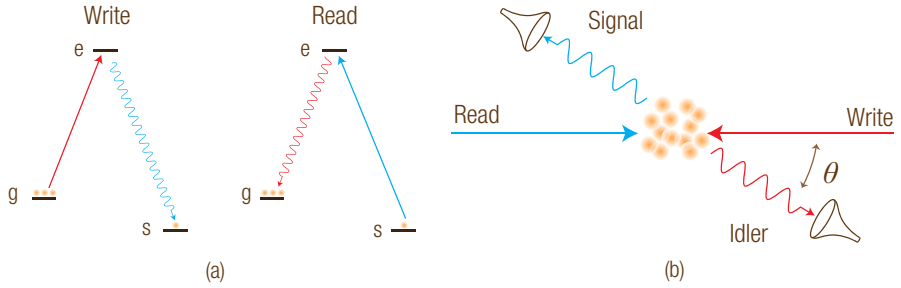

FIGURE 6.1: The energy levels used (a) and geometry configuration (b) of the DLCZ type protocols.

write direction.[1] This scattered photon is called the *signal* photon.[2] Conditioned on a detection of a signal photon, the atomic ensemble will result in a collective excitation (spin-wave) state:

$$|\psi\rangle_a = \frac{1}{\sqrt{N}} \sum_j e^{i\Delta\mathbf{k}\cdot\mathbf{r}_j} |g...s_j...g\rangle \tag{6.1}$$

with $\mathbf{k}_w$ the wave vector of the write photon, $\mathbf{k}_s$ the wave vector of the signal photon, $\Delta\mathbf{k} = \mathbf{k}_w - \mathbf{k}_s$ the wave vector of the spin-wave, and $\mathbf{r}_j$ the coordinate of the j-th atom.

The phase in the collective state in Eq. 6.1 can be understood in the following way. Before the write process, the quantum state for the write and the atoms can be written as:

$$|\Psi\rangle = |\psi\rangle_a \otimes |\psi\rangle_w = |g...g_j...g\rangle \otimes e^{-i(\omega_w t - \mathbf{k}_w\cdot\mathbf{r})}. \tag{6.2}$$

Assuming that at $t = 0$, one scattered signal photon is generated, therefore the phase given by the write beam for the j-th atom is $\phi_j^w = \mathbf{k}_w \cdot \mathbf{r}_j$. Now the new state after Raman scattering is

$$|\Psi\rangle' = \frac{1}{\sqrt{N}} \sum_j e^{i\phi_j^w} |g...s_j...g\rangle |\psi\rangle_s^j, \tag{6.3}$$

where $|\psi\rangle_s^j$ is the state for the scattering signal photon with the wave function of $e^{-i(\omega_s t - \mathbf{k}_s\cdot\mathbf{r} + \phi_j^o)}$. ϕ_j^o is the original phase for the signal field coming from the j-th atom. Since we assume the signal photon is created at time $t = 0$, the entire phase of $|\psi\rangle_s^j$ for each atom at $t = 0$ should be the same. It will give $\phi_j^o = \mathbf{k}_s \cdot \mathbf{r}_j$. By substituting the

[1] Generally the creation of scattered photons is isotropic. Among the first several experimental investigations, colinear configuration ($\theta = 0$) was adopted. The main limitation for this configuration is the strong leakage of the write pulse in the single-photon detectors, which requires complicated filtering schemes. Later on, V. Balić *et al.* [87] made the first attempt to use the small angle configuration. After that, the small angle configuration becomes more popularly used.

[2] Somtimes, it is also called the anti-Stokes photon since the energy of $|g\rangle$ is higher than $|s\rangle$. With consistency, the readout photon is called the Stokes photon.

form of ϕ_j^o and $|\psi\rangle_s^j$ into Eq. 6.3, we will get

$$\begin{aligned} |\Psi\rangle' &= \frac{1}{\sqrt{N}}\sum_j e^{i(\Delta\phi_j^w-\phi_j^o)}|g...s_j...g\rangle e^{-i(\omega_s t-\mathbf{k}_s\cdot\mathbf{r})} \\ &= \frac{1}{\sqrt{N}}\sum_j e^{i\Delta\mathbf{k}\cdot\mathbf{r}_j}|g...s_j...g\rangle e^{-i(\omega_s t-\mathbf{k}_s\cdot\mathbf{r})} \\ &= |\psi\rangle_a\otimes|\psi\rangle_s \end{aligned} \tag{6.4}$$

with $|\psi\rangle_s$ the state for the signal photon. Thus we proved the form in Eq. 6.1. The above derivation will also give us another conclusion that there is no enhanced effect in the write process, scattering photons from individual atoms do not interfere each other since the scattered photon is entangled with the atoms. In principle, we can detect which atom is in the state $|s\rangle$ and know from which atom the scattered signal photon comes from, therefore no interference will happen.

6.1.2 Read process using collective enhancement

After the write process, the spin-wave state will be stored in the atomic ensemble. Usually it is difficult to manipulate the spin-wave state, for many applications, such as quantum repeater, one has to convert the spin-wave back to single-photons. This conversion is realized through the read process, in which by shining in a strong *read* pulse, the spin-wave will convert to a single-photon which emits to a definite direction. The readout single-photon is usually called the *idler* photon. The emission direction for the idler photon is determined by the phase matching condition:

$$\mathbf{k}_w+\mathbf{k}_r=\mathbf{k}_s+\mathbf{k}_i \tag{6.5}$$

with $\mathbf{k}_r$ the wave vector of read photon, $\mathbf{k}_i$ the wave vector of the idler photon. In the following paragraphs the reason for this phase matching condition will be discussed in detail.

During the read process, before the spin-wave converts to the idler photon, the combined state for atomic ensemble and read photon can be express as:[3]

$$|\Psi\rangle=|\psi\rangle_a\otimes|\psi\rangle_r=\frac{1}{\sqrt{N}}\sum_j e^{i\Delta\mathbf{k}\cdot\mathbf{r}_j}|g...s_j...g\rangle\otimes e^{-i(\omega_r t-\mathbf{k}_r\cdot\mathbf{r})}. \tag{6.6}$$

[3]During the storage, it is assumed that all the atoms do not move. The random movement of individual atoms will cause spinwave dephasing, which will be discussed in detail in Sec. 7.1.3.

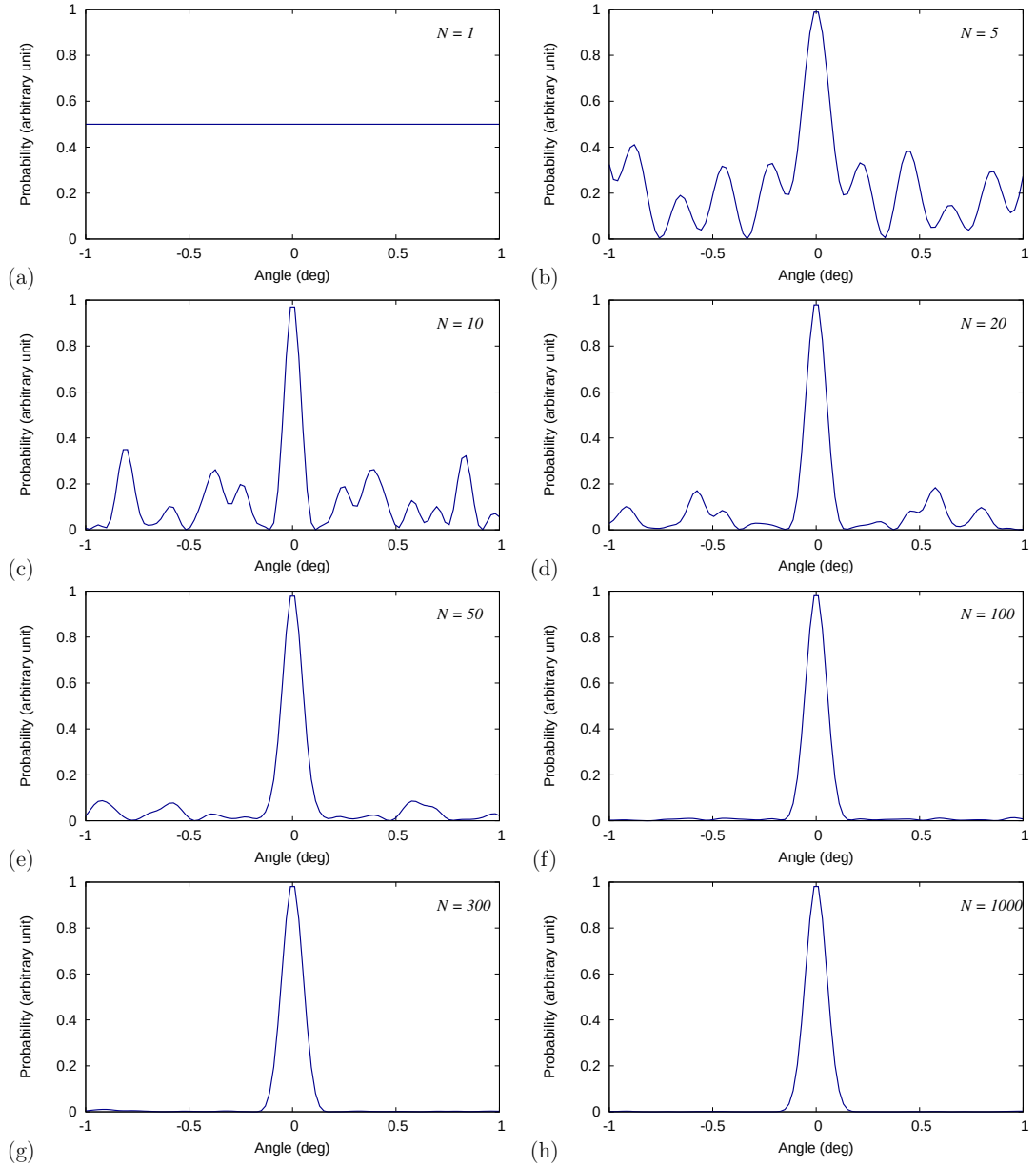

FIGURE 6.2: Simulated angular distribution of the idler photon as a function of atom number. The background pattern shown is related to the random distribution of the atom positions. A new assignment of the positions will give new background patterns.

Let's assume that the at $t = 0$, the spin-wave converts to the idler photon, giving the new combined state:

$$|\Psi\rangle' = |g...g_j...g\rangle \otimes \frac{1}{\sqrt{N}} \sum_j e^{i(\Delta\mathbf{k}+\mathbf{k}_r)\cdot\mathbf{r}_j} |\psi\rangle_i^j = |\psi\rangle_a \otimes |\psi\rangle_i, \tag{6.7}$$

where $|\psi\rangle_i^j$ is the spherical wave from each atom. The angular distribution for the idler photon is determined by the interference of the these spherical waves. The original phase for each spherical wave is $\phi_i^j = (\Delta\mathbf{k} + \mathbf{k}_r) \cdot \mathbf{r}_j$. For two arbitrary atoms (the l-th and

m-th atom), the difference for the original phase is

$$\phi_i^l - \phi_i^m = (\Delta\mathbf{k} + \mathbf{k}_r) \cdot (\mathbf{r}_l - \mathbf{r}_m). \tag{6.8}$$

For the idler propagation direction of $\mathbf{k}_i$, the propagation phase between the l-th atom and the m-th atom is $\Delta\phi^{l,m} = \mathbf{k}_i \cdot (\mathbf{r}_l - \mathbf{r}_m)$. If $\mathbf{k}_i$ is equal to $\Delta\mathbf{k} + \mathbf{k}_r$, we will have $\Delta\phi^{l,m}$ $= \phi_i^l - \phi_i^m$ which means that for every two atoms, the emission from they will always give constructive interference. The constructive interference in this special direction of $\mathbf{k}_i$ is just the reason for phase matching condition of Eq. 6.5, also the essence of collective enhancement. More atoms mean stronger interference in this special direction, thus higher probability it is able to readout the idler photon.

A simulation for the angular distribution for the idler photon as a function of the number of atoms (N) is made. Within the assumption, the shape of atomic ensemble used is of cigar shape with radius of 100 μm and length of 1 mm; emission wavelength is 795 nm. The position of each atom is created using Gaussian distribution. The Emission probability is calculated around the direction of $\mathbf{k}_i$ with the range of $\pm 1°$. Result is shown in Fig. 6.2. From it we can see that, when N is small, there is relative large background probability distribution; when N goes lager, the background becomes smaller, the emission angle becomes more definite. The angular width ($\Delta\theta$) of the emission angle is determined by the width (w) of the atomic ensemble with the relation of $\Delta\theta = 2\lambda/\pi w$.

6.1.3 Creation of remote entanglement

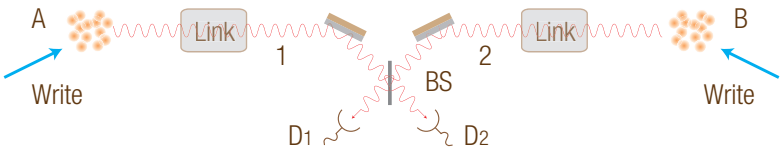

FIGURE 6.3: Creation of remote entanglement in the DLCZ protocol.

A crucial process in a quantum repeater is the creation of remote entanglement. In the DLCZ protocol, the proposed method is shown in Fig. 6.3. Both sites (A and B) repeat synchronized write process until a click is got in the detector of D_1 or D_2. Such a click may come from site A or B. Excluding measuring the spinwave state in each site, there is no other method in principle to distinguish from which ensemble the detected single-photon comes from, thus the two ensembles result in a superposition of spinwave states:

$$|\psi\rangle = 1/\sqrt{2}(|0\rangle_A|1\rangle_B + e^{i\phi}|0\rangle_A|1\rangle_B) \tag{6.9}$$

with $|1\rangle_j$ ($|0\rangle_j$) denotes there is (is not) an excitation in the j-th ensemble. In this way the remote entanglement between site A and B is created.[4]

An obvious drawback of the above idea is that the resulting phase ϕ of the remote entanglement in Eq. 6.9 is related to the propagation phase of photon 1 and photon 2. Considering the practical case of link distance of several km, due to the temperature fluctuation and air flowing in the link, for sure this phase will be rather unstable.[5] An intuitive idea is to use a second beam of with the same (or rather close) frequency and let it travel through the same link, and track the phase fluctuation. From the technical point of view, it will be rather difficult. So far to the best of my knowledge, there is no such realizations.

The phase problem comes along with the type interference used. In the DLCZ protocol, due to the adoption of single-photon interference in the middle site, it is inevitable to meet this phase problem. If we change the interference type from single-photon interference to two-photon interference, the phase problem can be easily solved, which will be discussed in detail in the next section.

6.2 A robust scheme resistent to phase noise

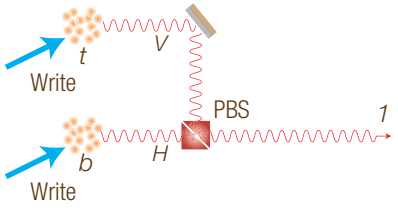

FIGURE 6.4: Creation of local entanglement using two ensembles.

The idea to use two-photon interference to solve the phase problem in the DLCZ protocol was proposed by Zhao et al. [128]. The first step of this two-photon scheme is the local creation of entanglement between the spin-wave spacial modes and the polarization of the scattered signal photon. The basis idea is shown in Fig. 6.4. Two atomic ensembles are utilized.The scattered signal fields from these two ensembles are combined on a PBS. By shining a write pulse, there is a small probability that one excitation is created in either the top ($|t\rangle$) or the bottom ($|b\rangle$) ensemble. If the excitation is in the top ensemble, the polarization for the signal photon is $|H\rangle$; if it is in the bottom, the polarization will

[4] There is some controversial argument about whether of not this type of state can be called an entangled state. One example is the case that a single-photon enters into a MZ interferometer, obviously it will result in the same type of state in Eq. 6.9. However, traditionally people do not regard it an entangled state.

[5] Even in the laboratory condition, we have the experience that the phase of interferometer of 1 m size will not be able longer than 10 min (drifting of π phase) without active stabilization.

be $|V\rangle$. Therefore the entangled state between the signal photon and the spin-wave stored in the ensembles can be express as:[6]

$$|\psi\rangle = 1/\sqrt{2}(|b\rangle|H\rangle_1 + |t\rangle|V\rangle_1). \tag{6.10}$$

The second step is the creation of remote entanglement using two-photon interference, which is shown in Fig. 6.5. In comparison with the DLCZ protocol, in the middle site two-photon Bell state measurement is adopted instead to entangle remote atomic ensembles. Once there is a coincidence count between the two detectors, it heralds the creation of remote entanglement.[7] The propagation phase for each photon is the overall phase for the system, which is not necessary to consider. The only requirement is to make sure that the two photons really meet each other, i.e., they have good time overlap. Typically the coherence length for the signal photon is about 20 m, which gives rise a upper bound for the length fluctuation for the quantum link. In the practical situation, let's make the following assumption: thermal expansion is the main origin for the change of link length; the thermal expansion coefficient is 10^{-5}; temperature fluctuation range is 10 K. The calculated possible communication distance is 200 km!

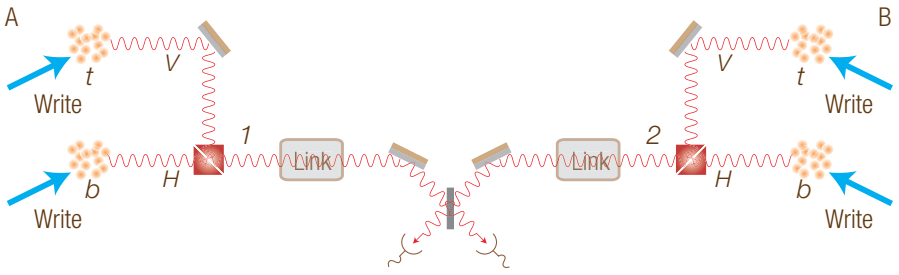

FIGURE 6.5: Creation of remote entanglement using four ensembles.

6.3 Efficient creation of remote entanglement

Due to the probabilistic character of the write process, in the DLCZ protocol and the two-photon scheme, it is not possible to know whether or not an excitation has been created locally. Only the clicks of the BSM in the middle site will herald a successful creation of excitations Therefore the write process can not be repeated very fast since the minimum cycle time is the propagation delay (T_L) which is the time for signal to

[6] There are some other methods to create this type of entanglement with only one ensemble involved, including the double-path scheme in [143] and the scheme in [144, 145] using multi ground states for the storage of "polarization" mode of spinwave.

[7] Once there is a coincidence count between the two detectors, for half the change it corresponds the creation of single excitation in each site (expected), for the other half change it corresponds the creation of double excitations in one site either A or B (unexpected). The double excited events in one site can eliminated in the second stage of entanglement connection [128].

TABLE 6.1: A comparison for the creation of remote entanglement in different schemes. η_L is the link attenuation from each site to the middle site. p is the excitation probability. Unit retrieval efficiency is assumed for calculation of the last scheme.

Scheme	DLCZ	Two-photon	Local preparation
Links	Fig. 6.3	Fig. 6.5	Fig. 6.7
Phase sensitive	yes	no	no
Ensembles used	2	4	8
Creation time	$\frac{1}{2p\eta_L}T_L$	$\frac{2}{p^2\eta_L^2}T_L$	$\frac{4}{p\eta_L^2}T$

transmit from one site to the middle and back. For each write trial, if we are able to know locally whether or not the write precess is successful without destructing the created atom-photon entanglement, we can repeat the write process much faster with the minimum cycle time limited only by the parameters like pumping time, delay of acousto-optic modulators, etc., which is usually much shorter compared with T_L.

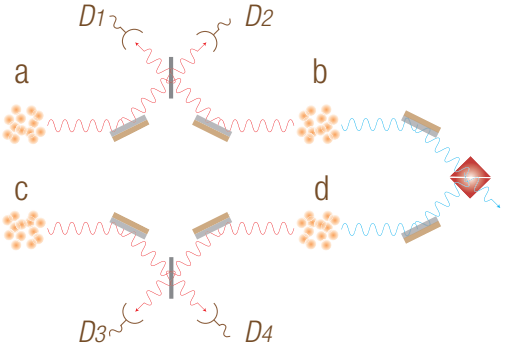

FIGURE 6.6: A efficient way to create local entanglement.

There are several ways to create local atom-photon entanglement deterministically.[8] One method is utilizing the way in Fig. 6.5.[9] The time required to prepare a pair of entanglement is $2T/p^2$ with p the excitation probability, T the write cycle time and a factor 2 with the reason that only two Bell states can be distinguished in the linear optical BSM. Since usually p is rather small ($\sim 0.1\%$), this method seems to be not so efficient. Actually there is a method which only scales with $1/p$ [24]. It is shown in Fig. 6.6. The write process will proceed in parallel for the top two (a and b) and the bottom two (c and d) ensembles. Once a click is got in D_1 or D_2, the write process for ensemble a and b will stop; once there is a click in D_3 or D_4, the write process for ensemble c and d will stop. Conditioned on such two clicks the state for these four

[8] There are some proposals which I don't think are experimentally feasible will not be talked in the following paragraphs. It includes the proposal based on creation of deterministic entangled photon pairs with four single-photon sources in [146], and the proposal based on partial memory readout in [147].

[9] One atomic qubit can be easily converted to the polarization state of a single-photon.

ensembles can be expressed as:

$$|\psi\rangle = 1/2(|a\rangle + |b\rangle)(|c\rangle + |d\rangle) = 1/\sqrt{2}(|\psi\rangle_1 + |\psi\rangle_2) \tag{6.11}$$

with

$$|\psi\rangle_1 = 1/\sqrt{2}(|a\rangle|d\rangle + |b\rangle|c\rangle) \quad |\psi\rangle_2 = 1/\sqrt{2}(|a\rangle|c\rangle + |b\rangle|d\rangle). \tag{6.12}$$

For half of the change,[10] the state be in $|\psi\rangle_1$ which means that one excitation is in the left two ensembles and the other in the right two ensembles. If we read the right ensembles b and d simultaneously and combine the readout idler photon on a PBS, we are able to create the entanglement between the left ensembles and the polarization state of the idler photon with the form

$$|\psi\rangle_1' = 1/\sqrt{2}(|a\rangle|V\rangle + |c\rangle|H\rangle). \tag{6.13}$$

The further way to utilize this state $|\psi\rangle_1'$ to build remote entanglement is sketched in Fig. 6.7. Similar as Fig. 6.5, two-photon interference is used for the BSM in the middle site. Two photon coincidence heralds the creation of remote entanglement between site A and B. A comparison for these schemes is shown in Tab. 6.1. The local preparation scheme is roughly T_L/pT times faster than the original two-photon interference scheme.

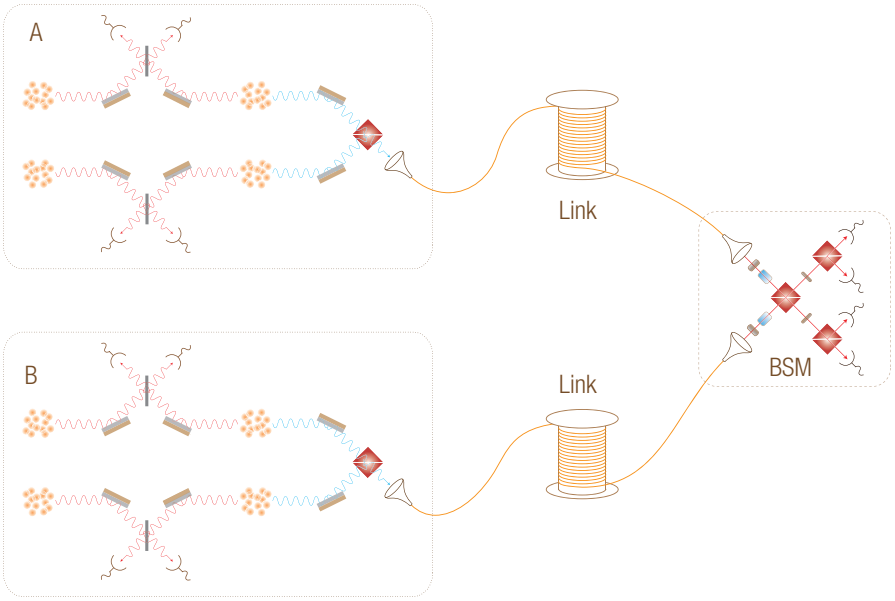

FIGURE 6.7: A efficient way to create remote entanglement.

[10] For the other half change, the four ensembles will be entangled in $|\psi\rangle_2$ for which state it is not possible to readout a idler photon either to the left direction or to the right direction, therefore this state will not contribute the final remote entanglement. In the next stage of entanglement connection, these terms will be removed.

Chapter 7

Improving the Performance of Quantum Memory

In the last chapter, atomic ensembles serve as the quantum memories in different quantum repeater schemes. There are two important parameters for a quantum memory, i.e., storage lifetime and retrieval efficiency. Storage lifetime mainly limits the maximal communication distance. Retrieval efficiency mainly limits entanglement connection efficiency. Higher retrieval efficiency means lower resource consumption. In this chapter, we analyze main limiting mechanisms and discuss feasible improving methods.

7.1 Extension of storage lifetime

7.1.1 Inhomogeneity of magnetic field

One main reason will limit the storage lifetime is the inhomogeneity of the ground states over the whole ensemble. The mechanism of this type of decoherence can be understood by referring to the spinwave state in Eq. 6.1. The evolution phase given by each atom is

$$\phi_{e\,j} = \frac{E_{s\,j} - E_{g\,j}}{\hbar} t = \frac{\Delta E_j}{\hbar} t. \tag{7.1}$$

When the average inhomogeneity of $\phi_{e\,j}$ over the whole ensemble equals to 1, the retrieval efficiency will drop to $1/e$ of its peak value.[1] Therefore, the lifetime given by this inhomogeneity is

$$\tau_{inh} = \frac{\hbar}{\sigma_{\Delta E}}. \tag{7.2}$$

[1] See Appendix A for the reason.

TABLE 7.1: Calculated lifetime (μs) for different pair of ground states.

	$m_s=-2$	$m_s=-1$	$m_s=0$	$m_s=+1$	$m_s=+2$
$m_g=-1$	15.2	22.8	45.5	$+\infty$	
$m_g=0$	22.8	45.5	$+\infty$	45.5	22.8
$m_g=+1$		$+\infty$	45.5	22.8	15.2

The magnetic field is the main origin for the inhomogeneity of $\sigma_{\Delta E}$ due to the Zeeman effect. In our experiments, we usually choose a pair ground states $|m_g, m_s\rangle$ with m_g from the Zeeman sublevels of the $5S_{1/2}$ $F=1$ hyperfine level and m_s from $5S_{1/2}$ $F=2$ of ^{87}Rb. In total, there are 15 combinations with 13 of them being allowable. Since the maximal Δm allowed is 2 for a two-photon process, the combinations of $|-1,2\rangle$ and $|1,-2\rangle$ are not physically allowed. For all the 13 combinations, we make a calculation for the corresponding lifetime by assuming magnetic inhomogeneity of $\sigma_{\mathrm{B}}=0.005$ G, with the results shown in Tab. 7.1. In this calculation, we only consider the first order dependence of ΔE over magnetic field. Within the results, there are 10 combinations showing a lifetime from 15 μs to 45 μs, which is consistent with the experimental observations like [148]. There are also three combinations, $|-1,1\rangle$, $|0,0\rangle$ and $|1,-1\rangle$, showing infinite long lifetime. These three pairs are usually called the "clock states".

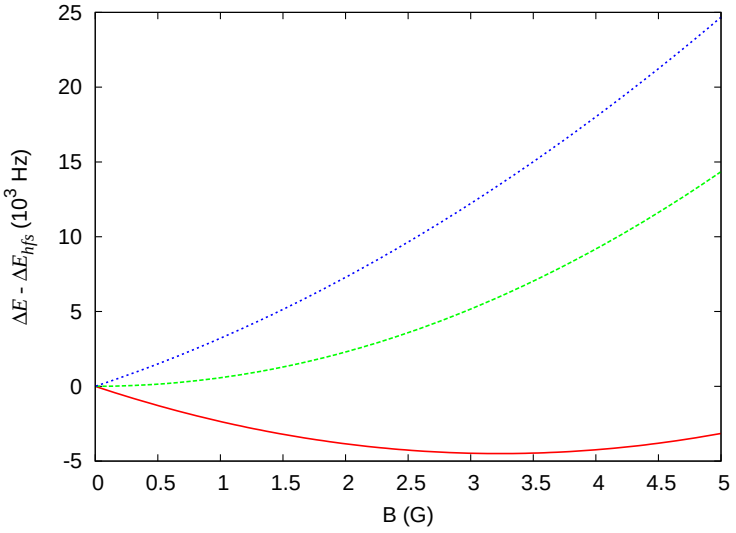

FIGURE 7.1: Dependence of ΔE on the magnetic field for the three pairs of clock states with red for $|-1,1\rangle$, green for $|0,0\rangle$ and blue for $|1,-1\rangle$. $\Delta E_{hfs}=6.83468261090429$ GHz is the $5S_{1/2}$ hyperfine split of ^{87}Rb.

Actually, it not enough to merely consider the first-order dependence of ΔE over B for the clock states. In order to consider the high-order dependence, we need to adopt the Breit-Rabi formula [149]. The calculated dependence ΔE over B for the three pairs of clock states are shown in Fig. 7.1. For the same value of σ_{B}, the smaller slope means

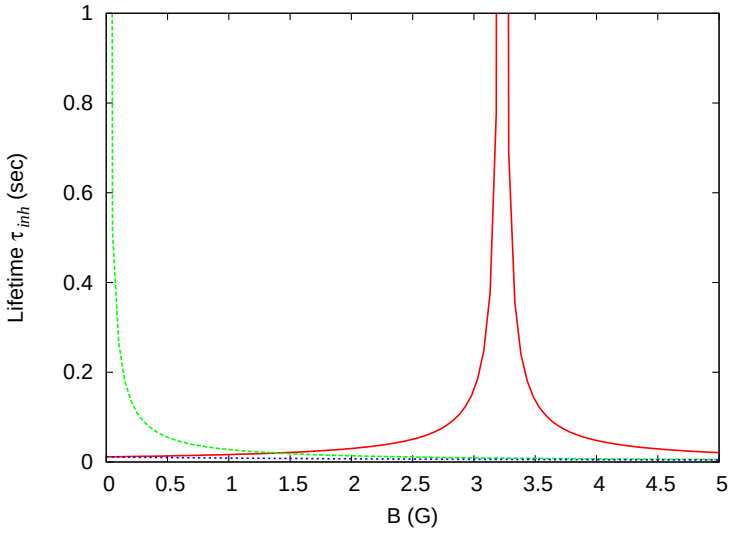

FIGURE 7.2: Lifetime estimation of the three pairs of clock states with red for $|-1,1\rangle$, green for $|0,0\rangle$ and blue for $|1,-1\rangle$. A magnetic field inhomogeneity of 0.02 G is assumed.

TABLE 7.2: Calculated lifetime τ_{loss} for different coditions.

	Temperature	τ_{loss} at $r_0 = 100\,\mu$m	τ_{loss} at $r_0 = 1\,$mm
MOT	100 μK	1.05 ms	10.5 ms
Optical Molasses	10 μK	3.33 ms	33.3 ms

longer lifetime time. The calculated lifetimes for these three pairs of clock sates are shown in Fig. 7.2. For the pair $|-1,1\rangle$, the slope equals to 0 at $B = 3.23$ G, which gives a maximal lifetime of 45 sec. For the pair of $|0,0\rangle$, there is a zero slope points at $B = 0$ G, which gives a maximal lifetime of 11 sec. For the last pair of $|1,-1\rangle$, the minimum slope points is also at $B = 0$ G, but with a value larger than 0, it only gives a maximal lifetime of 11 ms.

7.1.2 Loss of atoms

Loss of atoms is another main mechanism limiting the storage lifetime. There are two reasons which will result in loss of atoms, the gravity and atomic random motion due to the finite temperature. In most of the experiments due to the ease of alignment, the write/read, signal/idler beams are arranged in the horizontal plane. Therefore the gravity will play an important roll. Typical radius of the signal/idler field is 100 μm. The lifetime calculated due to the gravity effect is 4.6 ms ($1/e$ atoms left in the interaction region). The gravity induced loss of atoms can be minimized by arranging the signal/idler modes in the vertical direction.

Due to the finite temperature of the atoms, the size of the atomic could will expand as a function of time. The radius of the cigar shape cloud will increase in the form of

$$r^2(t) = r_0^2 + v_r^2 t^2 \tag{7.3}$$

with the average speed in radial direction $v_r = \sqrt{\pi k_{\mathrm{B}} T/2m}$; k_B the Boltzmann's contant; m the atom mass; T the atom temperature. The ratio of the atoms remaining in the original mode equals to $\gamma(t) = r_0^2/r^2(t)$. When $\gamma(t) = 1/e$, the retrieval efficiency will drop to the 1/e point, giving a lifetime of

$$\tau_{loss} = \frac{\sqrt{e-1}\, r_0}{v_r}. \tag{7.4}$$

For several typical experimental conditions, the calculated resut is shown in Tab. 7.2. Considering the best reasonable values of $T = 10\,\mu\mathrm{K}$ and $r_0 = 1\,\mathrm{mm}$, the longest lifetime is 33.3 ms.

7.1.3 Spinwave dephasing due to random atomic movement

In the last chapter, when we discuss the read process in Sec. 6.1.2, we assume the atoms do not move during storage. Actually, the random movement of the individual atoms constitutes another important mechanism which limits the storage lifetime. Considering the form of stored spinwave in Eq. 6.1, the random movement of individual atoms will give a phase for each atom

$$\phi_{\mathrm{sw},j} = \Delta\mathbf{k} \cdot \Delta\mathbf{r}_j \tag{7.5}$$

with $\Delta\mathbf{r}_j$ the random movement during the storage time of t. When the random phase $\phi_{\mathrm{sw},j}$ is large enough, the emission of all atoms will not be able to give constructive interference in the mode-matched direction, thus no collective enhancement. Since $\Delta k = 2\pi/\lambda_{sw}$, the requirement given by this mechanism is that the random movement should be much smaller than the spinwave wavelength λ_{sw}. It is able to suppress this dephasing either by increasing the spinwave wavelength or confining the atomic movement in the direction of $\Delta\mathbf{k}$.

In the case without confinement, the random movement $\Delta\mathbf{r}_j$ is determined by the temperature T and storage time t. When the random phase equals to 1,[2] it gives a lifetime of

$$\tau_{sw} = \frac{1}{\Delta k\, \overline{v}} \tag{7.6}$$

[2]The reason to choose this phase is shown in Appendix A

with $\overline{v} = \sqrt{2k_BT/\pi m}$. Since the amplitude of the spinwave vector is $\Delta k = |\mathbf{k_w} - \mathbf{k_s}| \simeq k_w\theta$, lifetime τ_{sw} is thus inverse proportional with the angle θ between the write beam and the signal field direction, when θ is small. Therefore, by reducing the detection angle, we reduce the wave vertor Δk, i.e., increase the spinwave wavelength, thus increase the tolerance of random movements. For a temperature of $T = 100\,\mu$k, the relation between τ_{sw} and θ is plotted in Fig. 7.3. When θ equals to 0, the lifetime will be maximized. However, τ_{sw} will not be infinite long, since the wave vectors k_w and k_s are not equal, there is slight difference between them. In our case due to the separation of 6.8 GHz between $|g\rangle$ and $|s\rangle$, the relative difference is 1.8×10^{-6}, which gives a spinwave wavelength of 4.4 cm, and lifetime τ_{sw} of 88.6 ms.[3]

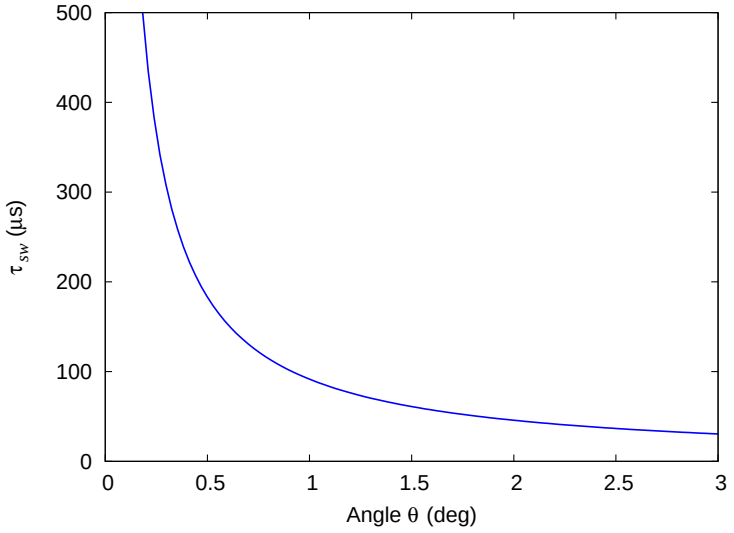

FIGURE 7.3: τ_{sw} caused by random movement through spinwave dephasing as a function of detection angle θ.

7.1.4 Confining the atoms with optical dipole trap

The problem of loss of atoms due to the free expansion of the atomic cloud can be suppressed by using additional confinement. While as discussed in Sec. 7.1.1, magnetic gradient will cause dephasing of the collective spinwave state, therefore magnetic trap is usually not a good choice. A popular method is using the optical dipole trap. When the detuning Δ is much larger than the D1/D2 separation of Δ_{hf}, the dipole potential can be expressed as [150]

$$U = \frac{3\pi c^2}{2\omega_0^3}\frac{\Gamma}{\Delta}I(r) \tag{7.7}$$

with ω_0 the resonant frequency, c speed of light, Γ decay rate of the excited state, $I(r)$ intensity of trapping beam. If $\Delta < 0$, it is called a red detuned trap, the atoms will be

[3] In the case of back scattering $\theta = \pi$, spinwave wavelength is minimized with the value of 397.5 nm, and a lifetime of τ_{sw}=799 ns.

trapped in the region with maximal intensity. While if $\Delta > 0$, it is called blue detuned trap, the atoms will be trapped in the region with minimum intensity. Therefore, for a red detuned trap, one just needs to focus the trapping beam to create a maximal intensity point. For the blue detuned trap, one needs to create a light box.

The main decoherence mechanism for the stored spinwave is the so called differencial light shift. In our case, the two ground state $|g\rangle$ and $|s\rangle$ has a separation of $\Delta_{\text{hfs}} = 2\pi \times 6.8\,\text{GHz}$, which will give a slightly difference between U_g and U_s. Consider this difference in detuning in Eq. 7.7, we have

$$U_{\text{diff}} = \frac{\Delta_{\text{hfs}}}{\Delta} U. \tag{7.8}$$

Since U is position dependent, atoms in different positions will experience different $\Delta E = E_s - E_g$, thus the integration over time will give a random phase for each atom in the spinwave state in Eq. 6.1, which causes decoherence.

7.1.4.1 Red detuned trap

For the calculation of lifetime, first we consider the case of a red detuned trap. When the trap depth U is much higher than the atomic kinetic energy $k_B T$ and the trap beam is Gaussian, the trap potential can be approximated with a harmonic potential

$$U = U_{r=0} + \alpha\, r^2. \tag{7.9}$$

For an atom with the original condition $r_{t=0} = 0$ and $v_{t=0} = \sqrt{2k_B T/m}$, it will start to oscillate with the form of

$$r(t) = r_{\max} \sin \omega_{\text{tr}} t \tag{7.10}$$

with $r_{\max} = \sqrt{k_B T/\alpha}$ the maximal oscillation distance from the trap center, $\omega_{\text{tr}} = \sqrt{2\alpha/m}$ the trap frequency. The phase which has been gained by this atoms compared with the atoms which stay still in the trap center (r=0) in one oscillating cycle is

$$\Delta\phi_{\text{cy}} = \frac{1}{\hbar} \int_0^{2\pi/\omega_{\text{tr}}} [U_{\text{diff}}(r(t)) - U_{\text{diff}}(r=0)]\mathrm{d}t = \frac{\pi k_B T}{\hbar \omega_{\text{tr}}} \frac{\Delta_{\text{hfs}}}{\Delta}. \tag{7.11}$$

Therefore the phase for an atoms at $t \gg 2\pi/\omega_{\text{tr}}$, the total phase is

$$\Delta\phi = \frac{t}{2\pi/\omega_{\text{tr}}} \Delta\phi_{\text{cy}} = t \frac{k_B T}{2\hbar} \frac{\Delta_{\text{hfs}}}{\Delta}. \tag{7.12}$$

When the phase $\Delta\phi$ equals to 1, it gives a lifetime of

$$\tau_{\text{tr}} = \frac{2\hbar}{k_B T} \frac{\Delta}{\Delta_{\text{hfs}}}. \tag{7.13}$$

From this formula we know that the lifetime τ_{tr} is not dependent on the trap parameters like, trap potential and trap frequency. It only depends on the trap detuning Δ and the atom temperature. Lower temperature and larger detuning give longer lifetime. By using the typical temperature of $T = 10\,\mu\mathrm{K}$, and a detuning of $\Delta = 2\pi \times 90\,\mathrm{THz}$ ($\lambda_{tr} = 1030\,\mathrm{nm}$), the calculated lifetime is $\tau_{\mathrm{tr}} = 20\,\mathrm{ms}$.

7.1.4.2 Blue detuned trap

In the case of a blue box trap, since in most of time there is no interaction with the trap, the trap frequency is mainly determined by the atom temperature and dimension of the trap. In the case of a cylindrical box, the estimated trap frequency is

$$\omega_{\mathrm{tr}} = \frac{\pi v_r}{d} = \frac{\pi}{d}\sqrt{\frac{2k_B T}{m}} \tag{7.14}$$

with d the diameter of the trap. The main task is to calculate the phase shift coming from differential light shift during each click with wall. We assume that the trap potential has the following form

$$U(r) = \frac{\pi c^2 \Gamma}{2\omega_0^3}\left(\frac{1}{\Delta_1} + \frac{2}{\Delta_2}\right) \cdot \frac{\sqrt{2}P}{\pi^{3/2}\delta d} e^{-\frac{2(r-d/2)^2}{\delta^2}} \tag{7.15}$$

with Δ_1 (Δ_2) the detuning relative to D_1 (D_2) line, P the power of trapping laser, δ the width of the trap wall. Considering the hyperfine split between $|g\rangle$ and $|s\rangle$, we get the differential light shift formula

$$U_{\mathrm{diff}}(r) = \frac{\Delta(2\Delta_1^2 + \Delta_2^2)}{\Delta_1\Delta_2(\Delta_1 + \Delta_2)} U(r). \tag{7.16}$$

The phase shift gained through a single click of box edge can be calculated in a similar way

$$\Delta\phi_{\mathrm{sc}} = \frac{1}{\hbar}\int_0^{\pi/\omega_{\mathrm{tr}}} U_{\mathrm{diff}}(r)\mathrm{d}t \tag{7.17}$$

By considering the typical experiment parameters, $\Delta_1 = 2\pi \times 9.2\,\mathrm{THz}$, $\Delta_2 = 2\pi \times 2.0\,\mathrm{THz}$, $P = 1\,\mathrm{W}$, $d = 200\,\mu\mathrm{m}$, $\delta = 10\mu\mathrm{m}$, $T = 10\,\mu\mathrm{K}$, and assuming $r_{t=0} = 0$ and $v_{t=0} = \sqrt{2k_B T/m}$, we get the calculated result of $\Delta\phi_{\mathrm{sc}} = 0.61$. Base on this phase shift we calculate the lifetime using the following formula

$$\tau_{\mathrm{tr}} = \frac{1}{\Delta\phi_{\mathrm{sc}}}\frac{2\pi}{\omega_{\mathrm{tr}}} \tag{7.18}$$

and get a result of $\tau_{\mathrm{tr}} = 15\,\mathrm{ms}$. Intuitively higher potential amplitude means higher potential slope, thus longer lifetime. However in the numerical calculation we find that

by increasing the laser power of trap beam, the resulting lifetime will increase very slowly, as shown in Fig. 7.4. It can be understood in the following way. when the trap potential is high, the atoms can only reach the weak tail of trap potential, the maximal slope of potential the atoms feel is mainly determined not by the trap amplitude, but by the atomic kinetic energy instead. Therefore the lifetime will hardly increase when increasing the trap potential.

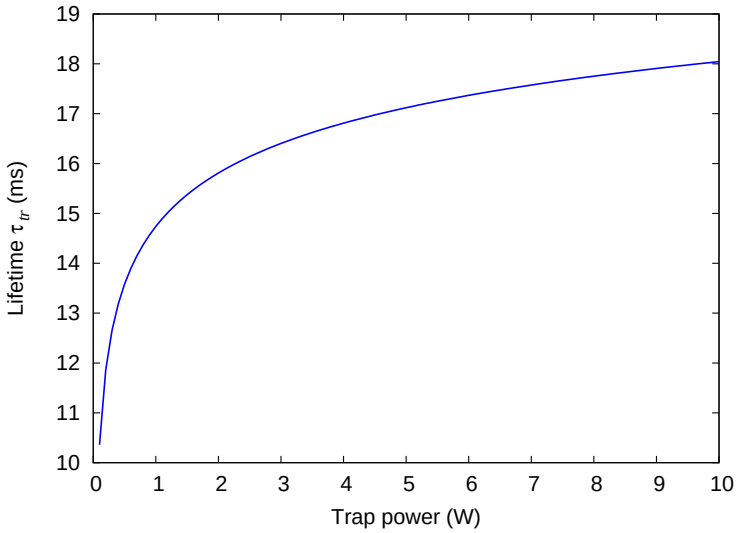

FIGURE 7.4: Calculated lifetime τ_{tr} as a function of the blue trap power.

No matter whether to use a red detuned or a blue detuned dipole trap to confine the atoms, differential light shift always limits the storage lifetime to the order of several tens ms. In order to have even longer lifetime, one has to compensate this differential light shift using another trap beam with similar intensity profile, which is beyond the scope of this thesis.

7.2 Increasing retrieval efficiency

In the read process, the most important parameter is retrieval efficiency, which is defined as the probability to convert the stored spinwave back to a single-photon. As discussed in Sec. 6.1.2, interference of light emission from individual atoms enhances the emission probability in the mode matched direction. In this section, we analyze quantitatively the relation between the retrieval efficiency and the experimental parameters, and discuss feasible ideas to improve it.

TABLE 7.3: ξ_g values for three pairs of clock states

Pair	$\|g\rangle$, $5^2S_{1/2}$, $F=1$	$\|s\rangle$, $5^2S_{1/2}$, $F=2$	$\|e\rangle$, $5^2P_{1/2}$, $F=2$	ξ_g
$\|-1,1\rangle$	$m_F=-1$	$m_F=1$	$m_F=0$	1/12
$\|1,-1\rangle$	$m_F=1$	$m_F=-1$	$m_F=0$	1/12
$\|0,0\rangle$	$m_F=0$	$m_F=0$	$m_F=1$	1/4
			$m_F=-1$	1/4

7.2.1 Relation with optical depth

We consider an atomic ensemble of N atoms in a cylindrical shape with diameter of w. For simplicity, we assume that spontaneous emission from $|e\rangle$ to the ground sates is isotropic and the transition $|e\rangle \rightarrow |g\rangle$ probability in any direction θ is $p\,\xi_g$. ξ_g is the branch ratio of the $|e\rangle \rightarrow |g\rangle$ transition over all the available transitions from $|e\rangle$ to the ground states. In the mode matched direction, $|e\rangle \rightarrow |g\rangle$ probability is N^2 times larger than the emission from a single atoms. The angular width of the enhanced emission is $\Delta\theta = 2\lambda/\pi w$, with a corresponding solid angle of $\Delta\Omega = \pi(\Delta\theta/2)^2$. Therefore, the total emission probability within $\Delta\Omega$ is

$$P_{\Delta\Omega} = p\,\xi_g N^2 \Delta\Omega = \frac{p\,\xi_g N^2}{\pi}\,\frac{\lambda^2}{w^2}. \tag{7.19}$$

This part of emission is useful since they are able to be collected into a single-mode fiber for further use. While the emission in to directions outside of $\Delta\Omega$ are difficult to collect, is the part to be minimized. In all the directions outside of $\Delta\Omega$, the interference of light from all atoms will not be in phase anymore, by with random phases instead. Therefore this part of emission can be treated incoherently, with the total emission probability of $P_{4\pi} = (4\pi - \Delta\Omega)Np \simeq 4\pi Np$.

Retrieval efficiency is defined to be the ratio of emission within $\Delta\Omega$ over the emission in all directions, with the form of

$$\eta = \frac{P_{\Delta\Omega}}{P_{4\pi} + P_{\Delta\Omega}} = \frac{\chi}{1+\chi} \tag{7.20}$$

with

$$\chi = \frac{\xi_g N}{4\pi^2}\,\frac{\lambda^2}{w^2} = \frac{\xi_g \lambda^2}{4\pi}\rho L \tag{7.21}$$

where ρ is the atom density and L is the length of the atoms cloud. Therefore we get the conclusion that retrieval efficiency is not dependent on the atom number N but the longitudinal density (ρL) instead. Longitudinal density is proportionally related with optical density in the formula of od $= \rho\sigma L$, with σ the cross section. Usually optical

depth is measured with a cycling transition. In our case it is the ^{87}Rb D_2 transition of $|F = 2, m_F = 2\rangle \rightarrow |F' = 3, m_F = 3\rangle$. The cross section for this transition is $\sigma = 3\lambda^2/2\pi$ [149]. Therefore we get the relation between χ and od of

$$\chi = \frac{\xi_g}{6} \cdot \text{od}. \tag{7.22}$$

The branch ratio ξ_g can be looked up in [149]. For the three pair of clock states mentioned in Sec. 7.1.1, the values are shown in Tab. 7.3. For the case of $\xi_g = 1/4$, the relation between optical density and retrieval efficiency is plotted in Fig. 7.8. In order to achieve a 90% retrieval efficiency, the optical depth required is 216. While for the case of $\xi_g = 1/12$, optical depth required is 648.

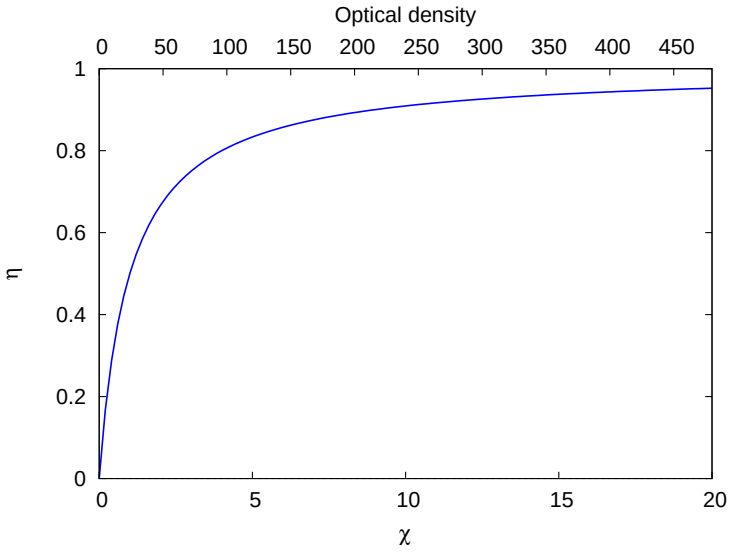

FIGURE 7.5: Relation between retrieval efficiency η and optical density when $\xi_g = 1/4$.

7.2.2 The ring cavity experiment

According to the analysis result in the last section, optical depth needs to be rather high in order to reach unit retrieval efficiency. Typical value of od for a MOT ranges from several to tens [151]. There are several ways to get larger optical depth, including putting the atoms inside a hollow fiber [152], using an optical cavity [153], etc.

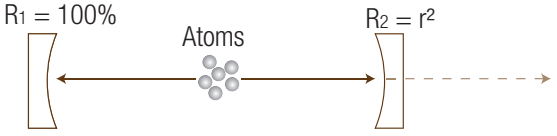

FIGURE 7.6: Using a cavity to enhance the emission into the cavity mode.

The reason why an optical cavity can be used to enhance the retrieval efficiency can be understood in the following simple way. We consider an atomic ensemble insider a one-end cavity, which is shown in Fig. 7.6. The reflection rate for one mirror is 100%, and for the other is $R = r^2$. We assume that there is one atom in the excited state. In the case without a cavity the probability to emit a single-photon in the cavity direction within unit time is p. When adding a cavity, there are several ways for the emission to go outside the cavity. First, it may come out directly after the emission. Second, it may have traveled in one round trip in the cavity already, or two times, or even more. We write down the possibility amplitudes

$$\begin{aligned} \sqrt{p_1} &= \sqrt{p} \cdot t \\ \sqrt{p_2} &= \sqrt{p} \cdot r \cdot t \\ &\vdots \\ \sqrt{p_n} &= \sqrt{p} \cdot r^{n-1} \cdot t \\ &\vdots \end{aligned} \tag{7.23}$$

with $t^2 = T = 1 - R$ being the transmission rate of the second mirror. By aligning the cavity length, one is able to make the phase gained during one round trip in the cavity equals to 2π multiplying an integer. Therefore, all the above possibilities will be in phase, and interfere constructively. The possibility to for the emission to go outside of the cavity within unit time can be calculated by summing up the possibility amplitudes in Eq. 7.23

$$p_{\text{out}} = |\sum_{j}^{+\infty} \sqrt{p_j}\,|^2 = \frac{p\,t^2}{(1-r)^2} \simeq \frac{4p}{T}. \tag{7.24}$$

The enhanced factor is $\eta_{\text{en}} = p_{\text{out}}/p \simeq 2F/\pi$, with F the cavity finesse. If we add such a cavity which is resonant with with the idler photon in our quantum memory setup, the emission probability $P_{\Delta\Omega}$ in Eq. 7.19 can be further enhanced by $2F/\pi$ times. Since $P_{\Delta\Omega}$ is proportional with optical depth, we can also say that optical depth is enhanced by $2F/\pi$ times.

In the previous experiment [153] in Vuletic's group in MIT, they used a linear cavity to enhance the read process. One problem for their experiment is that in the write process, forward and backward scattered signal photons are not able to be distinguished. The backward scattered case projects the atoms to a spinwave state with rather short wavelength, which corresponds to a lifetime of only about 200 ns. Another drawback is that if the cavity is placed outside of vacuum chamber, the idler photon will travel four times through the chamber windows, which will result in large unwanted losses.

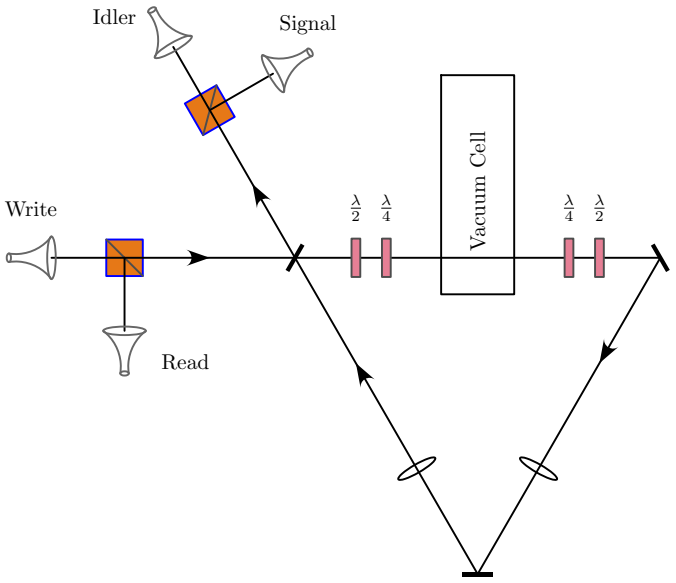

FIGURE 7.7: The ring cavity setup to increase retrieval efficiency.

If we use a ring cavity instead as shown in Fig. 7.7, the forward scattering and backward scattering in the write process can be distinguished since they will exit the cavity through different ports. And also the idler photon only needs to travel two times through the cavity windows, which gives less unwanted loss within the cavity. The cavity length can be configured to make all the four beams write/read, signal/idler, resonant with some longitudinal modes. Stabilization for the cavity length can be done during MOT loading. At the time of writing this thesis, this experiment is actively under going.

7.2.3 The big cavity idea

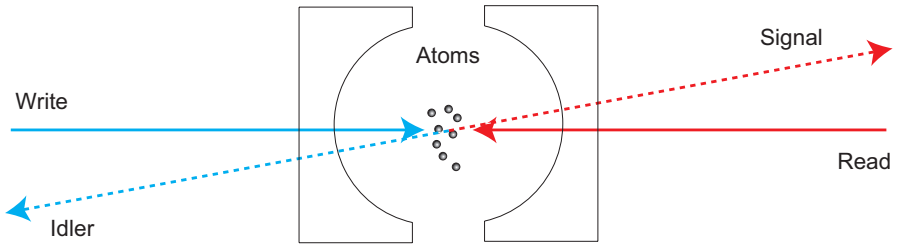

FIGURE 7.8: The big cavity idea to increase retrieval efficiency.

As discussed in Sec. 7.2.2, by using a cavity, we can enhance the emission in one special mode and and improve the retrieval efficiency. On the other hand, we can also align the cavity length to make the phase gained in one round trip equals to $(2n+1)\pi$. The interference between the terms in Eq. 7.23 will be destructive. In a similar way, we get the calculated suppression rate of $\eta_{\text{sup}} = \pi/2F$. The emission into the cavity mode is suppressed roughly by a factor of F. Considering this, we can can also construct a big

cavity, i.e., a 4π sphere mirror, with several holes opened for the experiment beams. Emissions into most directions within the 4π solid angle are suppressed by a factor of F. In this way, $P_{4\pi}$ in Eq. 7.20 can be suppressed by a factor of F. The extent of improvement for the retrieval efficiency is similar.

An advantage for this big cavity scheme is that, the requirement for the cavity stabilization is much easier, since it is only required the laser frequency to be roughly in the middle of two longitudinal modes, not like the case in Sec. 7.2.2 where the laser frequency is required to be precisely in the center of the narrow cavity linewidth. Second advantage is that, we do not suffer from the problem of intra cavity loss as in the ring cavity scheme in Sec. 7.2.2. However, the above scheme is just an idealized scheme. There many practical limitations, such as the manufacture of the big cavity, arrangement of the relatively wider cooling beams, the flatness of the chamber window, areas not possible to cover near the corner of the glass cell chamber, etc.

Chapter 8

Experimental Realization of 1 Millisecond Storage

In this chapter, we report our experimental investigations on extending the storage time of atomic ensemble based quantum memories. By exploiting the magnetic field insensitive state, "clock state", and generating a long-wavelength spinwave to suppress the dephasing, we succeed in extending the storage time of the quantum memory to 1 ms.

8.1 Motivation

Quantum repeater with atomic ensembles and linear optics has attracted broad interest in recently years, since it holds the promise to implement long-distance quantum communication and distribution of entanglement over quantum networks. Following the protocol proposed by Duan *et al.* [20] and the subsequent improved schemes [128, 154–156], significant progresses have been accomplished, including coherent manipulation of the stored excitation in one atomic ensemble [148, 157] and two atomic ensembles [123, 158, 159], demonstration of memory-built-in quantum teleportation [116], and realization of a building block of the quantum repeater [24, 25]. In these experiments, the atomic ensembles serve as the storable and retrievable quantum memory for single excitations.

Despite the advances achieved in manipulating atomic ensembles, long-distance quantum communication with atomic ensembles remains challenging due to the short coherence time of the quantum memory for single excitations. For example, to directly establish entanglement between two memory qubits over a few hundred kilometers, one needs a

memory with a storage time of a few hundred microseconds. However, the longest storage time reported previous to this work is only on the order of 10 μs [24, 148, 157, 160].

It is long believed that the short coherence time is mainly caused by the residual magnetic field [115, 161]. Thereby, storing the collective state in the superposition of the first-order magnetic-field-insensitive state [162], i.e. the "clock state", is suggested to inhibit this decoherence mechanism [161]. A numerical calculation[1] shows that the lifetime of the collective excitation stored in the "clock state" is on the order of seconds.

8.2 Experimental setup

The architecture of our experiment is depicted in Fig. 8.1.a and Fig. 8.1.b. A cold ^{87}Rb atomic ensemble in a MOT at a temperature of about 100 μK serves as the quantum memory. The two ground states $|g\rangle$ and $|s\rangle$, together with the excited state $|e\rangle$ form a Λ-type system. A bias magnetic field of about 3.2 G is applied along the axial direction to define the quantization axis. Note that there are three pairs of "clock states" for the ground states of ^{87}Rb atom, i.e. $(|1,1\rangle, |2,-1\rangle)$, $(|1,0\rangle, |2,0\rangle)$, and $(|1,-1\rangle, |2,1\rangle)$, where we have defined $|i,j\rangle = |5S_{1/2}, F=i, m_F=j\rangle$. In a timescale of milliseconds, we can use any of them to store the collective excitation, because the decoherence of the "clock states" caused by magnetic field is negligible. In our experiment, we prepare the atoms in $|1,0\rangle$ to exploit the clock state ($|g\rangle = |1,0\rangle$, $|s\rangle = |2,0\rangle$). An off-resonant σ^- polarized write pulse with wave vector $\mathbf{k}_\mathrm{W}$ is applied to the atomic ensemble along the axial direction, inducing spontaneous Raman scattering. The Stokes photon with σ^- polarization and wave vector $\mathbf{k}_\mathrm{S}$ is collected at an angle of $\theta = 3°$ relative to the write beam, as in most of the previous experiments [24, 115, 123, 143, 157–159]. The beam waist of the detection mode is about 100 μm in the atomic ensemble. Conditional on detecting a Stokes photon, a collective excited state or a spinwave is imprinted in the atomic ensemble [20], described by

$$|\psi\rangle = \frac{1}{\sqrt{N}} \sum_j e^{i\Delta\mathbf{k}\cdot\mathbf{r}_j} |g...s_j...g\rangle, \tag{8.1}$$

with $\Delta\mathbf{k} = \mathbf{k}_\mathrm{W} - \mathbf{k}_\mathrm{S}$ the wave vector of the spinwave, and $\mathbf{r}_j$ the coordinate of the j-th atom. After a controllable delay δt, a strong σ^+ polarized read light, counter-propagating with the write light, converts the collective excitation into an anti-Stokes photon, which is σ^+ polarized and spatially mode-matched with the Stokes photon from the opposite direction. The Stokes (anti-Stokes) photon and the write (read) light are spatially separated.

[1] See Sec. 7.1.1 for the detailed calculation.

In the experiment, the MOT is loaded for 20 ms at a repetition rate of 40 Hz. The trapping magnetic field and repumping beams are then quickly switched off. After 0.5 ms, the bias magnetic field is switched on, whereas the cooler beams stay on for another 0.5 ms before being switched off to prepare the atoms in the $|5S_{1/2}, F = 1\rangle$ ground state. Then, within another 4 ms, experimental trials (each consisting of pumping, write and read pulses) are repeated with a controllable period depending on the desired retrieval time. In order to optically pump the atoms to the desired sub-level, we switch on two pumping beams in each experimental trial before write and read process: one couples the transition $|5S_{1/2}, F = 2\rangle \rightarrow |5P_{3/2}, F' = 2\rangle$ with linear polarization for 2 μs, and the other couples the transition $|5S_{1/2}, F = 1\rangle \rightarrow |5P_{1/2}, F' = 1\rangle$ for 1.7 μs, which is linearly (σ^+) polarized for $|1, 0\rangle$ ($|1, 1\rangle$). From the experimental result, we estimate more than 80% of the atoms are prepared to the desired state.

For $\theta > 0.5°$, the Stokes (ant-Stokes) photon and the write (read) light can be spatially separated and thus we can choose any of the three pairs of "clock states". Because the retrieval efficiency is proportional to the coupling strength of the transition $|e\rangle \rightarrow |g\rangle$, we choose the clock state ($|1, 0\rangle$, $|2, 0\rangle$) to get higher retrieval efficiency. While for smaller angles $\theta < 0.5°$, the two beams with the same polarization cannot be spatially separated, and thereby we have to use the other two "clock states". In this case, we choose the "clock state" ($|1, 1\rangle$, $|2, -1\rangle$), since the energy level $|1, 1\rangle$ is lower than $|1, -1\rangle$ under the bias magnetic field and the pumping effect is better.

8.3 Experimental results

The quality of the quantum memory can be well characterized by the cross correlation $g_{\mathrm{S,AS}} = p_{\mathrm{S,AS}}/(p_{\mathrm{S}} \cdot p_{\mathrm{AS}})$ (See Methods), with p_{S} (p_{AS}) the probability of detecting a Stokes (anti-Stokes) photon and $p_{\mathrm{S,AS}}$ the coincident probability between the Stokes and anti-Stokes channels. The larger the cross correlation is, the higher-quality single photon source [148, 157] or atom-entanglement source [25, 143] we can acquire. In the experiment, to evaluate the coherence time of the quantum memory, we measure the cross correlation as a function of the time delay, described as [148]

$$g_{\mathrm{S,AS}}(\delta t) = 1 + C\gamma(\delta t), \tag{8.2}$$

with C a fitting parameter, and $\gamma(\delta t)$ the time dependent retrieval efficiency. Note that $g_{\mathrm{S,AS}} > 2$ means that the Stokes and anti-Stokes photon are nonclassically correlated [161, 163].

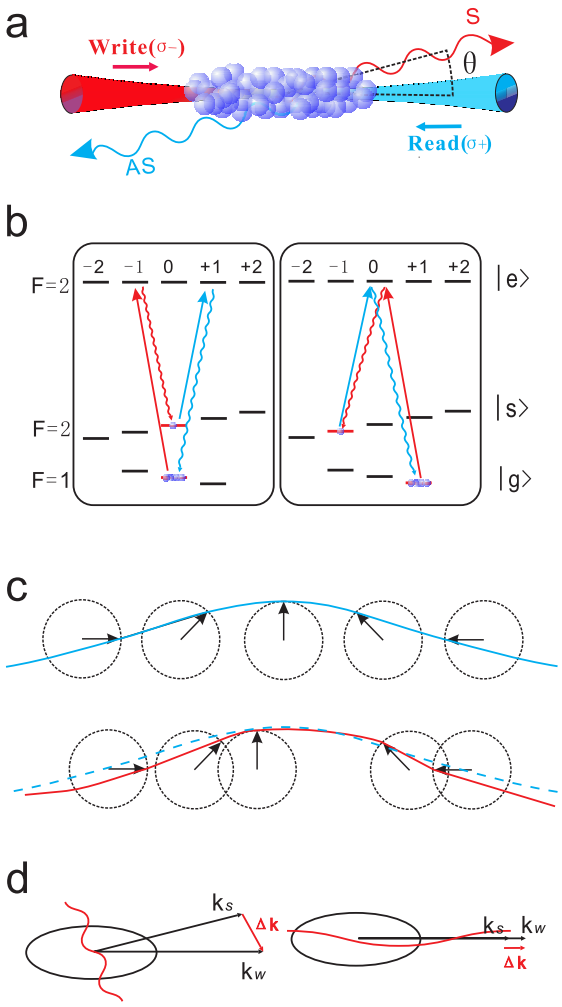

FIGURE 8.1: (a) Schematic view of the experiment. The atoms are initially prepared in $|g\rangle$. A weak σ^- polarized write pulse is applied to generate the spinwave and Stokes photon via spontaneous Raman transition $|g\rangle \rightarrow |e\rangle \rightarrow |s\rangle$. The Stokes photon are detected at an angle of θ relative to the write beam. After a controllable delay, a strong σ^+ polarized read light induces the transition $|s\rangle \rightarrow |e\rangle \rightarrow |g\rangle$, converting the spinwave into an anti-Stokes photon. (b) The structure of atomic transitions (^{87}Rb) under a weak magnetic field. The left panel corresponds to the experiment with $(|1,0\rangle, |2,0\rangle)$. The right one corresponds to the experiment with $(|1,1\rangle, |2,-1\rangle)$. The photons emitted in undesired transitions are filtered by polarization filter and filter cell. (c) Illustration of the spinwave dephasing induced by atomic random motion. The blue curve represents the spinwave initially stored in the quantum memory. The atoms randomly move along the wave vector direction, resulting in a phase fluctuation. The perturbed spinwave is represented by the red curve. (d) The wavelength of the spinwave can be controlled by changing the detection configuration. In the collinear case, we have the maximum wavelength.

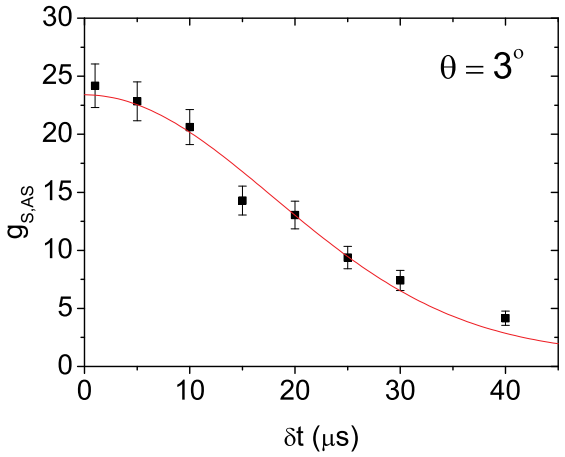

FIGURE 8.2: The cross correlation $g_{\mathrm{S,AS}}$ versus the storage time δt for $(|1,0\rangle, |2,0\rangle)$ at $\theta = 3°$. The data are fitted by using $g_{\mathrm{S,AS}}(\delta t) = 1 + C\exp(-\delta t^2/\tau_{\mathrm{D}}^2)$. Our data give a lifetime of $\tau_{\mathrm{D}} = 25 \pm 1$ μs, which is much less than the theoretical estimation for the "clock state". Error bars represent statistical errors.

The experimental result is given in Fig. 8.2. Our data shows that the lifetime is a little bit longer than our previous results [148], but still far from the theoretical predication for the "clock state". According to the calculation in Sec. 7.1.3, the spinwave dephasing is possible to be the main limiting mechanism. For $\theta = 3°$, a simple calculation gives[2] $\lambda = 15$ μm and then $\tau_{\mathrm{D}} = 25$ μs. By fitting the data in Fig. 8.2 with $g_{\mathrm{S,AS}}(\delta t) = 1 + C\exp(-\delta t^2/\tau_{\mathrm{D}}^2)$, we obtain a lifetime of $\tau_{\mathrm{D}} = 25 \pm 1$ μs, which is consistent with the theoretical calculation. Note that besides the atomic random motion, the collisions between atoms may also affect the phase of the spinwave. While in our experiment, the effect of collisions is negligible. The collisions rate can be estimated by $\Gamma \sim nv_s\sigma \simeq 1$ Hz, where the atomic density $n = 10^{10}/\mathrm{cm}^3$, the s-wave scattering cross section $\sigma = 8\pi a^2$ with the scattering length $a = 6$ nm. Thereby, in the time scale of milliseconds, the collisions can be safely neglected.

To further confirm that the decoherence is mainly caused by the dephasing induced by atomic motion, we increase the wavelength of the spinwave by decreasing the detection angle (see Fig. 8.1.d). In this way the dephasing will be suppressed and the storage time will be extended. In our experiment, we reduce the angle by choosing $\theta = 1.5°$, $0.6°$, and $0.2°$ and measure the lifetime of the quantum memory for each configuration. Note that, for $\theta = 0.2°$, the two beams with the same polarization can not be spatially separated, and thereby we use another "clock state" ($|g\rangle = |1,1\rangle$, $|s\rangle = |2,-1\rangle$) by preparing the atoms in $|1,1\rangle$. In this case, the Stokes (anti-Stokes) photon is σ^+ (σ^-)

[2] See Sec. 7.1.3 for the detailed calculation.

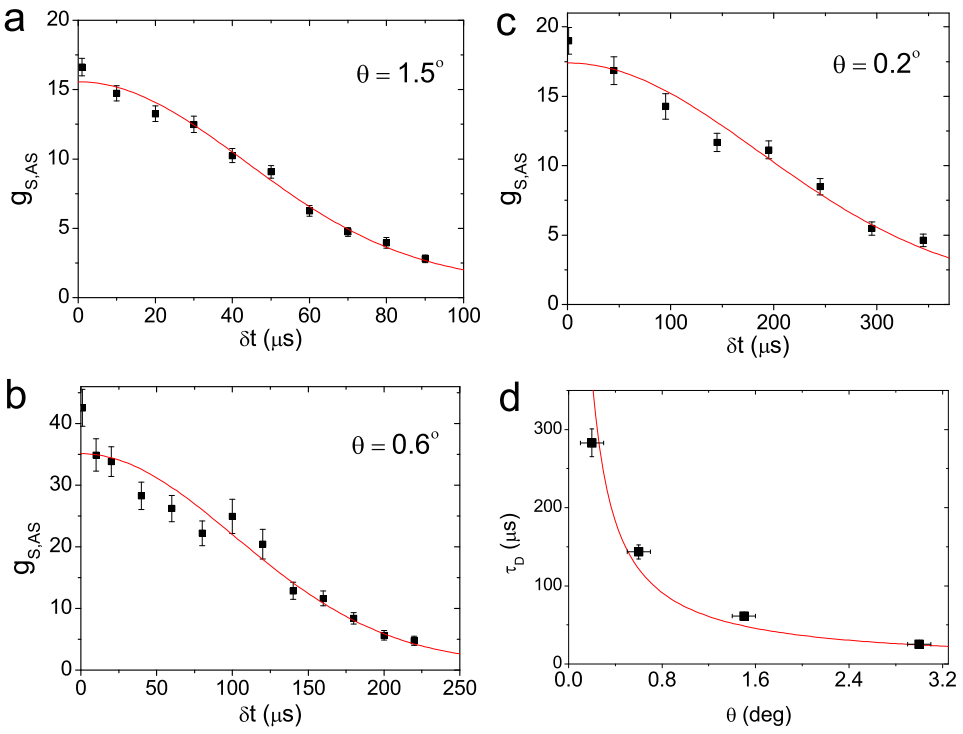

FIGURE 8.3: The cross correlation $g_{\mathrm{S,AS}}$ versus the storage time δt for different angles (a)-(c) and the measured lifetime τ_{D} as a function of detection angle θ (d). Panels (a) and (b) are for $(|1,0\rangle, |2,0\rangle)$ at $\theta = 1.5°$ and $0.6°$, respectively. The data are fitted by using $g_{\mathrm{S,AS}}(\delta t) = 1 + C\exp(-\delta t^2/\tau_{\mathrm{D}}^2)$, where τ_{D} is the lifetime due to dephasing. Panel (c) is for $(|1,1\rangle, |2,-1\rangle)$ at $\theta = 0.2°$. In this case we take into account the effect of loss of atoms and fit the data by using $g_{\mathrm{S,AS}}(\delta t) = 1+C\exp(-\delta t^2/\tau_{\mathrm{D}}^2)/(1+A\delta t^2)$, with A the fitting parameter obtained from the collinear configuration. The fitted lifetime for each case is: (a) $\tau_{\mathrm{D}} = 61 \pm 2$ μs, (b) $\tau_{\mathrm{D}} = 144 \pm 9$ μs, (c) $\tau_{\mathrm{D}} = 283 \pm 18$ μs. The first data are a little bit higher than the fitted curves, which might be caused by the imperfection in the pumping process. By reducing the angle, the lifetime is increased from 25 μs to 283 μs, which implies the decoherence is mainly caused by the dephasing induced by atomic random motion. Panels (d) depicts the measured lifetime τ_{D} as a function of detection angle θ, where the horizontal error bars indicate measurement errors in the angles. The solid line is the theoretical curve with $T \simeq 100$ μK. The experimental results are in good agreement with the theoretical predications. The vertical error bars indicate statistical errors.

polarized. The write (read) and Stokes (anti-Stokes) lights have orthogonal polarizations and are separated by a Glan-Laser prism.

The experimental results are displayed in Fig. 8.3.a-c. As expected, the dephasing of the spinwave dominates, when the effect of magnetic field is inhabited by using the "clock state". The lifetime increases from 25 μs to 283 μs by reducing θ or, in other words, increasing the wavelength of spinwave. Our results clearly show that the dephasing of the spinwave is extremely sensitive to the small angle between the write beam and Stokes modes, and that the long-wavelength spinwave is robust against the dephasing induced

by atomic random motion. Note that, for $\theta = 0.2°$, the data are fitted by taking into account the effect of loss of atoms. The measured lifetime τ_{D} is shown in Fig. 8.3.d as a function of angle θ. The solid line is the theoretical curve $\tau_{\mathrm{D}} = \frac{1}{\Delta k v_s}$, with $v_s = 0.1$ m/s corresponding to a temperature of $T \simeq 100$ μK. The good agreements between theory and experiment imply that our work provides an alternative approach to measure the temperature of an atomic ensemble. Moreover, since the lifetime is only sensitive to the velocity of the atoms in the interaction region, which is determined by the waist of the detection mode and is controllable, one can also use our method to measure the velocity distribution of the atomic ensemble by performing measurement in different regions.

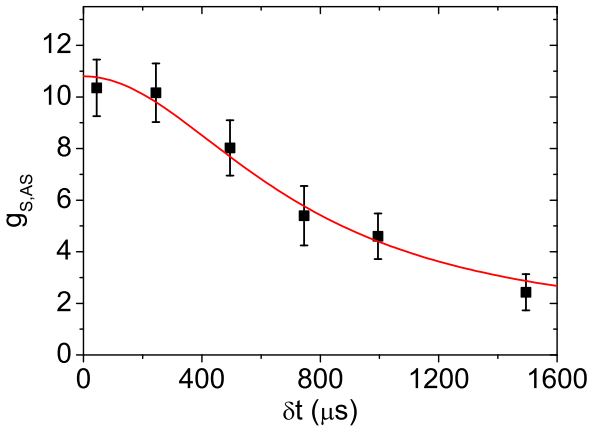

FIGURE 8.4: The cross correlation $g_{\mathrm{S,AS}}$ versus the storage time δt for $\theta = 0°$ and $(|1,1\rangle, |2,-1\rangle)$. The data are fitted by using $g_{\mathrm{S,AS}}(\delta t) = 1 + \frac{C}{1+A\delta t^2}$, with A the fitting parameter. Our data give a lifetime of $\tau_{\mathrm{L}} = 1.0 \pm 0.1$ ms, when the retrieval efficiency $\gamma(\delta t) = \frac{1}{1+A\delta t^2}$ has dropped to $1/e$. Error bars represent statistical errors.

To further suppress the dephasing and achieve a longer storage time, we use the collinear configuration ($\theta = 0°$), where we have the maximum wavelength of the spinwave $\lambda \simeq 4.4$ cm and thus $\tau_{\mathrm{D}} \simeq 72$ ms. In this case, the decoherence due to loss of atoms, is isolated as the principal decoherence mechanism. For $r_0 = 100$ μm as the waist of the detection mode and $T = 100$ μK, a direct calculation[3] gives $\tau_{\mathrm{L}} = 1.05$ ms. The experimental result is shown in Fig. 8.4, where the "clock state" $(|1,1\rangle, |2,-1\rangle)$ is also used. Our data give a lifetime of $\tau_{\mathrm{L}} = 1.0 \pm 0.1$ ms, when the retrieval efficiency has dropped to $1/e$. The experiment result is in good agreement with the theoretical estimation.

[3]See Sec. 7.1.2 for the detailed calculation.

8.4 Discussion

In summary, we have successfully realized a long-lived quantum memory for single collective excitation by exploiting the "clock state" and long-wavelength spinwave. The storage time of 1 ms is 30 times longer than the best result reported so far [157], and is long enough for photons transmission over 100 kilometers. In our experiment, the coherence time of the quantum memory is limited by the decoherence due to loss of atoms, which can be suppressed by lowering the temperature via optical molasses. A storage time of 3 ms is achievable by reducing the temperature to 10 μK. This will be the upper limit for the atomic memory in MOT, since longer storage time is prohibited by the free falling of the atoms under gravity. Further improvement might be achieved by trapping the atoms in an optical dipole trap [161, 164], where the decoherence due to loss of atoms and the dephasing induced by atomic random motion can both be suppressed. In this case, the principal decoherence mechanism is the diffusion caused by collisions, which will give a lifetime of a few tens of milliseconds. To inhibit the collision-induced diffusion, one has to trap the atoms in a deep optical lattice [165] or use solid state system [166], where each atom is tightly confined in a single site and collisions are avoided. The optical lattice has the potential to store the collective excitation for a few tens of seconds, which will reach the requirement in the storage time for a robust and efficient quantum repeater with atomic ensembles [147]. The idea presented in this work can also be applied to the quantum memory based on electromagnetically induced transparency [23, 115, 167]. By using the same method as in our experiment, a storage time of a few hundred microseconds can be expected.

Our work opens up the exciting possibility to implement many tasks of quantum information processing. Combined with the techniques developed in recent years, one can implement a high-quality on-demand single-photon source, deterministic preparation of multi-qubit entanglement, generation of entanglement between two remote atomic memory qubits over a few hundred kilometers, and even construction of long-lived quantum nodes for quantum repeater. More generally, our work presents an experimental investigation on the decoherence of the spinwave at single quanta level. It is clearly shown that a long-wavelength spinwave is robust against dephasing. Besides, our work also provides an approach to measure the temperature or the velocity distribution of an atomic ensemble. Furthermore, since the decoherence of the spinwave is controllable, one can measure certain important physical quantities by introducing additional physical mechanisms. For example, when performing experiments in optical dipole trap, the lifetime is determined by collision between atoms [168]. Thereby, the s-wave scattering cross section or scattering length might be measured using our approach.

Chapter 9

Entanglement Assisted Spinwave Interferometer

In this chapter, we report the heralded generation of atomic NOON state by observation of phase-super resolution in a motion-sensitive spinwave interferometer. The spinwave interferometer is implemented by generating a superposition of two spinwaves and observing the interference between them, where the interference fringe is sensitive to the atomic collective motion. By heralded generation of a second order NOON state in the spinwave interferometer, we observe the interference pattern which provides a strong evidence of phase super-resolution. The demonstrated spinwave interferometer can in principle be scaled up to highly entangled state, and thus is of fundamental importance, and might be used as an inertial sensor.

9.1 Motivation

The optical interferometer [169] and the atom interferometer [170] have become essential tools for measuring position, displacement or acceleration. In these devices, a light pulse or the wave-packet of neutral atoms in an ensemble are coherently split and recombined in space or time domain by applying mechanical or optical gratings. The gravity or platform rotation will cause a motion-sensitive phase shift, which can be measured from the interference fringes.

As is well known, by exploiting suitable quantum entanglement, e.g. NOON state ($|\text{NOON}\rangle = \frac{1}{\sqrt{2}}(|N\rangle_a|0\rangle_b + |0\rangle_a|N\rangle_b)$, which denotes the N-particle entanglement in Fock states basis) or GHZ state ($|\text{GHZ}\rangle = \frac{1}{\sqrt{2}}(|1\rangle_{a_1}|0\rangle_{b_1}...|1\rangle_{a_N}|0\rangle_{b_N} + |0\rangle_{a_1}|1\rangle_{b_1}...|0\rangle_{a_N}|1\rangle_{b_N}$, which denotes the N-particle entanglement in qubit basis), the measurement precision

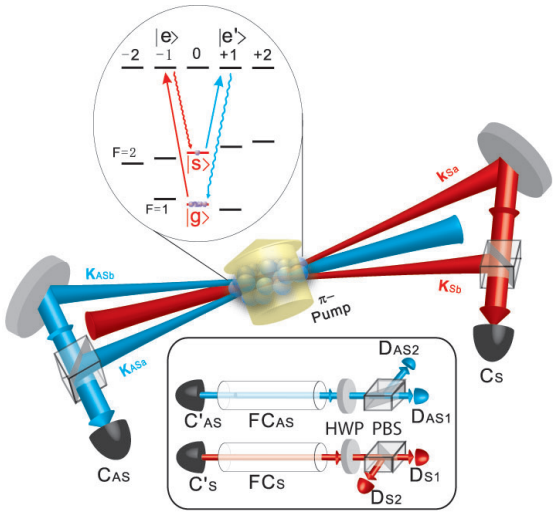

FIGURE 9.1: Experimental setup of the spinwave interferometer. The inset at the top shows the relevant Zeeman levels for the $|5S_{1/2}\rangle \rightarrow |5P_{1/2}, F' = 2\rangle$ transition of ^{87}Rb atoms. Before the experimental cycles we optically pump the atoms in $|g\rangle$ by applying two pumping lights (see Appendix), one of which is shining in from the lateral side (π-Pump) to introduce radiation pressure force. A weak σ^- polarized write pulse is applied to generate two modes of spinwave and Stokes fields via spontaneous Raman transition $|g\rangle \rightarrow |e\rangle \rightarrow |s\rangle$. The Stokes fields are collected at the angle of $\pm 0.6^0$ relative to the write beam, combined on a PBS and directed into a single mode fiber via a fiber coupler (C_S). After a controllable delay, a strong σ^+ polarized read beam induces the transition $|s\rangle \rightarrow |e'\rangle \rightarrow |g\rangle$, converting the two spinwaves into two anti-Stokes fields, which are overlapped in another PBS and then directed to a coupler (C_{AS}). Passing through two filter cells (FC) respectively, the anti-Stokes photon from C'_{AS} and Stokes photon from C'_S are then sent to the polarization analyzers combined with half wave plate (HWP), polarized-beam splitter (PBS) and single photon detectors (D), as illustrated in the inset at bottom. Filter cells are properly pumped in order to absorb the remaining leakage from read or write beams while to be transparent for the signals.

can be improved [169, 171]. For optical interferometers, the principle of the quantum-enhanced-measurement has been demonstrated by exploiting photonic NOON state, where phase super-resolution [133, 172, 173] and phase super-sensitivity [174] have been observed. However, generating atomic NOON state or GHZ state and exploiting them in atom interferometers are still challenging for current technology.

9.2 Generation of first order NOON state

To illustrate the working scheme of spinwave interferometer, we consider a cold atomic cloud with the Λ-type level structure shown in Fig. 9.1. About 10^6 atoms are initially optically pumped to $|g\rangle$. An off-resonant σ^- polarized write pulse coupling the transition $|g\rangle \rightarrow |e\rangle$ with wave vector $\mathbf{k}_{\mathrm{W}}$ is applied to the atomic ensemble along the axial direction, inducing spontaneous Raman scattering. Two Stokes fields with σ^- polarization and wave vector $\mathbf{k}_{\mathrm{S}a}$ and $\mathbf{k}_{\mathrm{S}b}$ are collected at an angle of $\theta_{a,b} = \pm\theta$ relative to the write

beam. The atom-light field in each mode can be expressed as [20] $|\Psi\rangle_i \sim |0\rangle_i^{\mathrm{S}}|0\rangle_i + \sqrt{\chi_i}|1\rangle_i^{\mathrm{S}}|1\rangle_i + \chi_i|2\rangle_i^{\mathrm{S}}|2\rangle_i + O(\chi_i^{3/2})$, where $\chi_a = \chi_b \ll 1$ is the excitation probability of one collective spin excitation in mode i ($i = a, b$), $|j\rangle_i^{\mathrm{S}}$ denotes the Stokes field S_i with photon number j, while $|j\rangle_i = S_i^{\dagger j}|0\rangle_i$ denotes the j-fold collective spin excitation in mode i, with $|0\rangle_i = \bigotimes_l |g\rangle_l$ the vacuum, $S_i^\dagger = \frac{1}{\sqrt{M_i}}\sum_l e^{i\Delta\mathbf{k}_i\cdot\mathbf{r}_l^i}|s\rangle_l\langle g|$ the creation operator of spinwave$_i$, where $\Delta\mathbf{k}_i = \mathbf{k}_{\mathrm{W}} - \mathbf{k}_{\mathrm{S}i} \simeq \mathbf{k}_{\mathrm{W}}\sin\theta_i$ is the wave vector of spinwave$_i$ and $\mathbf{r}_l^i$ the coordinate of the l-th atom in mode i.

The two Stokes fields are rotated to be horizontally ($|H\rangle$) and vertically ($|V\rangle$) polarized for mode a and b respectively, and are combined on a polarized beam splitter (PBS). The half-wave plate (HWP$_s$) is set to 22.5° to measure the Stokes photons under $|\pm\rangle = \frac{1}{\sqrt{2}}(|H\rangle \pm |V\rangle)$ basis. Neglecting high order excitations, a click on detector D_{S1} or D_{S2} will project the atomic ensembles into the superposition state

$$|\Psi\rangle = \frac{1}{\sqrt{2}}(|1\rangle_a|0\rangle_b \pm |0\rangle_a|1\rangle_b). \tag{9.1}$$

Such a spinwave superposition state can be exploited to implement the Mach-Zehnder interferometer.

Assume the atoms undergo a collective motion, e.g. motion caused by gravitational acceleration, described as $\mathbf{r}_l'^i = \mathbf{r}_l^i + \mathbf{r}_c$. Since $|1\rangle_i = S_i^\dagger|0\rangle_i = \frac{1}{\sqrt{M_i}}\sum_l e^{i\Delta\mathbf{k}\cdot\mathbf{r}_l^i}|g...s_l...g\rangle$, after the collective motion the spinwave will change to $|1'\rangle_i = e^{i\phi_i}|1\rangle_i$ with $\phi_i = \Delta\mathbf{k}_i\cdot\mathbf{r}_c$, where $\Delta\mathbf{k}_a = -\Delta\mathbf{k}_b \equiv \Delta\mathbf{k}$. Thereby, we obtain

$$|\Psi'\rangle \sim \frac{1}{\sqrt{2}}(|1\rangle_a|0\rangle_b \pm e^{-i\ 2\Delta\phi}|0\rangle_a|1\rangle_b), \tag{9.2}$$

with $\Delta\phi = \Delta\mathbf{k}\cdot\mathbf{r}_c$. It can be readily seen that the collective motion of the atoms is mapped to a relative phase in the superposition state. This phase and thus the collective motion can be measured by converting the spinwave back into photons and observing the interference pattern. In this way, if $\Delta\mathbf{k}$ is set in the direction of the gravity, one can measure the gravitational acceleration. The measurement precision is corresponding to the sensitivity of the interferometer determined by length of the wave vector $\Delta\mathbf{k}$, which is controllable in practice.

Such a single-excitation spinwave interferometer can be looked upon as the first order of a NOON state [175]. Higher order NOON state can be generated in a heralded way by using the linear optical methods (See Appendix for detail), described as $|\mathrm{NOON}\rangle = \frac{1}{\sqrt{2}}(|N\rangle_a|0\rangle_b + |0\rangle_a|N\rangle_b)$, where $|N\rangle_i = \frac{1}{sqrtN!}S_i^{\dagger N}|0\rangle_i$ denotes the N-fold excitation in mode i ($i = a, b$). Thus the collective motion of the atoms will induce a phase as $|\mathrm{NOON}'\rangle \sim \frac{1}{\sqrt{2}}(|N\rangle_a|0\rangle_b + e^{-i\ 2N\Delta\phi}|0\rangle_a|N\rangle_b)$. Note that, although the method is in principle extendable [133] to arbitrary N, the efficiency of generating the desired NOON

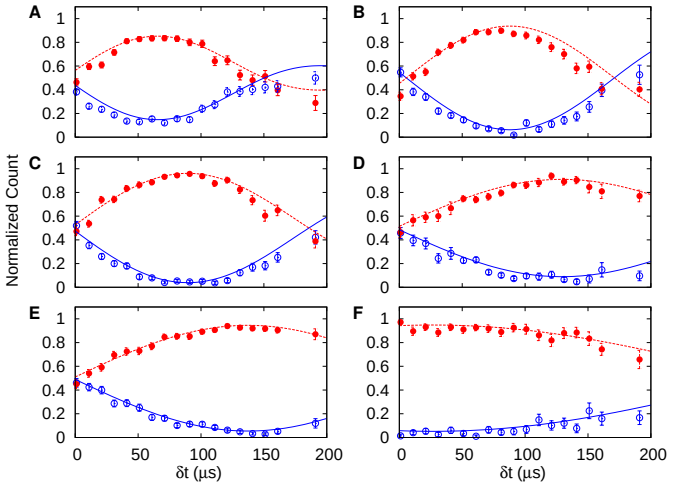

FIGURE 9.2: The fidelity of anti-Stokes field on $|+\rangle$ as a function of δt. Solid circles (open circles) represents the measured fidelity of anti-Stokes field on $|+\rangle$ on condition of a click of Stokes field on state $|+\rangle$ ($|-\rangle$). The power of the π-Pump is: **(A)** 6 mW, **(B)** 4.5 mW, **(C)** 3mW, **(D)** 1.5 mW, **(E)** 0.75 mW, **(F)** 0 mW. The experimental data are jointly fitted by using $f_{+|+}(\delta t) = (0.5 + a\sin^2(\pi\frac{\delta t}{T} + \phi_0)e^{-\delta t^2/\tau^2})/(1 + a\,e^{-\delta t^2/\tau^2})$ and $f_{+|-}(\delta t) = (0.5 + a\cos^2(\pi\frac{\delta t}{T} + \phi_0)e^{-\delta t^2/\tau^2})/(1 + a\,e^{-\delta t^2/\tau^2})$ (See Appendix for detail.). The evolution period $T = \frac{\pi}{\Delta\mathbf{k}\cdot\mathbf{v_c}}$ is measured to be **(A)** 317±18 μs, **(B)** 330±15 μs, **(C)** 378±14 μs, **(D)** 555±47 μs, **(E)** 591±30 μs, **(F)** 1177 ±152 μs. Error bars represent statistical errors, which are ±1 s.d.

state drops off exponentially [175] with N. In order to be more efficient in employing entanglement, one can exploit multiple atomic ensembles to prepare N-quanta GHZ state [64], which can be deterministically generated in a scalable way [106, 176] and share the same sensitivity as NOON state (See Appendix for details). Therefore, the spinwave interferometer would be N times more sensitive to the motion with the help of these highly entangled states and thus can be exploited to demonstrate the phase super-resolution and phase super-sensitivity.

Demonstration of the spinwave interferometers critically depends on the coherence time of the spinwave excitation. In the experiment, we implement the spinwave interferometer with ^{87}Rb atoms trapped in a magneto-optical trap at a temperature of about 100 μK. By exploiting the clock transitions of, $|g\rangle = |5S_{1/2}, F = 1, m_F = 0\rangle$ and $|s\rangle = |5S_{1/2}, F = 2, m_F = 0\rangle$ as the two ground states to avoid the deleterious effects induced by magnetic field, e.g. Larmor precession or inhomogeneous broadening, we achieve the coherence time of the spinwave of about 200 μs, which is limited by the dephasing of the spinwave induced by atomic random motion [26]. With such a coherence time, it is now possible to study the motion sensitivity of the spinwave interferometer. With our setup we obtain a typical generation probability for the spinwave superposition state (Eq. 9.1) of about 300 per second.

To show the motion sensitivity, we introduce a collective motion during the pumping

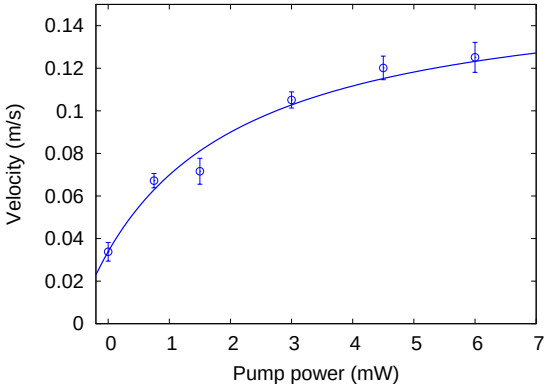

FIGURE 9.3: The atomic velocity as a function of the π-Pump power. The initial velocity induced by the unbalance of other lasers is about 0.03 m/s. The velocity acquired in the pumping stage increases with the pumping power until reaching a plateau of about 0.12 m/s. Error bars represent statistical errors, which are ± 1 s.d.

stage, where the atoms absorb photons from the π-Pump light and the $2 \rightarrow 2$ pump, and then decay spontaneously. Since the $2 \rightarrow 2$ pump is shined with the cooler light from six directions, and spontaneous emission is in arbitrary directions, on average they give no contribution to the collective motion. While the π-Pump light from the lateral side acts as a pushing laser, which causes a radiation pressure force and accelerates the atoms [177] until they are pumped to $|g\rangle$. We denote the velocity acquired in this process by $\mathbf{v_p} = v_p \hat{\mathbf{e}}_p$. Besides, the unbalance of other lasers, i.e. cooler, repumper, and etc., will also induce an initial velocity $\mathbf{v_0}$ when the atoms are released. Therefore the generated superposition state $|\Psi\rangle$ (Eq. 9.1) will evolve to $|\Psi'\rangle$ (Eq. 9.2) after a free evolution time of δt, where $\Delta\phi = \Delta\phi(\delta t) = \Delta\mathbf{k} \cdot \mathbf{v_c}\delta t$ with $\mathbf{v_c} = \mathbf{v_p} + \mathbf{v_0}$ and in which the atomic random motion is neglected.

To measure $\Delta\phi(\delta t)$, a strong σ^+ polarized read light, coupling the transition $|e'\rangle \rightarrow |g\rangle$, counter-propagating with the write light, converts the collective excitations into σ^+ polarized anti-Stokes fields. The anti-Stokes fields from two atomic ensembles are rotated to be perpendicular to each other and combined on a PBS (Fig. 9.1), which can be described by $|\Psi\rangle_{\mathrm{AS}} \sim \frac{1}{\sqrt{2}}(|H\rangle_{\mathrm{AS}} \pm e^{-i(2\Delta\phi(\delta t))} e^{i(\phi_1+\phi_2)} |V\rangle_{\mathrm{AS}})$, where ϕ_1 (ϕ_2) represents the propagating phase difference between two Stokes (anti-Stokes) fields before overlapping. In the experiment, the total phase $\phi_1 + \phi_2$ is actively stabilized and set to a fixed value [116]. The interference pattern is observed by setting the HWP_{AS} at 22.5° to detect the anti-Stokes fields under $+/-$ basis. The experiment results are shown in Fig. 9.2. We change the power of the π-pump and measure the fidelity of anti-Stokes field on $|+\rangle$ as a function of δt, on condition of a click of Stokes field on state $|+\rangle$ (solid circles) and $|-\rangle$ (open circles). The collective motion can be obtained from the period of the interference pattern $T = \frac{\pi}{\Delta\mathbf{k}\cdot\mathbf{v_c}}$, which varies from 300 μs to 1200 μs.

The velocity that the atoms acquired as a function of the π-Pump power is shown in Fig. 9.3. One can see that the average velocity will first increase with the π-Pump power, and reach a plateau when the π-Pump is sufficient strong. This might be related with the pumping efficiency in the pumping stage, since when all the atoms are pumped to the $|g\rangle$, the atoms will not absorb photons from π-Pump any more. Note that, the population in other Zeeman sub-levels arising from insufficient pump will not affect the interference pattern since the decoherence time in other states is very shot (about microseconds) due to inhomogeneous broadening.

9.3 Generation of second order NOON state

To demonstrate the advantage of quantum entanglement, we generate the second order NOON state, which can be described as $|\Psi\rangle_{NOON} = \frac{1}{\sqrt{2}}\left(|2\rangle_a|0\rangle_b - |0\rangle_a|2\rangle_b\right)$. This is achieved with the help of a feedback circuit [148] by registering the coincidence count between single photon detectors D_{S1} and D_{S2}, with a typical generation probability of 1 per second. Note that, the noise in preparing the NOON state is negligible (see appendix for details). After a free evolution time of δt, we have $|\Psi\rangle_{NOON'} \sim \frac{1}{\sqrt{2}}(|2\rangle_a|0\rangle_b - e^{-i(4\Delta\phi(\delta t)}|0\rangle_a|2\rangle_b)$. By converting the second order state to anti-Stokes fields and measuring the coincidence count between detectors D_{AS1} and D_{AS2}, we obtain the phase $\Delta\phi(\delta t)$. The coincidence count per successful generation of NOON state event is shown in Fig. 9.4.a. For comparison, we give the interference fringe for the first order NOON state under the same condition as shown in Fig. 9.4.b, which is taken directly after the measurement of the second order interference pattern. One can see that interference fringes for N=2 state oscillates about twice faster than that of N=1, which provides a strong evidence of phase super-resolution. Besides, the interference fringe for N=2 also decays faster than N=1, since NOON state is also sensitive to decoherence [169]. The N=2 data are fitted using a model by taking into account both the oscillation and decoherence, where the parameters are determined by optimizing the reduced chi-square (see Appendix for details). The fitting gives an evolution period of $T' = (73 \pm 7)\ \mu$s) for N=2, which is slightly shorter that half of $T = (220 \pm 17)\ \mu$s for N=1. This is mainly because that due to decoherence, we can not observe more than one evolution period, and some imperfections in experiment such as the drifting of the laser power and drifting of the coupling between different channels, will contribute errors to the signal. Note that, the data in Fig. 9.4 are taken under π-pump power of 6 mW. There's a slightly change of the initial velocity of the atomic ensemble compared to the original condition, which makes the first order evolving period slightly different to the one given in Fig. 9.2.a.

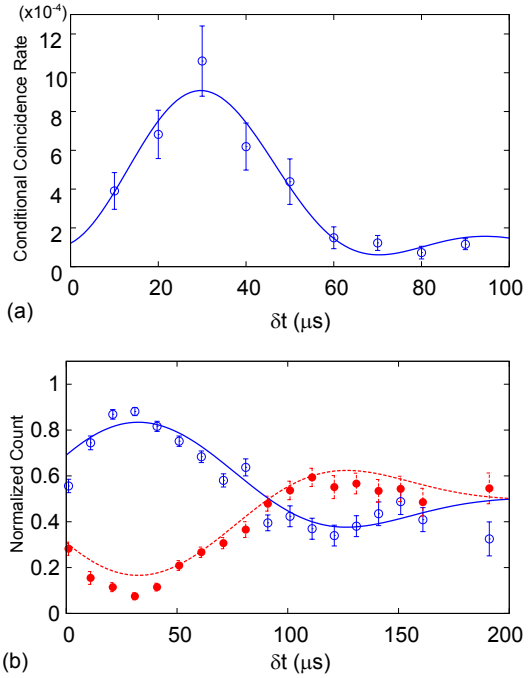

FIGURE 9.4: Comparison of the performance of the first and second order NOON state. (a), The normalized coincidence count for the second order NOON state as a function of δt. The experimental data are fitted by using $c(\delta t) = b\sin^2\left(\pi\frac{\delta t}{T'} + \phi_0'\right)e^{-2\delta t^2/\tau^2} + de^{-\delta t^2/\tau^2}$. The optimization fitting gives an evolution period of $T' = (73 \pm 7)$ μs (See Appendix for details). (b), The interference pattern for $N = 1$ under the same condition. The lines are the fitted with the same method as in Fig. 9.2. The fitting evolution period is $T = (220 \pm 17)$ μs. Error bars represent statistical errors, which are ± 1 s.d.

9.4 Discussion

With emphasis, we note that NOON state is not only more sensitive to the collective motion, but also more sensitive to decoherence [169, 178]. Therefore, to achieve phase super-sensitivity, the coherence time of our NOON state has to be much larger than its free evolution time [179, 180]. However, in our experiment, since the coherence time is comparable to the free evolution time, the gain obtained by using N=2 NOON state is partially offset by the corresponding faster decoherence, and thus we failed to achieve phase super-sensitivity. It is expected that, our NOON state will show the desired phase super-sensitivity with the improvement of the coherence time.

In summary, we have demonstrated a heralded atomic NOON state in a spinwave interferometer. In the experiment, the second order NOON state is generated, which provides a strong evidence of phase super-resolution. Higher order spinwave NOON state with small N= 4 or 5 can be generated in current setup to further demonstrate the principle of quantum-enhanced-measurement. Besides, since the quantum memory is automatically built in our system, N-quanta spinwave GHZ state can be deterministically generated

in a scalable way, which is a distinct advantage compared with photonic entanglement. Thus the spinwave interferometer might be used as an inertial sensor.

Chapter 10

Efficient Entanglement Swapping with Quantum Memories

In the chapter we report experimental realization of efficient entanglement swapping by using quantum memories and the quantum feedback technique. Previously, due to the probabilistic character of entangled photon sources, entanglement swapping will success with a rather small probability only when two pair of photons are created simultaneously. In our experiment, two pairs of photon-spinwave entanglement are created asynchronously in separate cold atomic ensembles. The swapping process is realized by converting the spinwave state for each site to photons again and measuring the converted photon pair in Bell basis. An enhanced factor of 257 is observed. Entanglement property after swapping is characterized by a violation of Bell-CHSH inequality.

10.1 Motivation

Entanglement swapping [17, 71] lies at the heart of quantum repeater [18] and quantum relay [181, 182]. However, generally the photonic entanglement are created in a probabilistic way. In a typical spontaneous parametric down-conversion (SPDC) setup [58], when an ultraviolet pulse goes through a nonlinear crystal, with a rather small probability (p is usually less than 1 percent) a pair of entangled photons can be created. If one uses two pairs of this type entangled photons to do quantum swapping, the success probability would be p^2. If the stages of entanglement swapping become larger, the success probability would decrease exponentially as a function of number of stages (p^n). This problem largely limits further application of entanglement swapping in quantum repeater and quantum relay.

On the other hand, atomic ensembles provide another method to create photon-photon entanglement [143–145] with one photon stored in the collective state of atoms. A typical cycle of these experiments consists of the following steps. First, a weak write pulse will shine on the ensemble, with a rather small probability, there will be one atom in the ensemble got a Raman transition, and simultaneously creating an anti-Stokes photon. In this stage, the scattered anti-Stokes photon is entangled with the collective spinwave state of the atoms. The atomic ensemble can preserve the spinwave state for a period typically between several μs to several ms [24, 26, 27]. After a controllable delay, by shining a read pulse, the stored spinwave will convert to the Stokes photon by using collective enhancement [20]. The Stokes photon is entangled with the anti-Stokes photon.

If we use this type of delayable entangled photons from cold atomic ensembles to replace the traditional SPDC entangled photons to do entanglement swapping, by incorporating the quantum feedback technique [157], it is possible to increase the efficiency of entanglement swapping significantly. In the case of SPDC, assuming that the experiment period is T, and the possibility to generate one photon pair with one experiment cycle is p (typically less than 1 percent), then the time required for one time successful entanglement swapping would be proportional to $(1/p^2)T$. While in the case of delayable entangled photons, we can use the feedback technique, which means that we will start to read out the Stokes photon only if we detect an anti-Stokes photon. The complete procedure is in three steps. First, the first source (A) repeats the write process until one anti-Stokes photon is detected with its polarization state measurement result recorded. Second, the second source (B) repeats the write process until an anti-Stokes photon is detected on his site. Third, both sites (A and B) simultaneously start the read process, converting the atomic spinwave states to the polarization states of Stokes photons, which are subjected to a joint Bell state measurement. In this scheme, the total time required is only proportional to $(2/p)T$, in which the writing cycle is assumed to be T. In the above new scheme, one critical requirement is the long coherence time required for site A, if the coherence time is shorter than $(1/p)T$ which means that within the lifetime of the spinwave at site A the probability to detect an anti-Stocks at site B is less than 1, the enhanced effect will be weakened.

10.2 Experimental setup

The architecture for our experiment is shown in the Fig. 10.1(b). Two cold ^{87}Rb atomic ensembles released from magneto-optical traps (MOT) are utilized, for the two sites. Within each site, the geometric configuration for the control beams (read, write) and

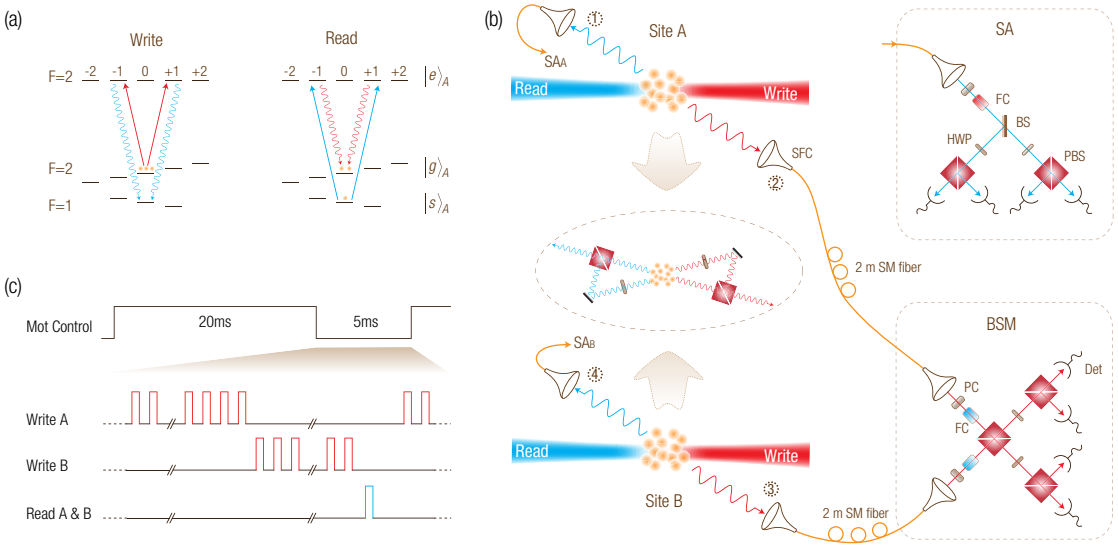

FIGURE 10.1: (a) Energy levels used for site A, with $|g\rangle_A = |5S_{1/2}, F = 2, m_F = 0\rangle$, $|s\rangle_A = |5S_{1/2}, F = 1, m_F = 0\rangle$ and $|e\rangle_A = |5P_{1/2}, F = 2\rangle$. Linear polarization is used both for read/write and anti-Stokes/Stokes. (b) Experimental Setup. BS, beam-splitter; PBS, polarized beam-splitter; PC, polarization controller; Det, single-photon detector. (c) Time sequence diagram of our experiment. The duration for the write and read pulses is 50 ns. The write cycle time for site A is $T_A = 2.9\,\mu$s, for B is $T_B = 0.9\,\mu$s).

detection beams (anti-Stokes, Stokes) is show in the inset of Fig. 10.1(b). All of the four beams are in the horizontal plane. In order to have good quality of mode-matching, all the four beams are coupled with single-mode (SM) fibers. The direct distance between these sites is about 60 cm. The write-out anti-Stokes photons are led to their polarization state analyzers (SA), respectively. The read-out Stokes photons are led to a joint Bell state measurement (BSM) apparatus by using two SM fibers of 2 m length. Within the BSM apparatus, by setting two half-wave plates (HWP) to 45°, we are able to distinguish two Bell states out of four, i.e., the state $|\Phi^+\rangle$ and $|\Phi^-\rangle$. The leakage of write (read) to the mode of anti-Stokes (Stokes) is suppressed through utilizing Rb filtering cells (FC) [148].

The energy levels used for site A, is shown in Fig. 10.1(a). A pair of ground states $|g\rangle_A$ and $|s\rangle_A$ are chosen since they are a pair of "clock states" for which the transition frequency is insensitive to magnetic field. A magnetic field of about 3 G is applied along the read/write direction to define the quantization axis. Initially the atoms are pumped to $|g\rangle_A$ by using two pumping beams. One couples the transition $|5S_{1/2}, F = 1\rangle \rightarrow |5P_{3/2}, F = 2\rangle$, and the other couples the transitions $|5S_{1/2}, F = 2\rangle \rightarrow |5P_{1/2}, F = 2\rangle$ with $\Delta m_F = 0$ which is called the "Π pump". In a previous work [183], the Π pump was applied in the horizontal directions. We found that it would induce a collective movement in the spinwave direction, which would give rise to a time-dependent phase shift in the stored spinwave state. In order to reduce this effect, we change the direction to be vertical from down to top. In this way, the movement induced by the Π pump

is perpendicular to the spinwave direction, the component in the spinwave direction is minimized. Due to the finite temperature for the atomic ensemble, during the period of spinwave storage, the random movement of atoms will distort the phase in the spinwave state, which will limit the spinwave coherence time. This decoherence will lower down if we reduce the detection angle (between write and anti-Stokes) [26]. The smaller the detection angle is, the longer wavelength the spinwave will have, thus less sensitive to the random movement of individual atoms. In our setup, the detection chosen is about 0.5°. For even smaller angles, the leakage of write and read to the modes of anti-Stokes and Stokes will be beyond the capability of our single-stage filtering cell. While for site B, since it is not required to have long coherence time, we choose a Λ system which is composed of $|g\rangle_B = |5S_{1/2}, F = 2\rangle$, $|s\rangle_B = |5S_{1/2}, F = 1\rangle$) and $|e\rangle_B = |5P_{1/2}, F = 2)$. Three pairs of Helmholtz coils are used to compensate the ambient magnetic field. The detection angle chosen is about 1.5°.

10.3 Experimental results

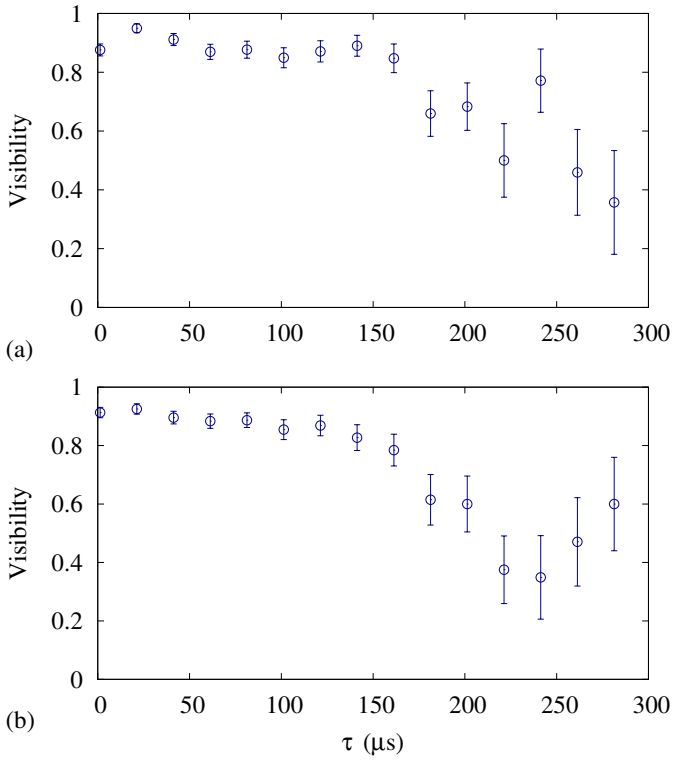

FIGURE 10.2: Measured polarization correlation visibility in $|H\rangle/|V\rangle$ basis (a) and $|+\rangle/|-\rangle$ basis (b), as a function of storage time for site A. Error bars represent statistical errors.

A prerequisite for the demonstration of efficient entanglement swapping is the long coherence time for the photon-spinwave entanglement of site A. There are three main mechanisms which will affect this coherence time, i.e., influence of residual magnetic

field [161], free expansion of the atom cloud and spinwave dephasing due to random movement of individual atoms. In our case the last mechanism is dominant [26]. We can calculate the lifetime given by this mechanism using the formula $\tau_L = 1/(\Delta k v)$, where Δk is the amplitude of the spinwave vector which is related with the detection angle θ in the relation of $\Delta k = 2\pi\theta/\lambda$, and v is the average velocity of individual atoms, which is related to the atomic temperature T_e with the relation of $v = \sqrt{k_B T_e/m}$ with k_B the Boltzmann's constant and m is the atomic mass. Given the typical temperature of 100 μK and detection angle of 0.5°, the resulting lifetime is $\tau_L = 148\,\mu$s, which coincides with our experimental result shown in Fig. 10.2. Slight phase shifting observed in the measurement of polarization correlation visibility in $|+\rangle/|-\rangle$ basis with $|\pm\rangle = 1/\sqrt{2}(|H\rangle \pm |V\rangle)$ in Fig. 10.2(b) is due to the misalignment of Π pump direction and the imbalance of cooling and repumping beams which are used during MOT loading.

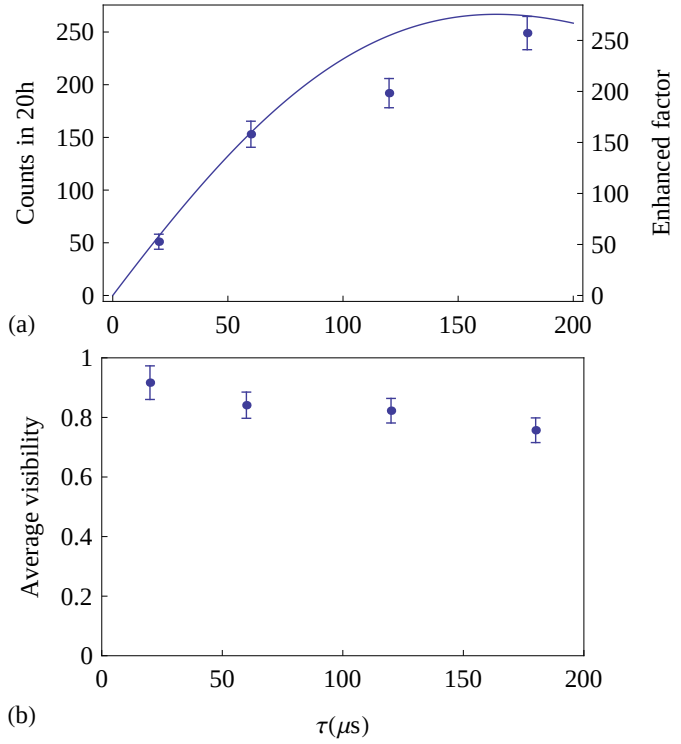

FIGURE 10.3: (a)Measured 4-photon coincidence count rate as a function of τ. (b)Measured polarization correlation visibility (averaged in $|H\rangle/|V\rangle$ and $|+\rangle/|-\rangle$ basis) of photon 1 and photon 4 as a function of τ. Error bars represent statistical errors.

With such a long-lifetime photon-spinwave entangled state, we are able to demonstrate the efficient entanglement swapping using quantum feedback. In our experiment all the electrical pulse sequences are generated using a FPGA card. A brief diagram for the time sequences is shown in Fig. 10.1(c). The repetition rate is 40Hz. For each 25 ms cycle, the beginning 20 ms is utilized for MOT loading for both sites. After mot loading, another 1 ms is spent on pumping all the atoms to the required original state for each site. Within the last 4 ms, we will start and repeat the write process for site A until we

get a click within the four detectors in SA_A. Then site A will halt, we start to repeat the write process for site B. How long site A can wait (τ) is determined by the coherence time of the spinwave. Within time τ, if a click is got with the four detectors in SA_B, the read process will start simultaneously for both sites. While if it is failed, the write process for site A will be restarted. During the write process for both sites, a clean pulse is applied to pump the atoms back to the required original state at the end of each write cycle.

After the read process, the entangle sate between photon 1 and 2 is $|\Phi^+\rangle_{12}$, while for photon 3 and 4 it is $|\Psi^-\rangle_{34}$. If the BSM result for photon 2 and 3 is $|\Phi^+\rangle_{23}$, the left photons 1 and 4 will be entangled in the state of $|\Psi^-\rangle_{14}$; if the BSM result is $|\Phi^-\rangle_{23}$, photon 1 and 4 will be entangle in $|\Psi^+\rangle_{14}$. In order to verify the enhanced effect, we measured 4-photon coincident count rate and the polarization correlation visibility averaged in $|H\rangle/|V\rangle$ and $|+\rangle/|-\rangle$ basis of photon 1 and 4 as a function of the waiting time τ at site A. The result is shown in Fig. 10.3. From it we can see that the count rate will rise as we increase the waiting time τ at site A. A theoretical curve for the count rate is calculated based on the experimental parameters, such as excitation probability, retrieval efficiency, and write cycle time for each site, etc. There are no free parameters used. The enhanced factor is defined as the ratio between the count rate in the case with and without feedback. When τ equals to 180 μs, a maximal enhanced factor of 257 ± 16 is observed; while at the same time the average visibility is 0.76 ± 0.04, which is still enough for a violation of Bell-CHSH inequality.

In order to evaluate the entanglement quality between photon 1 and 4 after entanglement swapping, we measure the Bell-CHSH inequality [90]. In this inequality the value S is defined as

$$S = |E(\phi_A, \phi_B) - E(\phi_A, \phi'_B) + E(\phi'_A, \phi_B) + E(\phi'_A, \phi'_B)|$$

where ϕ_A and ϕ'_A are two polarization measuring angles for photon A, and ϕ_B and ϕ'_B for photon B, and $E(\alpha, \beta)$ is the correlation coefficient between these two photons [58]. Violation of this inequality ($S > 2$) is a direct proof of entanglement. Our measure result is $S = 2.67 \pm 0.35$ for the BSM result of $|\Phi^+\rangle$, and $S = 2.40 \pm 0.37$ for the BSM result of $|\Phi^-\rangle$, which clearly confirms that it is a successful entanglement swapping experiment.

We note that this entanglement swapping experiment is done in a delayed choice way [184], since photon 1 and 4 are measured before photon 2 and 3 with a time interval of 3.35 μs. During this time interval, we have the choice to decide to measure photon 2 and 3 in all kinds of basis. One drawback given by this delayed choice feature is the difficulty for multi-stage entanglement swapping [185]. However, there are still a lot of other applications. One interesting idea is the concept of bank for quantum cryptography. The bank provides a large amount of photon-spinwave entangled pairs.

Each customer goes to the bank and measures the photonic states randomly in the basis of $|H\rangle/|V\rangle$ or $|+\rangle/|-\rangle$ in series, and records the information of basis chosen and measurement result for individual photons classically. The bank will store the quantum states of spin-wave. Afterwards, if customer A and B want to build a series of quantum keys, no matter where they are, they just telephone the bank to convert their stored spinwave states to photons and make joint Bell state measurement in series and send them the measured results classically. Based on this information, A and B just follow the standard procedure of quantum cryptography [129] to extract the final absolute secure keys. The above scheme has the advantage that the bank does not need to be trustful, there will be no information of the final keys leaked to the bank. We do a proof-of-principle demonstration of this scheme. In this experiment, the random basis selection of photon 1 and photon 4 is realized with the use of BS, see Fig. 10.1(b). The information for the basis chosen and measurement results are recorded on an electrical card. The spinwave states are stored for a duration of 3.35 μs. The measured quantum bits error rate (QBER) is $9.3 \pm 2.2\%$.

Additionally, We want to note that this experiment can also be viewed as quantum communication over a high-loss channel. In principle, we can assume that the excitation probability can reach 1, e.g., by using the Rydberg blockade effect [186]; the retrieval efficiency can be improved to near 1, e.g. by adding additional cavity in the mode of Stokes [160]. Therefore, we could make a further assumption that the relatively small excitation probability and retrieval efficiency are equivalent to a channel attenuation. In our case, the calculated attenuation is 1.1×10^{-9}. For a typical value of 0.2 db/km attenuation of standard telecommunication fibers, the equivalent communication distance is already 448 km.

10.4 Discussion

In summary, we have reported an experimental realization of efficient entanglement swapping by using quantum memories and quantum feedback technique. An enhanced factor of 257 is observed. The entanglement property after swapping is characterized by a violation of Bell-CHSH inequality. A proof-of-principle demonstration of the concept of quantum cryptography bank has been done with this efficiency-enhanced entanglement swapping. This realization and the methods developed in this experiment would have various novel applications in the field of quantum communication with photons and atoms.

Chapter 11

Quantum Teleportation Between Atomic Ensembles

11.1 Motivation

Quantum teleportation is a process to transfer a quantum state of an object without transferring the state carrier itself. So far, most of the teleportation experiments realized are within the photonic regime. For the teleportation of stationary states, the largest system reported is a single ion. Our purpose is to teleport the state of an atomic cloud to another atomic cloud.

11.2 Experimental setup

In our experiment two atomic ensembles are utilized. Each ensemble consists 10^8 ^{87}Rb atoms. All the atoms are cooled to a temperature about 100 μK in separate MOTs. The layout of our experiment is shown in Fig. 11.1. The atomic state is prepared in Site A. While in Site B, entanglement between a single-photon (3) and the collective spinwave sate of the atomic ensemble is created. To realize the teleportation between these two atomic ensembles, first, photon 2 in site B is sent to site A through a fiber link. Second, the atomic state prepared in site A is converted to a single-photon (photon 2). Third, these two single-photons (2 and 3) are subjected to a joint Bell state measurement. The fiber link can be switched between two case, namely the short fiber case (2 m) and the long fiber case (150 m).

The energy levels for both sites are shown in Fig. 11.1 For site A, originally all the atoms are prepared in the groud state of $|5S_{1/2}, F = 2\rangle$. While for site B, all the atoms are

prepared to be in the ground state of $|5S_{1/2}, F = 1\rangle$, in order to make sure that the frequency of readout photon of site A matches the frequency of writeout photon of site B. The excited state chosen is $|5P_{1/2}, F = 2\rangle$. The wavelength required for the read and write laser is arround 795 nm. The frequencies chosen for the write and read lasers are resonant to the corresponding transitions. The polarizations for write and read are linear, but orthogonal with each other. The polarization of writeout signal photon and the readout idle photon are also linear.

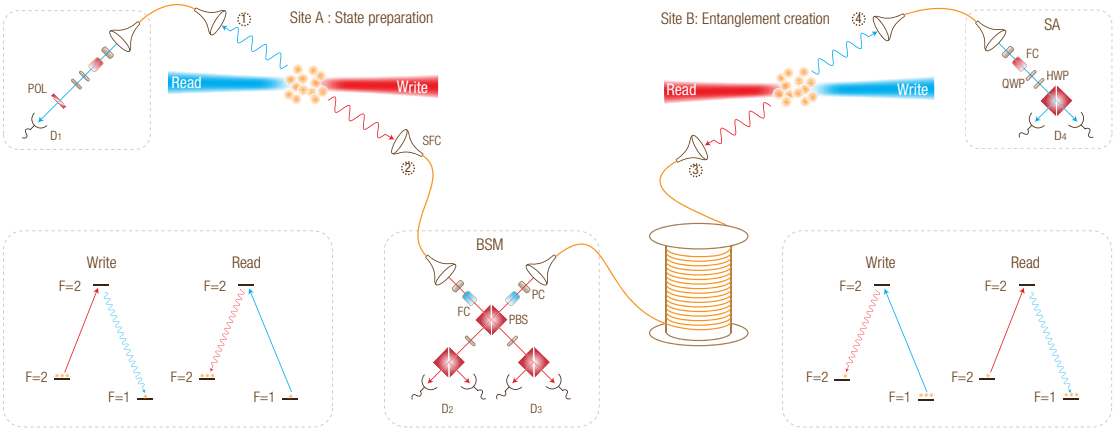

FIGURE 11.1: Layout of the experiment

For the detection of the signal and idler photons, we need to get rid the leakage of write and read pulses. We have three stages of filtering of the leakage. The first stage is the spacial filtering. In our case the angle between single-photon detection directions and the control beam (write and read) is about 0.5 degree (to be confirmed). This will give a suppression rate of 10^{-3} (needs to be calculated). The second stage is the polarization filtering. Since the polarization between signal (idler) photon and write (read) pulse is different, a PBS is used as a filter, which will give a suppression rate of 10^{-2}. The last stage is the frequency filtering with atomic vapor cells. Inside this vapor cells, the Rb atoms are heated to a temperature of about 70°. Before the signal (idler) enters the cell, the atoms are optical pumped the states for which the leakage of write (read) will be strongly absorbed. This will give a suppression rate of 10^{-2} for the leakage. With these three stage of filtering, we are able to get rid of the contributions of leakage light during single-photon detection.

11.3 Control sequences

The time sequences for the main control signals are shown in Fig. 11.3. All the signals are generated using a FPGA logic card. During the MOT load time (10 ms), the cooler and repumper lasers are tuned on to capture and cool down the atoms. During the

experiment time of 3 ms, we repeat the process of write and read. In the following we will use two modes, one is called the deterministic preparation mode, and the other is called heralded preparation mode. The main difference is that in the deterministic mode atomic state is prepared in predetermined periodical time points, while in the herald mode state preparation time is random. Details of each mode will be talk in the following sections. After a successful state preparation, we will start to convert the atomic state to a single photon in site A by applying the Read A signal and create the photon-spinwave entanglement in site B by applying the Write B signal. The relative delay between these two signals are adjusted precisely to make sure that photon 2 and photon 3 arriving at the PBS in the Bell state measurement simultaneously in order to achieve good time overlap. Avalanched single-photon detectors are gated according to the time when the control pulses are applied.

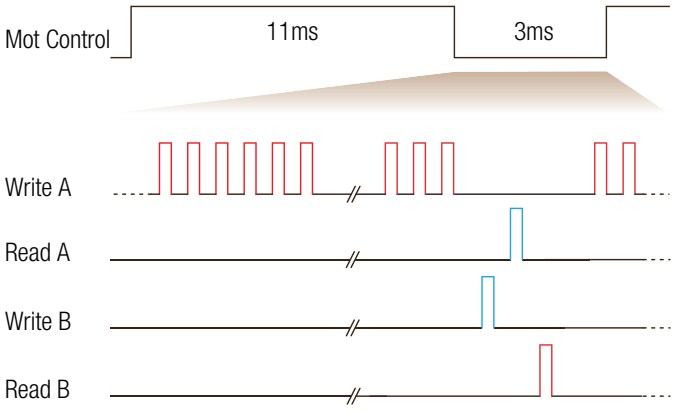

FIGURE 11.2: Time sequences for the experimental control signals.

11.4 Deterministic State preparation

Deterministic sate preparation means that one will know in advance when a state is prepared and ready for further use. Usually the time points are in a periodic sequence. We use the double-path Raman scattering precess [20, 143] to prepare the original state for the ensemble. Due to the probabilistic character of this process, the excitation probability (p) has to be rather small (usually bellow 1%) in order have high ratio between single excitation events and multi-excitation events. Therefore we have to write many times before we detect a write-out signal photon. This a also a probabilistic process, we can not predict at what time we will get such a click.

But if the spinwave state of the atomic ensemble has a long lifetime (τ_l), it possible to make the preparation process deterministic. Let us assume that the teleportation process is running periodically with a period of T. The write cycle time is Δ. In average, we have to write $1/p$ times in order to get a click of the signal photon. Therefore, we have

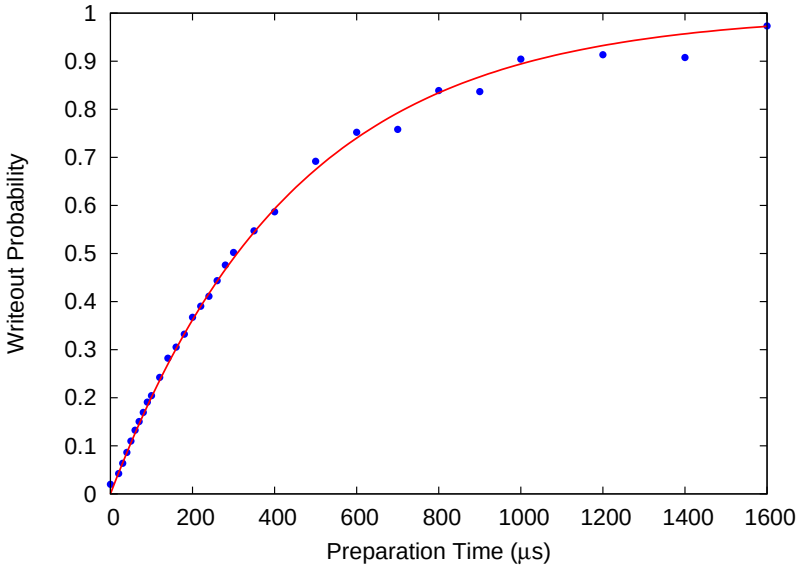

(a)

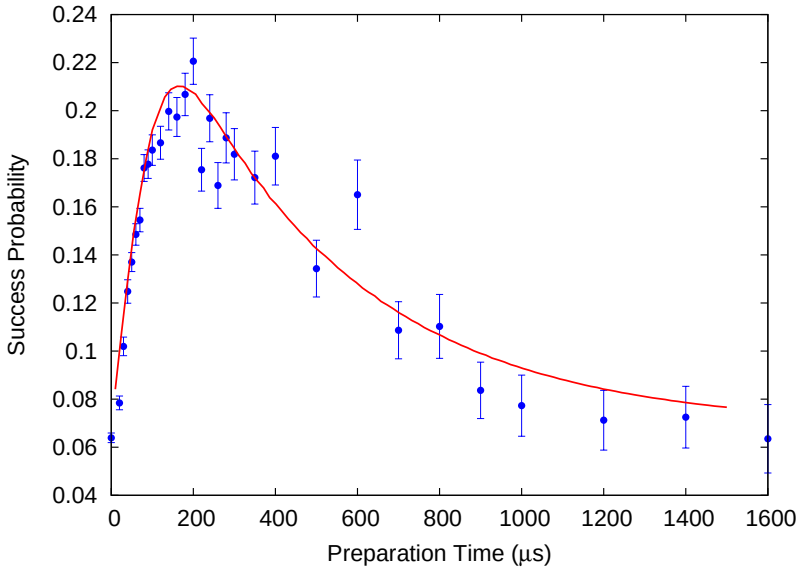

(b)

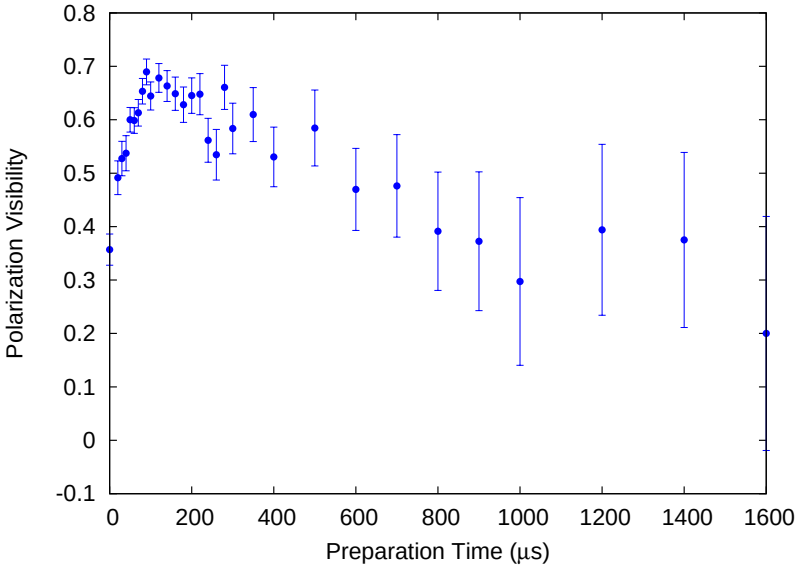

(c)

FIGURE 11.3: Deterministic state preparation results.

one requirement $\Delta/p \ll T$. Since the write process is probability, it is even possible to get a click at beginning of T, which means that the atomic spin-wave state has to be able preserved longer than the preparation time ($T \ll \tau_l$). In together, we have the following equation:

$$\Delta/p \ll T \ll \tau_l. \tag{11.1}$$

According to this equation, we should minimize Δ and have a reasonable large τ_l. In our case[1], The minimum Δ we can achieve is 1.35 μs. The main limitation is the π pumping beam. In our experiment, we apply the π pumping to $m_F = 0$ after every 4 times of write, with a duration of 3 μs. The excitation probability typically is 0.003. The average time to successfully write out a signal photon is about 450 μs. While the lifetime of the atomic spinwave state measure is 129 μs.[2] It is obvious no matter how we choose T, we will no be able to fulfill the relation in Eq. 11.1. Even through, we have done some preliminary experimental investigations.

First we measure the writeout probability as a function of preparation time T. It is defined to be the probability to detect a signal photon within T. The result is shown in Fig. 11.3(a). We fit the data with a function of $1-(1-p)^{T/\Delta}$. The second term in this function has the meaning that every write trial in T fails. During the fitting we make p as a parameter. The fitted result for p is rather close the value we measured in other methods.

Second we measure the successful probability as function of T. It is the probability to have the prepared atomic state well in the desired state at the end of T. Experimentally, it is measured as the ratio of $P_i(T)$ to η_0. $P_i(T)$ is the probability to detect an idler photon when we convert spinwave to single-photons at each end of T. η_0 is the retrieval efficiency without time delay. The result is shown in Fig. 11.3(b). When T is around 200 μs, the success probability reaches it peak value of 22%. Before 200 μs, the increase of writeout probability is main cause for it to rise. After 200 μs, since the spinwave lifetime is not long enough, at the end of T, spinwave dephasing already partially distorted the atomic state, thus reducing the conversion efficiency. The last, we measure the polarization correlation visibility. When T is small ($< 200\ \mu s$), the visibility is low due to two reasons. One is due the contribution of readout background noise. The other is due to the imperfect π pumping process. The visibility after 800 μs is higher than expected is caused but the imbalance of readout background noise in different channels.

[1] For this part of deterministic state preparation, the energy levels used for site A is different from Fig. 11.1. A pair of "clock" states $|5S_{1/2}, F = 2, m_F = 0\rangle$ and $|5S_{1/2}, F = 1, m_F = 0\rangle$ are used for the two ground states. In order to pump atoms to the specified m_F state, a pair of π polarized pumping beams are applied in the vertical direction coupling the transition of $|5S_{1/2}, F = 2\rangle \rightarrow |5P_{1/2}, F = 2\rangle$.

[2] Even through in a previous experiment [26] a lifetime of 1 ms was observed, we are not able to create photon-spinwwave entanglement with one MOT using the double-path scheme [143] since colinear configuration has to be adopted to have a long wavelength for the spinwave.

From the measurements, we have the following conclusions. First the π pumping process needs to be improved by increasing the pumping duration. Second and most importantly, the spinwave lifetime is far less than required. Fig. 11.4 is the numerically calculated result. For a successful preparation probability of 90%, the lifetime required is about 4.5 ms.

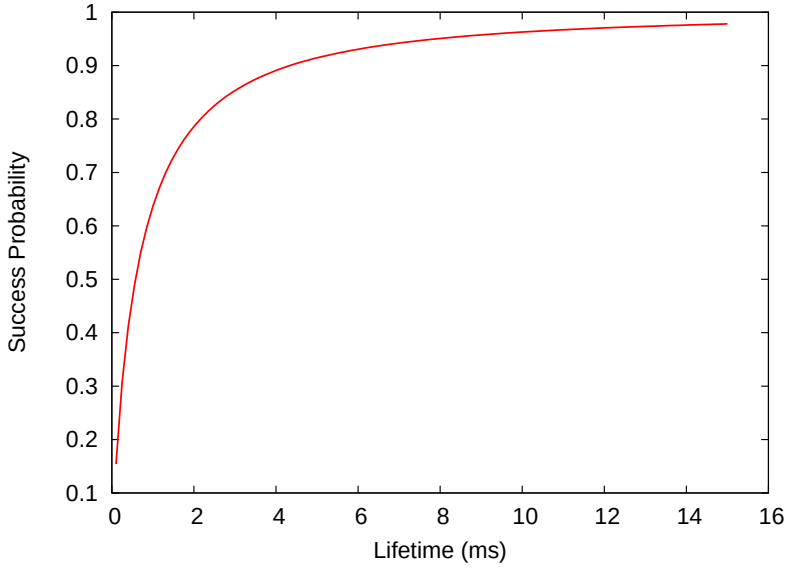

FIGURE 11.4: An estimation for the lifetime required

11.5 Heralded state preparation

Since we do not have a photon-spinwave entanglement with long enough lifetime as discussed in the previous section, in this teleportation experiment, we adopt the heralded preparation mode. It means that we can not predict when the state preparation will be ready, but will instead provide a trigger signal once the state preparation is ready. One we get such a trigger signal, the read precess of site A and write process of site B will be started immediately.

The entangled state created during the write process at site A can be expressed as:

$$|\Psi^-\rangle_{1A} = 1/\sqrt{2}(|0\rangle_1|1\rangle_A - |1\rangle_1|0\rangle_A) \tag{11.2}$$

where the subscript 1 denotes the writeout signal photon and A denotes the atomic state in site A; for the photonic state, $|0\rangle$ ($|1\rangle$) denotes horizontal (vertical) polarization; for the atomic state, $|0\rangle$ ($|1\rangle$) denotes the spinwave mode which is to the right (left) side of the write beam. In order to prepare atomics to the desired state, we just make a projection measurement of the photonic qubit in the corresponding basis. For experimental point

of view, we just need to add a polarizer before photon 1 goes to the detector, with the angle set orthogonal to the desired atomic state. Then repeat the process of write until a signal photon is detected. Once we get such a trigger signal, it mean that the state preparation is finished.

To verify the atomic state and evaluate the preparation fidelity, by shining a strong read pulse, we convert the atomic spinwave state back to a idler photon and measure its polarization. During the conversion, we have $|0\rangle_A \rightarrow |0\rangle_2$ and $|1\rangle_A \rightarrow |1\rangle_2$ where subscript 2 represents photon 2 in Fig. 11.1. The polarization state of photon 2 is analyzed using the quantum tomography technique [92], with the result shown in Fig. 11.5. Six states from three mutually unbiased bases are chosen, including $|0\rangle/|1\rangle$ $|+\rangle/|-\rangle$ and $|R\rangle/|L\rangle$ with $|\pm\rangle/ = 1/\sqrt{2}(|0\rangle \pm |1\rangle)$ and $|R/L\rangle/ = 1/\sqrt{2}(|0\rangle \pm i|1\rangle)$. The average fidelity for these six states is $97.5 \pm 0.2\%$.

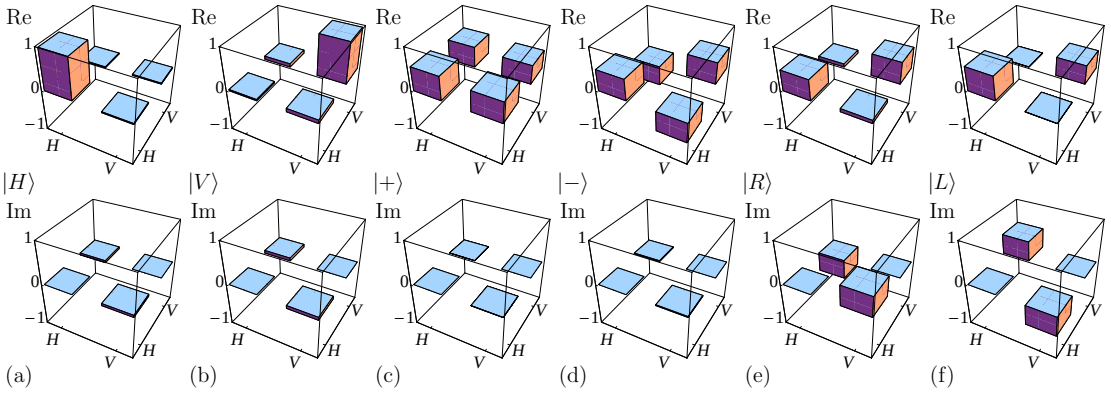

FIGURE 11.5: Tomography result for the prepared atomic states.

11.6 Teleportation: short fiber case

After a successful state preparation in site A, we start to create the photon-spinwave entanglement in site B, also using the double path scheme [143]. The entangled state can be expressed as:

$$|\Phi^+\rangle_{3B} = 1/\sqrt{2}(|0\rangle_3|0\rangle_B + |1\rangle_3|1\rangle_B) \tag{11.3}$$

where the subscript 3 represents photon 3 in Fig. 11.1, B represents the atomic spinwave state in site B. Photon 3 is sent to site A and subjected to joint Bell state measurement. In order have a good interference between photon 2 and 3 one a PBS, we optimize the relative delay and relative frequency between signal read A and write B in Fig. 11.3. In order to have a good spacial mode matching, the photons after interference are collected with single-mode fibers.

TABLE 11.1: Teleportation fidelities for the short fiber case.

State Index	1	2	3	4	5	6
Close to	$\|0\rangle$	$\|1\rangle$	$\|+\rangle$	$\|-\rangle$	$\|R\rangle$	$\|L\rangle$
Value	0.935	0.954	0.897	0.963	0.967	0.987
Deviation	0.0243	0.0214	0.0391	0.0222	0.0238	0.0153

In our setup by using a PBS, we are able to distinguish two bell states out four, $|\Phi^+\rangle$ and $|\Phi^-\rangle$. In case of $|\Phi^+\rangle$, no operation is required to apply on the teleported qubit. While in case of $|\Phi^-\rangle$, a π phase shift operation on $|1\rangle_B$ is required. In order to evaluate the performance for the teleportation process, we have done the quantum tomography measurement for all the six states prepared in Fig. 11.5 of Sec. 11.5, with the results shown in Fig. 11.6.

Generally the fidelity between two states (ρ_1 and ρ_2) is defined as:

$$F(\rho_1,\, \rho_2) = Tr(\rho_1\rho_2). \tag{11.4}$$

But this is only valid if one of these two states is a pure state. In our teleportation experiment, both the prepared state and the teleported state are mixed states, even through the fidelity for the prepared states is rather high. Theoretically there is another definition of fidelity [187] in general for which mixed states will apply:

$$F(\rho_1,\, \rho_2) = \{Tr[(\sqrt{\rho_1}\rho_2\sqrt{\rho_1})^{1/2}]\}^2. \tag{11.5}$$

In the specially case of two dimensions, the above formula can be simplified to a simple form:

$$F(\rho_1,\, \rho_2) = Tr(\rho 1\rho 2) + 2(\det \rho 1\, \det \rho 2)^{1/2}. \tag{11.6}$$

We calculate the teleportation fidelity between the prepared input states and the teleported state with the results shown in Tab. 11.1. The average fidelity is $95 \pm 1\%$, which is well above the classical boundary of 2/3 [140].

11.7 Teleportation: long fiber case

In order to show that our realization has potential applications in long-distance quantum communication, we replace the inter-connection fiber between site A and B with a 150 m long fiber. The loss induced by the fiber is about 13%. The main problem induced by this long fiber is the temperature dependent drift of its polarization rotation. In a previous experiment [116] we have to check the stability of it every half an hour. We

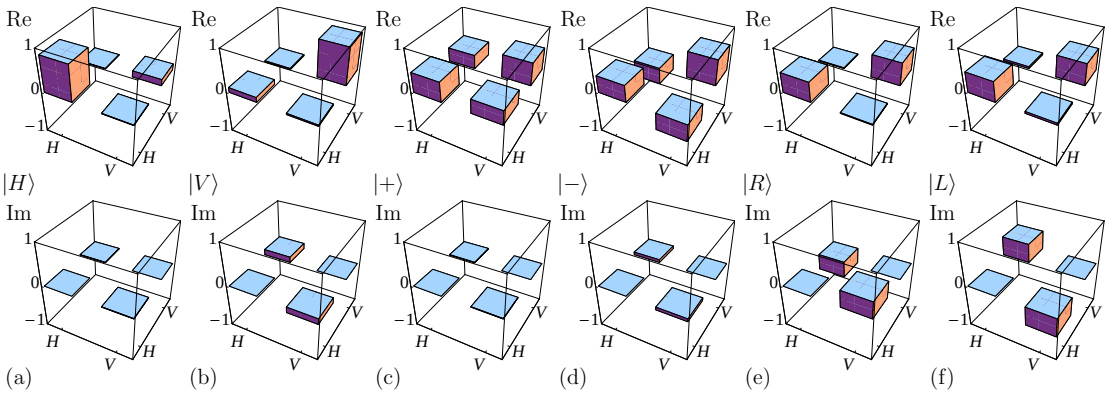

FIGURE 11.6: Tomography result of the short fiber case.

find that the drift for the polarization rotation is related to the diameter with which we wrap the fibers. If the diameter is larger, the birefringence effect will be small, thus small drift. By increasing the diameter from about 10 cm to about 1 m, we find that the fiber becomes more stable. One example measurement result is shown in Fig. 11.7. From it we can see that within a duration of 10 hours, the contrast ratio keeps higher than 1000:1. Based on this result and our experience, we periodically check the stability every 3 days during the data measurement. Similar as the short fiber case, we also make the quantum tomography measurement for all the six teleported states, with the result shown in Fig. 11.8. The average fidelity is $95.5 \pm 1\%$, which is comparable with the short fiber case.

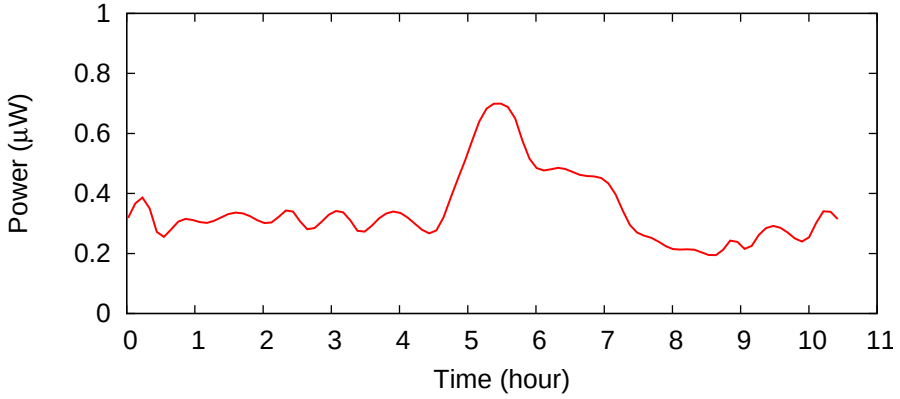

FIGURE 11.7: Measurement of polarization stability for the 150 m fiber used. Data shown is the power measured after a polarizer. The output power of the long fiber before the polarizer is 1.1 mW.

11.8 Heralded teleportation

For a lot of applications, such as distributed quantum computing, it is rather useful to have a trigger signal, which tells the teleportation process has succeeded without

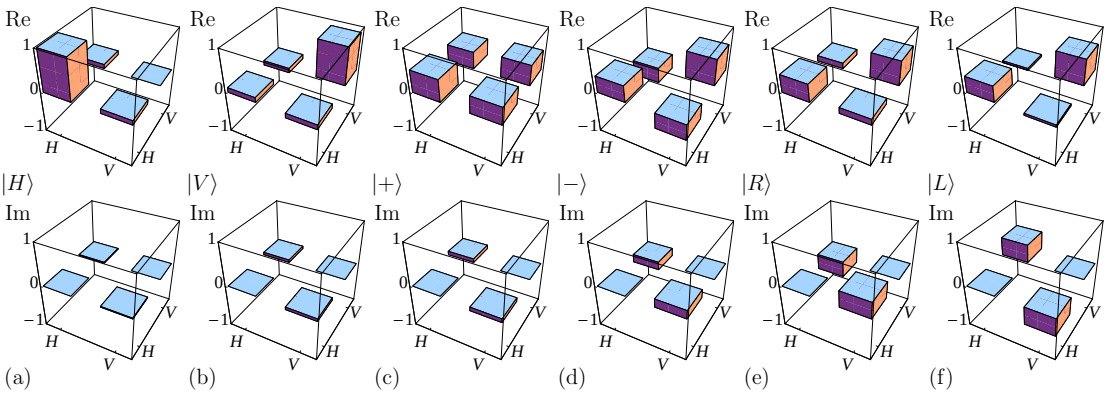

FIGURE 11.8: Tomography result of the long fiber case.

TABLE 11.2: Teleportation fidelities for the long fiber case.

State Index	1	2	3	4	5	6
Close to	$\|0\rangle$	$\|1\rangle$	$\|+\rangle$	$\|-\rangle$	$\|R\rangle$	$\|L\rangle$
Value	0.975	0.935	0.957	0.937	0.968	0.958
Deviation	0.0028	0.0297	0.0266	0.0279	0.0231	0.0228

converting the atomic qubit to a photonic qubit and detect it. In the ideal case, the BSM result can be used as this trigger signal. However, in the real case, if we consider the experimental noise and high order excitations in the write process, we will find that the BSM signal is mixed with too much noise. Mainly there are three contributions for the BSM signals, which is shown bellow,

$$\begin{array}{lccc} \text{from} & \text{A\&B} & \text{A} & \text{B} \\ \hline \text{probability} & \eta_A P_B & \eta_A P_A & {P_B}^2 \end{array} \tag{11.7}$$

where η_A is the retrieval efficiency of site A; P_A and P_B are the excitation probabilities for each site. The first term is the desired term which corresponds to the case one photon is retrieved out from site A and the other is the writeout photon from site B. The second term means that two photons are from site A, with one being the retrieved photon and the other the read noise which has a similar probability as the excitation probability. The third term means that both photons are from site B which originates from the double excitation process. Our purpose is to improve the proportion of the first term (P_{ut} in Fig. 11.9) as higher as possible. Therefore the follow requirement will be imposed:

$$P_A \ll P_B \ll \eta_A. \tag{11.8}$$

In our experiment, η_A is about 7%, P_B chosen is 3.0×10^{-3}, thus the second part in Eq. 11.8 is satisfied. In order to fulfill the first part of Eq. 11.8 and increase P_{ut}, we need

TABLE 11.3: Fidelities for the heralded teleportation

Basis	$\|0\rangle/\|1\rangle$	$\|+\rangle/\|-\rangle$	$\|R\rangle/\|L\rangle$
Polarization fidelity	0.927	0.873	0.917
Genuine fidelity	0.895	0.798	0.883
Deviation	0.129	0.118	0.122

to reduce the excitation probability P_A. The experimental result is shown in Fig. 11.9. When $P_A = 0.30 \times 10^{-3}$, the best value of $90 \pm 3\%$ is observed for P_{ut}. Under this condition, we remeasure the teleportation data, with the result shown in Tab. 11.3. The genuine fidelity is defined as:

$$F_{gen} = F_{pol}\frac{C_{234}}{C_{23}\eta_B} \tag{11.9}$$

where C_{xx} is the coincidence counts between corresponding detectors; η_B is the retrieval efficiency of site B. The average of F_{gen} is $86 \pm 7\%$, which overcomes the classical limit of 2/3 [140]. This result proves that our experiment is a genuine teleportation experiment.

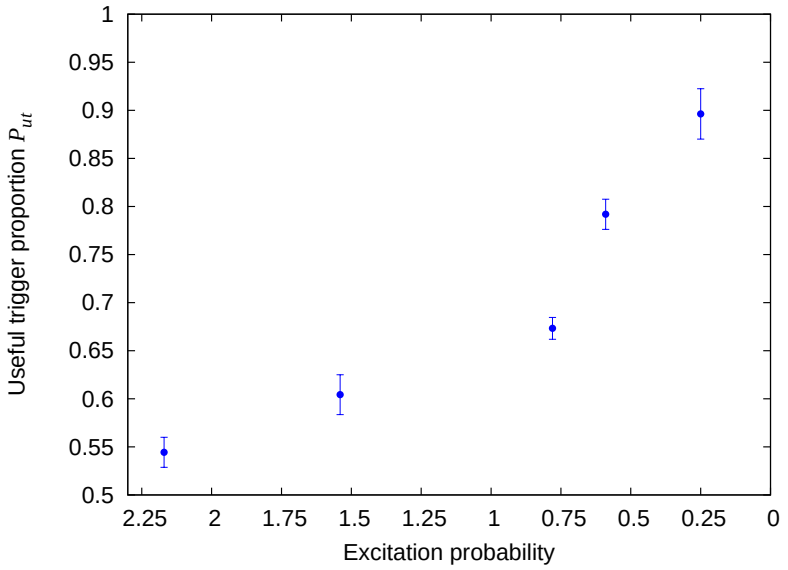

FIGURE 11.9: Proportion of useful triggers given by BSM as a function of excitation probability of site A.

Chapter 12

Conclusions and Outlook

In the previous chapters we have presented our experimental work of manipulating entangled photons and cold atomic ensembles for the applications in quantum information science. To conclude the present thesis, we want to make a summary of the main points and give an outlook to future work.

Due to the ease of high-precision single-qubit operation and detection and extremely weak coupling with the environment, entangled photons have been a major testbed for the quantum information protocols since the invention of SPDC based high-intensity source of polarization entangled photons [58]. Linear optical quantum computing (LOQC) is one of these protocols. The main difficulty in LOQC is to realize the controlled operation between independent photons. Previous schemes require an entangled photon pair as ancilla to realized a non-destructive CNOT gate. In Chap. 3 we have presented and realized a new scheme without using any entangled ancilla. However, all the realizations of linear optical CNOT gates are probabilistic, which will cause inefficiency for further applications without being assisted with quantum memories. Typically the frequency bandwidth of entangled photons from SPDC is of several THz. However most the quantum memories currently under developing are working with a frequency linewidth of several MHz. In order to solve this problem, we have presented our experimental investigations of using cavity-enhanced SPDC to create high-intensity narrowband entangled photons in Chap. 4. We have successfully realized single-mode operation of a PPKTP based cavity SPDC source, and suppressed the linewidth from 175 GHz to 9.6 MHz. In order to verify the validity of this source for multi-photon entanglement based applications in quantum information, in Chap. 5, we made an interference experiment between this narrowband entanglement source with an attenuated quasi single-photon from another completely independent diode laser. Three-photon entanglement was successfully observed.

In the latter half part of the thesis, we moved to the experimental work with cold atomic ensembles, which have been the best candidate for coherently storing the photonic states. In Chap. 6 we reviewed the famous DLCZ protocol of using atomic ensembles to realize quantum repeater to increase the quantum communication distance and also discussed about its drawback and subsequent revised schemes. In Chap. 7, we analyzed in detail the main mechanisms limiting the storage lifetime and retrieval efficiency of atomic ensemble based quantum memories. In Chap. 8 we presented our experimental results of extending the storage lifetime from several tens μs to 1 ms by increasing the spinwave wavelength. During the investigation of long-lifetime photon-spinwave entanglement, we found that the phase within the stored spinwave was changing as a function of storage time. Based on this finding we successfully created an second order spinwave NOON state, which has the potential of applications in the field of quantum enhanced measurements. There results have been presented in Chap. 9. Based on the techniques developed in the investigation of long-lifetime storage, in Chap. 10 we experimentally demonstrated that the entanglement swapping process with probabilistic sources could be made more efficient. A realization of quantum teleportation between atomic ensembles has been presented in Chap. 11. An atomic ensemble has been the largest stationary object which has been teleported at the time of this thesis.

Further work includes the following aspects. Utilizing the realized CNOT gate to create complicated cluster states for one-way quantum computing; Study the storage of narrowband entangled photons with EIT; Creation of narrowband entangled photons between telecom wavelength and near infrared, with one photon being suitable for transmission in the commercial low-loss telecom fibers and the other one suitable for storage with quantum memories; Creating large-scale multi-photon entanglement based on the narrowband entangled photons and quantum memories; Further extending the storage lifetime of cold atomic ensemble based quantum memories, by decreasing the temperature and using additional confinements; Improving the retrieval efficiency using the ring cavity scheme and the dark MOT technique; Investigating the possibility of connecting multi quantum repeater nodes and demonstrating the superiority of quantum repeater based transmission over direct transmission; Study of linear optical quantum computing based on quantum memories; etc.

Appendix A

Relation between Retrieval Efficiency and Atomic Random Phases

We assume that the individual phase ϕ_j of each atoms obeys normal distribution

$$f(\phi) = \frac{1}{\sqrt{2\pi}\sigma} e^{-\frac{\phi^2}{2\sigma^2}} \tag{A.1}$$

with σ being the standard deviation of ϕ. When the optical density is not high, retrieval efficiency is approximately proportional with the interference factor F_N of N atoms which is defined as

$$F_N = |f_N|^2 \text{ with } f_N = \sum_{j=1}^{N} e^{i\phi_j}. \tag{A.2}$$

The task is to find the relationship between F_N and σ when N is extremely large. We can expand the expression of F_N to the following form

$$\begin{aligned} F_N &= N + \textstyle\sum_{i\neq j}^{N} \cos(\phi_i - \phi_j) \\ &= N + N(N-1)\overline{\cos(\phi_i - \phi_j)} \\ &= N^2\overline{\cos(\phi_i - \phi_j)}. \end{aligned} \tag{A.3}$$

The average value of $\cos(\phi_i - \phi_j)$ can be calculate using the probability distribution function of ϕ:

$$\begin{aligned} \overline{\cos(\phi_i - \phi_j)} &= \textstyle\int_{-\infty}^{+\infty}\int_{-\infty}^{+\infty} f(\alpha)f(\beta)\cos(\alpha-\beta)\mathrm{d}\alpha\mathrm{d}\beta \\ &= e^{-\sigma^2}. \end{aligned} \tag{A.4}$$

Usually the lifetime of is defined at the $1/e$ point of F_N, therefore we have $\sigma_{1/e} = 1$. In this way, we explained why the lifetime is defined at the point when the random phase of each atom reaches 1 but not the intuitive value of π/e in Chap. 7.

List of Publications

Within the frame work of the presented thesis, some of the publications have been achieved.

[1] Claudia Wagenknecht, Che-Ming Li, Andreas Reingruber, **Xiao-Hui Bao**, Alexander Goebel, Yu-Ao Chen, Qiang Zhang, Kai Chen, and Jian-Wei Pan, *Experimental Demonstration of a Heralded Entanglement Source*, Nature Photonics, accepted (2010).

[2] Yu-Ao Chen, **Xiao-Hui Bao**, Zhen-Sheng Yuan, Shuai Chen, Bo Zhao, and Jian-Wei Pan, *Heralded Generation of an Atomic NOON State*, Phys. Rev. Lett. **104**, 043601 (2010). (Chap. 9)

[3] Jian Yang, **Xiao-Hui Bao**, Han Zhang, Shuai Chen, Cheng-Zhi Peng, Zeng-Bing Chen, and Jian-Wei Pan, *Experimental quantum teleportation and multiphoton entanglement via interfering narrowband photon sources*, Phys. Rev. A **80**, 042321 (2009). (Chap. 5)

[4] Bo Zhao, Yu-Ao Chen, **Xiao-Hui Bao**, Thorsten Strassel, Chih-Sung Chuu, Xian-Min Jin, Jörg Schmiedmayer, Zhen-Sheng Yuan, Shuai Chen, Jian-Wei Pan, *A millisecond quantum memory for scalable quantum networks*, Nature Physics **5**, 95-99 (2008). (Chap. 8)

[5] **Xiao-Hui Bao**, Yong Qian, Jian Yang, Han Zhang, Zeng-Bing Chen, Tao Yang, and Jian-Wei Pan, *Generation of Narrow-Band Polarization-Entangled Photon Pairs for Atomic Quantum Memories*, Phys. Rev. Lett. **101**, 190501 (2008). (Chap. 4)

[6] Qiang Zhang, **Xiao-Hui Bao**, Chao-Yang Lu, Xiao-Qi Zhou, Tao Yang, Terry Rudolph, and Jian-Wei Pan, *Demonstration of a scheme for the generation of "event-ready" entangled photon pairs from a single-photon source*, Phys. Rev. A **77**, 062316 (2008).

[7] **Xiao-Hui Bao**, Teng-Yun Chen, Qiang Zhang, Jian Yang, Han Zhang, Tao Yang, and Jian-Wei Pan, *Optical Nondestructive Controlled-NOT Gate without Using Entangled Photons*, Phys. Rev. Lett. **98**, 170502 (2007). (Chap. 3)

[8] Jun Zhang, **Xiao-Hui Bao**, Teng-Yun Chen, Tao Yang, Adan Cabello, and Jian-Wei Pan, *Experimental quantum Guess my Number protocol using multiphoton entanglement*, Phys. Rev. A, **75** 022302 (2007).

[9] Zeng-Bing Chen, Qiang Zhang, **Xiao-Hui Bao**, Jörg Schmiedmayer, and Jian-Wei Pan, *Deterministic and efficient quantum cryptography based on Bells theorem*, Phys. Rev. A **73**, 050302(R) (2006).

[10] Cheng-Zhi Peng, Tao Yang, **Xiao-Hui Bao**, Jun Zhang, Xian-Min Jin, Fa-Yong Feng, Bin Yang, Jian Yang, Juan Yin, Qiang Zhang, Nan Li, Bao-Li Tian, and Jian-Wei Pan, *Experimental Free-Space Distribution of Entangled Photon Pairs Over 13 km: Towards Satellite-Based Global Quantum Communication*, Phys. Rev. Lett. **94**, 150501 (2005).

Acknowledgements

First of all, I would like to enthusiastically thank Prof. Jian-Wei Pan for supervising this thesis. It was really a good pleasure to meet him at the right time and be led into this fascinating field of quantum optics and quantum information. Throughout the Ph.D study I really appreciate his continuous guidance, support and steady trust, and I really learned a lot from him.

I would like to thank Prof. Matthias Weidemüller for reviewing my thesis, and Dr. Jörg Evers and Prof. Thomas Gasenzer for being examiners for the final exam.

Many thanks to Dr. Yuao Chen, Dr. Zhen-Sheng Yuan, Prof. Shuai Chen, Xiao-Fan Xu, Andreas Reingruber, Peter Dietrich, Alexander Dueck, and Dr. Che-Ming Li, who have been working directly with me in the experiments with cold atomic ensembles. I really enjoyed the time working with them. Specially I want to thank Yuao Chen, for inviting me for meal so many times when he was in Heidelberg, and Andreas Reingruber for translating the abstract into German.

I also want to thank Jian Yang and Han Zhang for the experimental works about narrowband entangled photons. Without the nice team work with them, it would never be possible to have the good results.

For the theoretical study, I want to specially thank Dr. Bo Zhao. Anytime when I have some questions, he was always rather patient to answer. It was so nice to have such a theoretician who was sitting nearby.

I would like thank all other present group members including Dr. Claudia Wagenknecht, Dr. Fan Yang, Christian Lutz and Thorsten Mandel for their support and the pleasant working atmosphere. I also enjoyed every lunch time with them together.

I would also like to thank former group members including Dr. Thorsten Strassel, Dr. Alexander Goebel, Dr. Chih-Sung Chuu, Prof. You-Jin Deng, Prof. Kai Chen, Dr. Yong Zhao, Huan Nguyen, Maximilian Plenert and Valentin Hagel. The time working with them constitutes a good memory for me.

Many thanks to Prof. Tao Yang, Prof. Zeng-Bing Chen and Prof. Yong-De Zhang in USTC for the guidance in the beginning of my scientific career.

Also many thanks to the people who are working in the electronic workshop, mechanical workshop and the glass workshop of our institute. The strong supports from them have definitely accelerated our experimental progresses.

Finally I would like to thank my parents and my girlfriend Jing Ning for their constant understanding, support and love. Their encouragement gives me strong strength to go further.

Bibliography

[1] C. H. Bennett and G. Brassard. Quantum cryptography: Public key distribution and coin tossing. In *Proceedings of the IEEE International Conference on Computers, Systems, and Signal Processing*, page 175. Bangalore, 1984. 2

[2] Artur K. Ekert. Quantum cryptography based on bell's theorem. *Phys. Rev. Lett.*, 67(6):661–663, Aug 1991. 2

[3] Z.-B. Chen, Q. Zhang, X.-H. Bao, J. Schmiedmayer, and J.-W. Pan. Deterministic and efficient quantum cryptography based on bell's theorem. *Physical Review A (Atomic, Molecular, and Optical Physics)*, 73(5):050302, 2006. 2

[4] T. C. Ralph. Continuous variable quantum cryptography. *Phys. Rev. A*, 61(1):010303, Dec 1999. 2

[5] Xiang-Bin Wang. Beating the photon-number-splitting attack in practical quantum cryptography. *Phys. Rev. Lett.*, 94(23):230503, Jun 2005. 2

[6] Hoi-Kwong Lo, Xiongfeng Ma, and Kai Chen. Decoy state quantum key distribution. *Phys. Rev. Lett.*, 94(23):230504, Jun 2005. 2

[7] Danna Rosenberg, Jim W. Harrington, Patrick R. Rice, Philip A. Hiskett, Charles G. Peterson, Richard J. Hughes, Adriana E. Lita, Sae Woo Nam, and Jane E. Nordholt. Long-distance decoy-state quantum key distribution in optical fiber. *Phys. Rev. Lett.*, 98(1):010503, Jan 2007. 2

[8] Tobias Schmitt-Manderbach, Henning Weier, Martin Fürst, Rupert Ursin, Felix Tiefenbacher, Thomas Scheidl, Josep Perdigues, Zoran Sodnik, Christian Kurtsiefer, John G. Rarity, Anton Zeilinger, and Harald Weinfurter. Experimental demonstration of free-space decoy-state quantum key distribution over 144 km. *Phys. Rev. Lett.*, 98(1):010504, Jan 2007. 2

[9] C.-Z. Peng, J. Zhang, D. Yang, W.-B. Gao, M. a. Huai-Xin, H. Yin, H.-P. Zeng, T. Yang, X.-B. Wang, and J.-W. Pan. Experimental long-distance decoy-state quantum key distribution based on polarization encoding. *Phys. Rev. Lett.*, 98(1):010505, 2007. 2

[10] Charles H. Bennett, Gilles Brassard, Claude Crépeau, Richard Jozsa, Asher Peres, and William K. Wootters. Teleporting an unknown quantum state via dual classical and einstein-podolsky-rosen channels. *Phys. Rev. Lett.*, 70(13):1895–1899, Mar 1993. 3, 19, 35

[11] Dik Bouwmeester, Jian-Wei Pan, Klaus Mattle, Manfred Eibl, Harald Weinfurter, and Anton Zeilinger. Experimental quantum teleportation. *Nature*, 390(6660):575–579, 1997. 3, 35

[12] D. Boschi, S. Branca, F. De Martini, L. Hardy, and S. Popescu. Experimental realization of teleporting an unknown pure quantum state via dual classical and einstein-podolsky-rosen channels. *Phys. Rev. Lett.*, 80(6):1121–1125, Feb 1998. 4

[13] A. Furusawa, J. L. Sϕrensen, S. L. Braunstein, C. A. Fuchs, H. J. Kimble, and E. S. Polzik. Unconditional quantum teleportation. *Science*, 282(5389):706–709, 1998. 4

[14] M. Riebe, H. Haffner, C. F. Roos, W. Hansel, J. Benhelm, G. P. T. Lancaster, T. W. Korber, C. Becher, F. Schmidt-Kaler, D. F. V. James, and R. Blatt. Deterministic quantum teleportation with atoms. *Nature*, 429(6993):734–737, 2004. 4

[15] M. D. Barrett, J. Chiaverini, T. Schaetz, J. Britton, W. M. Itano, J. D. Jost, E. Knill, C. Langer, D. Leibfried, R. Ozeri, and D. J. Wineland. Deterministic quantum teleportation of atomic qubits. *Nature*, 429(6993):737–739, 2004. 4

[16] S. Olmschenk, D. N. Matsukevich, P. Maunz, D. Hayes, L.-M. Duan, and C. Monroe. Quantum teleportation between distant matter qubits 10.1126/science.1167209. *Science*, 323(5913):486–489, 2009. 4

[17] J.-W. Pan, D. Bouwmeester, H. Weinfurter, and A. Zeilinger. Experimental entanglement swapping: Entangling photons that never interacted. *Phys. Rev. Lett.*, 80(18):3891–3894, 1998. 4, 35, 83

[18] H.-J. Briegel, W. Dür, J. I. Cirac, and P. Zoller. Quantum repeaters: The role of imperfect local operations in quantum communication. *Phys. Rev. Lett.*, 81(26):5932–5935, Dec 1998. 5, 27, 43, 83

[19] Charles H. Bennett, Gilles Brassard, Sandu Popescu, Benjamin Schumacher, John A. Smolin, and William K. Wootters. Purification of noisy entanglement and faithful teleportation via noisy channels. *Phys. Rev. Lett.*, 76(5):722–725, Jan 1996. 6, 19

[20] L.-M. Duan, M. D. Lukin, J. I. Cirac, and P. Zoller. Long-distance quantum communication with atomic ensembles and linear optics. *Nature*, 414(6862):413–418, 2001. 6, 36, 43, 67, 68, 77, 84, 93

[21] A. Kuzmich, W. P. Bowen, A. D. Boozer, A. Boca, C. W. Chou, L.-M. Duan, and H. J. Kimble. Generation of nonclassical photon pairs for scalable quantum communication with atomic ensembles. *Nature*, 423(6941):731–734, 2003. 6

[22] M. D. Eisaman, A. Andre, F. Massou, M. Fleischhauer, A. S. Zibrov, and M. D. Lukin. Electromagnetically induced transparency with tunable single-photon pulses. *Nature*, 438(7069):837–841, 2005. 6

[23] T. Chaneliere, D. N. Matsukevich, S. D. Jenkins, S. Y. Lan, T. A. B. Kennedy, and A. Kuzmich. Storage and retrieval of single photons transmitted between remote quantum memories. *Nature*, 438(7069):833–836, 2005. 6, 27, 36, 74

[24] C.-W. Chou, J. Laurat, H. Deng, K. S. Choi, H. de Riedmatten, D. Felinto, and H. J. Kimble. Functional quantum nodes for entanglement distribution over scalable quantum networks 10.1126/science.1140300. *Science*, 316(5829):1316–1320, 2007. 6, 50, 67, 68, 84

[25] Z.-S. Yuan, Y. A. Chen, B. Zhao, S. Chen, J. Schmiedmayer, and J.-W. Pan. Experimental demonstration of a bdcz quantum repeater node. *Nature*, 454(7208):1098–1101, 2008. 6, 36, 67, 69

[26] B. Zhao, Y.-A. Chen, X.-H. Bao, T. Strassel, C.-S. Chuu, X.-M. Jin, J. Schmiedmayer, Z.-S. Yuan, S. Chen, and J.-W. Pan. A millisecond quantum memory for scalable quantum networks. *Nat. Phys.*, 5:95–99, 2009. 6, 78, 84, 86, 87, 95

[27] R. Zhao, Y. O. Dudin, S. D. Jenkins, C. J. Campbell, D. N. Matsukevich, T. A. B. Kennedy, and A. Kuzmich. Long-lived quantum memory. *Nat. Phys.*, 5:100–104, 2009. 6, 84

[28] P. Shor. Algorithms for quantum computation: Discrete log and factoring. In S. Goldwasser, editor, *Proc. 35th Annu. Symp. on the Foundations of Computer Science*, pages 124–134. IEEE Computer Society Press, Los Alamitos, California, 1994. 6

[29] Lov K. Grover. A fast quantum mechanical algorithm for database search. In *28th Annual ACM Symposium on the Theory of Computing (STOC)*, pages 212–219. May 1996. 7

[30] M. A. Nielsen and I. L. Chuang. *Quantum Computation and Quantum Information*. Cambridge Univ. Press, Cambridge, 2000. 7, 19

[31] N. A. Gershenfeld and I. L. Chuang. Bulk spin-resonance quantum computation. *Science*, 275(5298):350–356, 1997. 7

[32] F. Schmidt-Kaler, H. Haffner, M. Riebe, S. Gulde, G. P. T. Lancaster, T. Deuschle, C. Becher, C. F. Roos, J. Eschner, and R. Blatt. Realization of the cirac-zoller controlled-not quantum gate. *Nature*, 422(6930):408–411, 2003. 7

[33] J. L. O'Brien, G. J. Pryde, A. G. White, T. C. Ralph, and D. Branning. Demonstration of an all-optical quantum controlled-not gate. *Nature*, 426(6964):264–267, 2003. 7, 19

[34] X. Li, Y. Wu, D. Steel, D. Gammon, T. H. Stievater, D. S. Katzer, D. Park, C. Piermarocchi, and L. J. Sham. An all-optical quantum gate in a semiconductor quantum dot. *Science*, 301(5634):809–811, 2003. 7

[35] J. H. Plantenberg, P. C. de Groot, C. J. P. M. Harmans, and J. E. Mooij. Demonstration of controlled-not quantum gates on a pair of superconducting quantum bits. *Nature*, 447(7146):836–839, 2007. 7

[36] H. Haffner, W. Hansel, C. F. Roos, J. Benhelm, D. Chek-al kar, M. Chwalla, T. Korber, U. D. Rapol, M. Riebe, P. O. Schmidt, C. Becher, O. Guhne, W. Dur, and R. Blatt. Scalable multiparticle entanglement of trapped ions. *Nature*, 438(7068):643–646, 2005. 7, 17

[37] Robert Raussendorf and Hans J. Briegel. A one-way quantum computer. *Phys. Rev. Lett.*, 86(22):5188–5191, 2001. 7, 13, 20

[38] O. Mandel, M. Greiner, A. Widera, T. Rom, T. W. Hansch, and I. Bloch. Controlled collisions for multi-particle entanglement of optically trapped atoms. *Nature*, 425(6961):937–940, 2003. 7

[39] K. B. Soderberg, N. Gemelke, and C. Chin. Ultracold molecules: vehicles to scalable quantum information processing. *New Journal of Physics*, 11(5):055022, 2009. 7

[40] P. Walther, K. J. Resch, T. Rudolph, E. Schenck, H. Weinfurter, V. Vedral, M. Aspelmeyer, and A. Zeilinger. Experimental one-way quantum computing. *Nature*, 434(7030):169–176, 2005. 7, 35

[41] C. K. Hong and L. Mandel. Theory of parametric frequency down conversion of light. *Phys. Rev. A*, 31(4):2409–2418, 1985. 10, 31

[42] Morton H. Rubin, David N. Klyshko, Y. H. Shih, and A. V. Sergienko. Theory of two-photon entanglement in type-ii optical parametric down-conversion. *Phys. Rev. A*, 50(6):5122–5133, Dec 1994. 10

[43] Michael A. Horne, Abner Shimony, and Anton Zeilinger. Two-particle interferometry. *Phys. Rev. Lett.*, 62(19):2209–2212, May 1989. 10

[44] J. G. Rarity and P. R. Tapster. Experimental violation of bell's inequality based on phase and momentum. *Phys. Rev. Lett.*, 64(21):2495–2498, May 1990. 10

[45] T. J. Herzog, J. G. Rarity, H. Weinfurter, and A. Zeilinger. Frustrated two-photon creation via interference. *Phys. Rev. Lett.*, 72(5):629–632, Jan 1994. 10

[46] Tao Yang, Qiang Zhang, Jun Zhang, Juan Yin, Zhi Zhao, Marek Zukowski, Zeng-Bing Chen, and Jian-Wei Pan. All-versus-nothing violation of local realism by two-photon, four-dimensional entanglement. *Phys. Rev. Lett.*, 95(24):240406, 2005. 10, 15

[47] J. D. Franson. Bell inequality for position and time. *Phys. Rev. Lett.*, 62(19):2205–2208, May 1989. 11

[48] P. G. Kwiat, W. A. Vareka, C. K. Hong, H. Nathel, and R. Y. Chiao. Correlated two-photon interference in a dual-beam michelson interferometer. *Phys. Rev. A*, 41(5):2910–2913, Mar 1990. 11

[49] Z. Y. Ou, X. Y. Zou, L. J. Wang, and L. Mandel. Observation of nonlocal interference in separated photon channels. *Phys. Rev. Lett.*, 65(3):321–324, Jul 1990. 11

[50] H. de Riedmatten, I. Marcikic, H. Zbinden, and N. Gisin. Creating high-dimensional time-bin entanglement using mode-locked lasers. *Quantum Information and Computing*, 2:425–433, 2002. 12

[51] J. Brendel, N. Gisin, W. Tittel, and H. Zbinden. Pulsed energy-time entangled twin-photon source for quantum communication. *Phys. Rev. Lett.*, 82(12):2594–2597, Mar 1999. 12

[52] I. Marcikic, H. de Riedmatten, W. Tittel, H. Zbinden, M. Legre, and N. Gisin. Distribution of time-bin entangled qubits over 50 km of optical fiber. *Phys. Rev. Lett.*, 93(18):180502, 2004. 12

[53] I. Marcikic, H. de Riedmatten, W. Tittel, H. Zbinden, and N. Gisin. Long-distance teleportation of qubits at telecommunication wavelengths. *Nature*, 421(6922):509–513, 2003. 12

[54] Z. Y. Ou and L. Mandel. Violation of bell's inequality and classical probability in a two-photon correlation experiment. *Phys. Rev. Lett.*, 61(1):50–53, Jul 1988. 12

[55] Y. H. Shih and C. O. Alley. New type of einstein-podolsky-rosen-bohm experiment using pairs of light quanta produced by optical parametric down conversion. *Phys. Rev. Lett.*, 61(26):2921–2924, Dec 1988. 12

[56] J. Zak. Finite translations in time and energy. *Phys. Rev. Lett.*, 71(16):2623–2625, Oct 1993. 12

[57] Y. H. Shih, A. V. Sergienko, Morton H. Rubin, T. E. Kiess, and C. O. Alley. Two-photon entanglement in type-ii parametric down-conversion. *Phys. Rev. A*, 50(1):23–28, Jul 1994. 12

[58] Paul G. Kwiat, Klaus Mattle, Harald Weinfurter, Anton Zeilinger, Alexander V. Sergienko, and Yanhua Shih. New high-intensity source of polarization-entangled photon pairs. *Phys. Rev. Lett.*, 75(24):4337–4341, 1995. 12, 15, 20, 23, 27, 35, 83, 88, 103

[59] Christian Kurtsiefer, Markus Oberparleiter, and Harald Weinfurter. High-efficiency entangled photon pair collection in type-ii parametric fluorescence. *Phys. Rev. A*, 64(2):023802, Jul 2001. 13

[60] Paul G. Kwiat, Edo Waks, Andrew G. White, Ian Appelbaum, and Philippe H. Eberhard. Ultrabright source of polarization-entangled photons. *Phys. Rev. A*, 60(2):R773–R776, Aug 1999. 13

[61] J. B. Altepeter, E. R. Jeffrey, and P. G. Kwiat. Phase-compensated ultra-bright source of entangled photons. *Optics Express*, 13(22):8951–8959, 2005. 13

[62] Paul G. Kwiat, Philippe H. Eberhard, Aephraim M. Steinberg, and Raymond Y. Chiao. Proposal for a loophole-free bell inequality experiment. *Phys. Rev. A*, 49(5):3209–3220, May 1994. 13

[63] Marco Fiorentino, Gaétan Messin, Christopher E. Kuklewicz, Franco N. C. Wong, and Jeffrey H. Shapiro. Generation of ultrabright tunable polarization entanglement without spatial, spectral, or temporal constraints. *Phys. Rev. A*, 69(4):041801, Apr 2004. 13

[64] Daniel M. Greenberger, Michael A. Horne, and Anton Zeilinger. Going beyond bell's theorem. In M. Kafatos, editor, *Bell's Theorem, Quantum Theory, and Conceptions of the Universe*, pages 69–72. Kluwer Academic, Dordrecht, 1989. 13, 17, 38, 78

[65] Mark Hillery, Vladimír Bužek, and André Berthiaume. Quantum secret sharing. *Phys. Rev. A*, 59(3):1829–1834, Mar 1999. 13

[66] Valerio Scarani and Nicolas Gisin. Quantum communication between n partners and bell's inequalities. *Phys. Rev. Lett.*, 87(11):117901, Aug 2001. 13

[67] M. Zukowski, A. Zeilinger, M. A. Horne, and Weinfurter H. Quest for ghz states. *Acta Phys. Pol.*, 93:187, 1998. 13

[68] Adan Cabello and Antonio J. Lopez-Tarrida. Proposed experiment for the quantum "guess my number" protocol. *Physical Review A (Atomic, Molecular, and Optical Physics)*, 71(2):020301, 2005. 13

[69] Jun Zhang, Xiao-Hui Bao, Teng-Yun Chen, Tao Yang, Adan Cabello, and Jian-Wei Pan. Experimental quantum "guess my number" protocol using multiphoton entanglement. *Physical Review A (Atomic, Molecular, and Optical Physics)*, 75(2):022302, 2007. 13

[70] Q. Zhang, A. Goebel, C. Wagenknecht, Y.-A. Chen, B. Zhao, T. Yang, A. Mair, J. Schmiedmayer, and J.-W. Pan. Experimental quantum teleportation of a two-qubit composite system. *Nat Phys*, 2(10):678–682, 2006. 13

[71] M. Żukowski, A. Zeilinger, M. A. Horne, and A. K. Ekert. "event-ready-detectors" bell experiment via entanglement swapping. *Phys. Rev. Lett.*, 71(26):4287–4290, Dec 1993. 14, 83

[72] M. Zukowski, A. Zeilinger, and H. Weinfurter. Entangling photons radiated by independent pulsed sources. *Annals of the New York Academy of Sciences*, 755:91–102, 1995. 14, 27, 35, 38

[73] Anton Zeilinger, Michael A. Horne, Harald Weinfurter, and Marek Żukowski. Three-particle entanglements from two entangled pairs. *Phys. Rev. Lett.*, 78(16):3031–3034, Apr 1997. 14

[74] J.-W. Pan, M. Daniell, S. Gasparoni, G. Weihs, and A. Zeilinger. Experimental demonstration of four-photon entanglement and high-fidelity teleportation. *Phys. Rev. Lett.*, 86(20):4435–4438, 2001. 14

[75] Z. Zhao, Y.-A. Chen, A.-N. Zhang, T. Yang, H. J. Briegel, and J.-W. Pan. Experimental demonstration of five-photon entanglement and open-destination teleportation. *Nature*, 430(6995):54–58, 2004. 15

[76] C.-Y. Lu, X.-Q. Zhou, O. Guhne, W.-B. Gao, J. Zhang, Z.-S. Yuan, A. Goebel, T. Yang, and J.-W. Pan. Experimental entanglement of six photons in graph states. *Nat. Phys.*, 3:91–95, 2007. 15, 17, 36

[77] Manfred Eibl, Sascha Gaertner, Mohamed Bourennane, Christian Kurtsiefer, Marek Żukowski, and Harald Weinfurter. Experimental observation of four-photon entanglement from parametric down-conversion. *Phys. Rev. Lett.*, 90(20):200403, May 2003. 15

[78] P. G. Kwiat. Hyper-entangled states. *Journal of Modern Optics*, 44(11):2173–2184, 1997. 15

[79] Paul G. Kwiat and Harald Weinfurter. Embedded bell-state analysis. *Phys. Rev. A*, 58(4):R2623–R2626, Oct 1998. 15

[80] Christoph Simon and Jian-Wei Pan. Polarization entanglement purification using spatial entanglement. *Phys. Rev. Lett.*, 89(25):257901, Dec 2002. 15

[81] Zeng-Bing Chen, Jian-Wei Pan, Yong-De Zhang, Časlav Brukner, and Anton Zeilinger. All-versus-nothing violation of local realism for two entangled photons. *Phys. Rev. Lett.*, 90(16):160408, Apr 2003. 15

[82] Zeng-Bing Chen, Qiang Zhang, Xiao-Hui Bao, Jorg Schmiedmayer, and Jian-Wei Pan. Deterministic and efficient quantum cryptography based on bell's theorem. *Physical Review A (Atomic, Molecular, and Optical Physics)*, 73(5):050302, 2006. 15, 16

[83] C. Cinelli, M. Barbieri, R. Perris, P. Mataloni, and F. De Martini. All-versus-nothing nonlocality test of quantum mechanics by two-photon hyperentanglement. *Phys. Rev. Lett.*, 95(24):240405, 2005. 15

[84] Julio T. Barreiro, Nathan K. Langford, Nicholas A. Peters, and Paul G. Kwiat. Generation of hyperentangled photon pairs. *Phys. Rev. Lett.*, 95(26):260501, 2005. 16

[85] O. Alibart, J. Fulconis, G. K. L. Wong, S. G. Murdoch, W. J. Wadsworth, and J. G. Rarity. Photon pair generation using four-wave mixing in a microstructured fibre: theory versus experiment. *New Journal of Physics*, 8(5):67, 2006. 16

[86] R. M. Stevenson, R. J. Young, P. Atkinson, K. Cooper, D. A. Ritchie, and A. J. Shields. A semiconductor source of triggered entangled photon pairs. *Nature*, 439(7073):179–182, 2006. 16, 20

[87] V. Balić, D. A. Braje, P. Kolchin, G. Y. Yin, and S. E. Harris. Generation of paired photons with controllable waveforms. *Phys. Rev. Lett.*, 94(18):183601, 2005. 16, 44

[88] J. K. Thompson, J. Simon, H. Loh, and V. Vuletic. A high-brightness source of narrowband, identical-photon pairs. *Science*, 313(5783):74–77, 2006. 17, 28

[89] J. S. Bell. On the einstein-podolsky-rosen paradox. *Physics (Long Island City, N.Y.)*, 1:195–200, 1964. 17, 24

[90] John F. Clauser, Michael A. Horne, Abner Shimony, and Richard A. Holt. Proposed experiment to test local hidden-variable theories. *Phys. Rev. Lett.*, 23(15):880–884, 1969. 17, 24, 31, 88

[91] Alain Aspect, Philippe Grangier, and Gérard Roger. Experimental tests of realistic local theories via bell's theorem. *Phys. Rev. Lett.*, 47(7):460–463, Aug 1981. 17

[92] Daniel F. V. James, Paul G. Kwiat, William J. Munro, and Andrew G. White. Measurement of qubits. *Phys. Rev. A*, 64(5):052312, Oct 2001. 17, 31, 38, 97

[93] O. Gühne, P. Hyllus, D. Bruss, A. Ekert, M. Lewenstein, C. Macchiavello, and A. Sanpera. Detection of entanglement with few local measurements. *Phys. Rev. A*, 66(6):062305, Dec 2002. 17

[94] E. Knill, R. Laflamme, and G. J. Milburn. A scheme for efficient quantum computation with linear optics. *Nature*, 409(6816):46–52, 2001. 19, 27, 36

[95] Charles H. Bennett and Stephen J. Wiesner. Communication via one- and two-particle operators on einstein-podolsky-rosen states. *Phys. Rev. Lett.*, 69(20):2881–2884, 1992. 19

[96] T. B. Pittman, M. J. Fitch, B. C Jacobs, and J. D. Franson. Experimental controlled-not logic gate for single photons in the coincidence basis. *Phys. Rev. A*, 68(3):032316, Sep 2003. 19

[97] N. K. Langford, T. J. Weinhold, R. Prevedel, K. J. Resch, A. Gilchrist, J. L. O' Brien, G. J. Pryde, and A. G. White. Demonstration of a simple entangling optical gate and its use in bell-state analysis. *Phys. Rev. Lett.*, 95(21):210504, 2005. 19, 24

[98] Nikolai Kiesel, Christian Schmid, Ulrich Weber, Rupert Ursin, and Harald Weinfurter. Linear optics controlled-phase gate made simple. *Phys. Rev. Lett.*, 95(21):210505, 2005. 19, 24

[99] Ryo Okamoto, Holger F. Hofmann, Shigeki Takeuchi, and Keiji Sasaki. Demonstration of an optical quantum controlled-not gate without path interference. *Phys. Rev. Lett.*, 95(21):210506, 2005. 19

[100] Zhi Zhao, An-Ning Zhang, Yu-Ao Chen, Han Zhang, Jiang-Feng Du, Tao Yang, and Jian-Wei Pan. Experimental demonstration of a nondestructive controlled-[small-caps not] quantum gate for two independent photon qubits. *Phys. Rev. Lett.*, 94(3):030501, 2005. 19, 26

[101] Sara Gasparoni, Jian-Wei Pan, Philip Walther, Terry Rudolph, and Anton Zeilinger. Realization of a photonic controlled-[small-caps not] gate sufficient for quantum computation. *Phys. Rev. Lett.*, 93(2):020504, 2004. 19, 26

[102] L. M. Duan and R. Raussendorf. Efficient quantum computation with probabilistic quantum gates. *Phys. Rev. Lett.*, 95(8):080503, 2005. 20

[103] T. B. Pittman, B. C. Jacobs, and J. D. Franson. Probabilistic quantum logic operations using polarizing beam splitters. *Phys. Rev. A*, 64(6):062311, 2001. 20

[104] N. Akopian, N. H. Lindner, E. Poem, Y. Berlatzky, J. Avron, D. Gershoni, B. D. Gerardot, and P. M. Petroff. Entangled photon pairs from semiconductor quantum dots. *Phys. Rev. Lett.*, 96(13):130501, 2006. 20

[105] Xiang-Bin Wang. Possibility of producing the event-ready two-photon polarization entangled state with normal photon detectors. *Phys. Rev. A*, 68(4):042304, 2003. 20

[106] D. E. Browne and T. Rudolph. Resource-efficient linear optical quantum computation. *Phys. Rev. Lett.*, 95(1):010501, 2005. 20, 27, 36, 40, 78

[107] Q. Zhang, X.-H. Bao, C.-Y. Lu, X.-Q. Zhou, T. Yang, T. Rudolph, and J.-W. Pan. Demonstration of a scheme for the generation of "event-ready" entangled photon pairs from a single-photon source. *Phys. Rev. A*, 77(6):062316, 2008. 20

[108] Mikio Fujiwara and Masahide Sasaki. Multiphoton discrimination at telecom wavelength with charge integration photon detector. *Appl. Phys. Lett.*, 86(11):111119, 2005. 22

[109] H. S. Eisenberg, J. F. Hodelin, G. Khoury, and D. Bouwmeester. Multiphoton path entanglement by nonlocal bunching. *Phys. Rev. Lett.*, 94(9):090502, 2005. 22

[110] Charles Santori, David Fattal, Jelena Vuckovic, Glenn S. Solomon, and Yoshihisa Yamamoto. Indistinguishable photons from a single-photon device. *Nature*, 419(6907):594–597, 2002. 23

[111] J. F. Poyatos, J. I. Cirac, and P. Zoller. Complete characterization of a quantum process: The two-bit quantum gate. *Phys. Rev. Lett.*, 78(2):390–393, 1997. 24, 26

[112] J. L. O'Brien, G. J. Pryde, A. Gilchrist, D. F. V. James, N. K. Langford, T. C. Ralph, and A. G. White. Quantum process tomography of a controlled-[small-caps not] gate. *Phys. Rev. Lett.*, 93(8):080502, 2004. 24

[113] Holger F. Hofmann. Complementary classical fidelities as an efficient criterion for the evaluation of experimentally realized quantum operations. *Phys. Rev. Lett.*, 94(16):160504, 2005. 24, 25

[114] Holger F. Hofmann. Quantum parallelism of the controlled-not operation: An experimental criterion for the evaluation of device performance. *Phys. Rev. A*, 72(2):022329, 2005. 25

[115] K. S. Choi, H. Deng, J. Laurat, and H. J. Kimble. Mapping photonic entanglement into and out of a quantum memory. *Nature*, 452(7183):67–71, 2008. 27, 33, 36, 68, 74

[116] Y.-A. Chen, S. Chen, Z.-S. Yuan, B. Zhao, C.-S. Chuu, J. Schmiedmayer, and J.-W. Pan. Memory-built-in quantum teleportation with photonic and atomic qubits. *Nat. Phys.*, 4(2):103–107, 2008. 27, 67, 79, 98

[117] R. Kaltenbaek, B. Blauensteiner, M. Zukowski, M. Aspelmeyer, and A. Zeilinger. Experimental interference of independent photons. *Phys. Rev. Lett.*, 96(24):240502, 2006. 28, 36

[118] T. Yang, Q. Zhang, T.-Y. Chen, L. Shan, J. Yin, J.-W. Pan, Z.-Y. Wei, J.-R. Tian, and J. Zhang. Experimental synchronization of independent entangled photon sources. *Phys. Rev. Lett.*, 96(11):110501, 2006. 28, 36

[119] Z. Y. Ou and Y. J. Lu. Cavity enhanced spontaneous parametric down-conversion for the prolongation of correlation time between conjugate photons. *Phys. Rev. Lett.*, 83(13):2556–2559, 1999. 28

[120] J. H. Shapiro and N. C. Wong. An ultrabright narrowband source of polarization-entangled photon pairs. *J. Opt. B*, 2(1):L1–L4, 2000. 28

[121] H. Wang, T. Horikiri, and T. Kobayashi. Polarization-entangled mode-locked photons from cavity-enhanced spontaneous parametric down-conversion. *Phys. Rev. A*, 70(4):043804, 2004. 28

[122] C. E. Kuklewicz, F. N. C. Wong, and J. H. Shapiro. Time-bin-modulated biphotons from cavity-enhanced down-conversion. *Phys. Rev. Lett.*, 97(22):223601, 2006. 28, 30

[123] Z.-S. Yuan, Y.-A. Chen, S. Chen, B. Zhao, M. Koch, T. Strassel, Y. Zhao, G.-J. Zhu, J. Schmiedmayer, and J.-W. Pan. Synchronized independent narrow-band single photons and efficient generation of photonic entanglement. *Phys. Rev. Lett.*, 98(18):180503, 2007. 28, 67, 68

[124] E. D. Black. An introduction to pound–drever–hall laser frequency stabilization. *Am. J. Phys.*, 69(1):79–87, 2001. 29

[125] Y. J. Lu and Z. Y. Ou. Optical parametric oscillator far below threshold: Experiment versus theory. *Phys. Rev. A*, 62(3):033804, 2000. 29, 31

[126] Andrew G. White, Daniel F. V. James, Philippe H. Eberhard, and Paul G. Kwiat. Nonmaximally entangled states: Production, characterization, and utilization. *Phys. Rev. Lett.*, 83(16):3103–3107, Oct 1999. 31

[127] H. Goto, Y. Yanagihara, H. Wang, T. Horikiri, and T. Kobayashi. Observation of an oscillatory correlation function of multimode two-photon pairs. *Phys. Rev. A*, 68(1):015803, 2003. 31

[128] B. Zhao, Z.-B. Chen, Y.-A. Chen, J. Schmiedmayer, and J.-W. Pan. Robust creation of entanglement between remote memory qubits. *Phys. Rev. Lett.*, 98(24):240502, 2007. 33, 48, 49, 67

[129] Nicolas Gisin, Grégoire Ribordy, Wolfgang Tittel, and Hugo Zbinden. Quantum cryptography. *Rev. Mod. Phys.*, 74(1):145–195, Mar 2002. 35, 89

[130] M. Zukowski, A. Zeilinger, M. A. Horne, and A. K. Ekert. Event-ready-detectors bell experiment via entanglement swapping. *Phys. Rev. Lett.*, 71(26):4287–4290, 1993. 35

[131] J.-W. Pan, D. Bouwmeester, M. Daniell, H. Weinfurter, and A. Zeilinger. Experimental test of quantum nonlocality in three-photon greenberger-horne-zeilinger entanglement. *Nature*, 403(6769):515–519, 2000. 35

[132] J.-W. Pan, S. Gasparoni, R. Ursin, G. Weihs, and A. Zeilinger. Experimental entanglement purification of arbitrary unknown states. *Nature*, 423(6938):417–422, 2003. 35

[133] P. Walther, J.-W. Pan, M. Aspelmeyer, R. Ursin, S. Gasparoni, and A. Zeilinger. De broglie wavelength of a non-local four-photon state. *Nature*, 429(6988):158–161, 2004. 35, 76, 77

[134] F. Konig, E. J. Mason, F. N. C. Wong, and M. A. Albota. Efficient and spectrally bright source of polarization-entangled photons. *Phys. Rev. A*, 71(3):033805, 2005. 36

[135] M. Halder, A. Beveratos, N. Gisin, V. Scarani, C. Simon, and H. Zbinden. Entangling independent photons by time measurement. *Nat. Phys.*, 3(10):692–695, 2007. 36

[136] X.-H. Bao, Y. Qian, J. Yang, H. Zhang, Z.-B. Chen, T. Yang, and J.-W. Pan. Generation of narrow-band polarization-entangled photon pairs for atomic quantum memories. *Phys. Rev. Lett.*, 101(19):190501, 2008. 36

[137] Z. Zhao, Y. A. Chen, A.-N. Zhang, T. Yang, H. J. Briegel, and J.-W. Pan. Experimental demonstration of five-photon entanglement and open-destination teleportation. *Nature*, 430(6995):54–58, 2004. 36

[138] Jian-Wei Pan, Zeng-Bing Chen, Marek Zukowski, Harald Weinfurter, and Anton Zeilinger. Multi-photon entanglement and interferometry. arXiv:0805.2853v1 [quant–ph], 2008. 36

[139] T. P. Bodiya and L.-M. Duan. Scalable generation of graph-state entanglement through realistic linear optics. *Phys. Rev. Lett.*, 97:143601, 2006. 36

[140] S. Popescu. Bells inequalities versus teleportation: What is nonlocality? *Phys. Rev. Lett.*, 72(6):797–799, 1994. 38, 98, 101

[141] N. D. Mermin. What's wrong with these elements of reality? *Phys. Today*, 43(6):9–11, 1990. 40

[142] Michael Seevinck and Jos Uffink. Sufficient conditions for three-particle entanglement and their tests in recent experiments. *Phys. Rev. A*, 65(1):012107, 2001. 40

[143] Shuai Chen, Yu-Ao Chen, Bo Zhao, Zhen-Sheng Yuan, Jörg Schmiedmayer, and Jian-Wei Pan. Demonstration of a stable atom-photon entanglement source for quantum repeaters. *Phys. Rev. Lett.*, 99(18):180505, Nov 2007. 49, 68, 69, 84, 93, 95, 97

[144] D. N. Matsukevich, T. Chaneliere, M. Bhattacharya, S.-Y. Lan, S. D. Jenkins, T. A. B. Kennedy, and A. Kuzmich. Entanglement of a photon and a collective atomic excitation. *Phys. Rev. Lett.*, 95(4):040405, 2005. 49, 84

[145] H. de Riedmatten, J. Laurat, C.-W. Chou, E. W. Schomburg, D. Felinto, and H. J. Kimble. Direct measurement of decoherence for entanglement between a photon and stored atomic excitation. *Phys. Rev. Lett.*, 97(11):113603, 2006. 49, 84

[146] Z.-B. Chen, B. Zhao, Y.-A. Chen, J. Schmiedmayer, and J.-W. Pan. Fault-tolerant quantum repeater with atomic ensembles and linear optics. *Phys. Rev. A*, 76(2):022329, 2007. 50

[147] Nicolas Sangouard, Christoph Simon, Bo Zhao, Yu-Ao Chen, Hugues de Riedmatten, Jian-Wei Pan, and Nicolas Gisin. Robust and efficient quantum repeaters with atomic ensembles and linear optics. *Phys. Rev. A*, 77(6):062301, Jun 2008. 50, 74

[148] S. Chen, Y.-A. Chen, T. Strassel, Z.-S. Yuan, B. Zhao, J. Schmiedmayer, and J.-W. Pan. Deterministic and storable single-photon source based on a quantum memory. *Phys. Rev. Lett.*, 97(17):173004, 2006. 54, 67, 68, 69, 71, 80, 85

[149] Daniel A. Steck. Rubidium 87 d line data. available online at http://steck.us/alkalidata. 54, 62

[150] Rudolf Grimm, Matthias Weidemueller, and Yurii B. Ovchinnikov. Optical dipole traps for neutral atoms. In *Advances in Atomic, Molecular and Optical Physics Vol. 42*, pages 95–170. 2000. 57

[151] D. Wei, J. F. Chen, M. M. T. Loy, G. K. L. Wong, and S. Du. Optical precursors with electromagnetically induced transparency in cold atoms. *Phys. Rev. Lett.*, 103(9):093602, 2009. 62

[152] M. Bajcsy, S. Hofferberth, V. Balic, T. Peyronel, M. Hafezi, A. S. Zibrov, V. Vuletic, and M. D. Lukin. Efficient all-optical switching using slow light within a hollow fiber. *Phys. Rev. Lett.*, 102(20):203902, 2009. 62

[153] J. Simon, H. Tanji, J. K. Thompson, and V. Vuletic. Interfacing collective atomic excitations and single photons. *Phys. Rev. Lett.*, 98(18):183601, 2007. 62, 63

[154] Z.-B. Chen, B. Zhao, Y. A. Chen, J. Schmiedmayer, and J.-W. Pan. Fault-tolerant quantum repeater with atomic ensembles and linear optics. *Phys. Rev. A*, 76(2):022329, 2007. 67

[155] L. Jiang, J. M. Taylor, and M. D. Lukin. Fast and robust approach to long-distance quantum communication with atomic ensembles. *Phys. Rev. A*, 76(1):012301, Jul 2007. 67

[156] O. A. Collins, S. D. Jenkins, A. Kuzmich, and T. A. B. Kennedy. Multiplexed memory-insensitive quantum repeaters. *Phys. Rev. Lett.*, 98(6):060502, Feb 2007. 67

[157] D. N. Matsukevich, T. Chanelière, S. D. Jenkins, S.-Y. Lan, T. A. B. Kennedy, and A. Kuzmich. Deterministic single photons via conditional quantum evolution. *Phys. Rev. Lett.*, 97(1):013601, Jul 2006. 67, 68, 69, 74, 84

[158] D. Felinto, C. W. Chou, J. Laurat, E. W. Schomburg, H. de Riedmatten, and H. J. Kimble. Conditional control of the quantum states of remote atomic memories for quantum networking. *Nat Phys*, 2(12):844–848, 2006. 67, 68

[159] T. Chaneliere, D. N. Matsukevich, S. D. Jenkins, S.-Y. Lan, R. Zhao, T. A. B. Kennedy, and A. Kuzmich. Quantum interference of electromagnetic fields from remote quantum memories. *Phys. Rev. Lett.*, 98(11):113602, 2007. 67, 68

[160] Jonathan Simon, Haruka Tanji, James K. Thompson, and Vladan Vuletić. Interfacing collective atomic excitations and single photons. *Phys. Rev. Lett.*, 98(18):183601, May 2007. 68, 89

[161] D. Felinto, C. W. Chou, H. de Riedmatten, S. V. Polyakov, and H. J. Kimble. Control of decoherence in the generation of photon pairs from atomic ensembles. *Phys. Rev. A*, 72(5):053809, 2005. 68, 69, 74, 87

[162] D. M. Harber, H. J. Lewandowski, J. M. McGuirk, and E. A. Cornell. Effect of cold collisions on spin coherence and resonance shifts in a magnetically trapped ultracold gas. *Phys. Rev. A*, 66(5):053616, Nov 2002. 68

[163] C. W. Chou, S. V. Polyakov, A. Kuzmich, and H. J. Kimble. Single-photon generation from stored excitation in an atomic ensemble. *Phys. Rev. Lett.*, 92(21):213601, 2004. 69

[164] Rudolf Grimm, Matthias Weidemüller, and Yurii B. Ovchinnikov. Optical dipole traps for neutral atoms. In Benjamin Bederson and Herbert Walther, editors, *Advances in Atomic, Molecular and Optical Physics Vol. 42*, pages 95–170. ACADEMIC PRESS, 2000. 74

[165] M. Greiner, O. Mandel, T. Esslinger, T. W. Hansch, and I. Bloch. Quantum phase transition from a superfluid to a mott insulator in a gas of ultracold atoms. *Nature*, 415(6867):39–44, 2002. 74

[166] J. J. Longdell, E. Fraval, M. J. Sellars, and N. B. Manson. Stopped light with storage times greater than one second using electromagnetically induced transparency in a solid. *Phys. Rev. Lett.*, 95(6):063601, Aug 2005. 74

[167] M. Fleischhauer and M. D. Lukin. Dark-state polaritons in electromagnetically induced transparency. *Phys. Rev. Lett.*, 84(22):5094–5097, 2000. 74

[168] Claudia Mewes and Michael Fleischhauer. Decoherence in collective quantum memories for photons. *Phys. Rev. A*, 72(2):022327, Aug 2005. 74

[169] J. P. Dowling. Quantum optical metrology the lowdown on high-n00n states. *Contemporary Physics*, 49(2):125–143, 2008. 75, 76, 80, 81

[170] Alexander D. Cronin, Jörg Schmiedmayer, and David E. Pritchard. Optics and interferometry with atoms and molecules. *Rev. Mod. Phys.*, 81(3):1051–1129, Jul 2009. 75

[171] Vittorio Giovannetti, Seth Lloyd, and Lorenzo Maccone. Quantum-enhanced measurements: Beating the standard quantum limit. *Science*, 306(5700):1330–1336, 2004. 76

[172] M. W. Mitchell, J. S. Lundeen, and A. M. Steinberg. Super-resolving phase measurements with a multiphoton entangled state. *Nature*, 429(6988):161–164, 2004. 76

[173] K. J. Resch, K. L. Pregnell, R. Prevedel, A. Gilchrist, G. J. Pryde, J. L. O'Brien, and A. G. White. Time-reversal and super-resolving phase measurements. *Phys. Rev. Lett.*, 98(22):223601, May 2007. 76

[174] T. Nagata, R. Okamoto, J. L. O'Brien, K. Sasaki, and S. Takeuchi. Beating the standard quantum limit with four-entangled photons 10.1126/science.1138007. *Science*, 316(5825):726–729, 2007. 76

[175] P. Kok, H. Lee, and J. P. Dowling. Creation of large-photon-number path entanglement conditioned on photodetection. *Phys. Rev. A*, 65(5):052104, 2002. 77, 78

[176] S. D. Barrett, P. P. Rohde, and T. M. Stace. Scalable quantum computing with atomic ensembles. pages 0804.0962v1 [quant–ph], 2008. 78

[177] W. Wohlleben, F. Chevy, K. Madison, and J. Dalibard. An atom faucet. *The European Physical Journal D*, 15(2):237–244, August 2001. 79

[178] S. F. Huelga, C. Macchiavello, T. Pellizzari, A. K. Ekert, M. B. Plenio, and J. I. Cirac. Improvement of frequency standards with quantum entanglement. *Phys. Rev. Lett.*, 79(20):3865–3868, Nov 1997. 81

[179] M. Auzinsh, D. Budker, D. F. Kimball, S. M. Rochester, J. E. Stalnaker, A. O. Sushkov, and V. V. Yashchuk. Can a quantum nondemolition measurement improve the sensitivity of an atomic magnetometer? *Phys. Rev. Lett.*, 93(17):173002, Oct 2004. 81

[180] D. Leibfried, M. D. Barrett, T. Schaetz, J. Britton, J. Chiaverini, W. M. Itano, J. D. Jost, C. Langer, and D. J. Wineland. Toward heisenberg-limited spectroscopy with multiparticle entangled states 10.1126/science.1097576. *Science*, 304(5676):1476–1478, 2004. 81

[181] B. C. Jacobs, T. B. Pittman, and J. D. Franson. Quantum relays and noise suppression using linear optics. *Phys. Rev. A*, 66(5):052307, Nov 2002. 83

[182] Edo Waks, Assaf Zeevi, and Yoshihisa Yamamoto. Security of quantum key distribution with entangled photons against individual attacks. *Phys. Rev. A*, 65(5):052310, Apr 2002. 83

[183] Yu-Ao Chen, Xiao-Hui Bao, Zhen-Sheng Yuan, Shuai Chen, Bo Zhao, and Jian-Wei Pan. Heralded generation of an atomic noon state. *Phys. Rev. Lett.*, 104(4):043601, Jan 2010. 85

[184] A. Peres. Delayed choice for entanglement swapping. *Journal of Modern Optics*, 47:531, 2000. 88

[185] A. M. Goebel, C. Wagenknecht, Q. Zhang, Y.-A. Chen, K. Chen, J. Schmiedmayer, and J.-W. Pan. Multistage entanglement swapping. *Phys. Rev. Lett.*, 101(8):080403, 2008. 88

[186] Bo Zhao, Markus Mueller, Klemens Hammerer, and Peter Zoller. Efficient quantum repeater based on deterministic rydberg gates. arXiv:1003.1911v1 [quant–ph], 2010. 89

[187] R. Jozsa. Fidelity for mixed quantum states. *Journal of Modern Optics*, 41(12):2315–2323, 1994. 98